HOME AREA NETWORKS FOR SMART GRID COMMUNICATIONS

by

ZHUO LI

Presented to the Faculty of the Graduate School of

The University of Texas at Arlington in Partial Fulfillment

of the Requirements

for the Degree of

DOCTOR OF PHILOSOPHY

THE UNIVERSITY OF TEXAS AT ARLINGTON

May 2014

To my family.

For their love and support.

Acknowledgements

My deepest gratitude goes to my supervising professor Dr. Qilian Liang, who is invaluable for constantly motivating and encouraging me to explore my capability of doing research, training me to provide innovative solutions. I am also learning following traits from Dr. Qilian Liang: self-discipline, diligence and keep improving. He was and always will be the role model throughout my life.

I wish to thank Dr. Jonathan Bredow, Dr. Wen-Jen Lee, Dr. Ioannis D. Schizas, Dr. Saibun Tjuatja, and Dr. David A. Wetz for their interest in my research and for taking time to serve in my defense committee.

I would like to extend my appreciation to Prof. Zheng Zhou, Prof. Weixia Zou, and a senior Bin Li at Beijing University of Posts and Telecommunications (BUPT), for encouraging and inspiring me to pursue Ph.D studies.

I am also indebted to the members of the Wireless Communications and Networking Lab at UTA, including Dr. Jing Liang, Dr. Lei Xu, Dr. Davis Kirachaiwanich, Dr. Ji Wu, Junjie Chen, Ishrat Maherin, Xin Wang, Qiong Wu and so on. I am also grateful to my boyfriend Nan Zhang. I have benefited enormously from their experience inside and outside the classroom.

Finally, I would like to express my sincere gratefulness to my parents, my sister, and my brother-in-law, for their unceasing support and encouragement throughout my career. They set an example and made me who I am. I am extremely fortunate to be so blessed.

This work was supported in part by U.S. National Science Foundation under Grants CNS-1247848, CNS-1116749, CNS-0964713, and U.S. Office of Naval Research under Grants N00014-13-1-0043, N00014-11-1-0865, N00014-11-1-0071.

April 14, 2014

Abstract

HOME AREA NETWORKS FOR SMART GRID COMMUNICATIONS

Zhuo Li, Ph.D.

The University of Texas at Arlington, 2014

Supervising Professor: Qilian Liang

This dissertation studies five topic which are focused on but not limited to the area of Home Area Networks (HANs) in Smart Grid communications: capacity optimization for IR-UWB (Chapter 2), power consumption and downlink outage probability in a dynamic HAN (Chapter 3), uplink multiuser selection in a dynamic HAN (Chapter 4), capacity optimization in Heterogeneous HANs (Chapter5), hybrid models of OFDM-based power line and wireless communications for HAN security (Chapter 6), and scaling laws of ergodic capacity for hybrid wireless networks with distributed base stations (DBS) (Chapter 7).

We investigate the capacity optimization of Impulse Radio (IR) UWB user within the coexisting operating bandwidth with IEEE 802.11n user, while making sure that its cumulative interference to the coexisting IEEE 802.11n user is below a certain permissible threshold. The optimal power allocation scheme is presented by using water-filling algorithm with Karush-Kuhn-Tucher (KKT) conditions, which is also compared with a traditional equal power allocation scheme.

Considering the power saving potential of the emerging WiFi Direct technique, we evaluate the performance of WiFi Direct technique in HANs for Smart Grid Com-

munication from two aspects: power consumption and outage probability. By modeling the traffic intensity and the number of working devices in a dynamic HAN as a Markov chain, the power consumption of the dynamic HAN is evaluated. As to the outage performance, in the downlink of the HAN, the probability density function (PDF) of the signal to interference and noise ratio (SINR) for the active user is derived from the amplitude distribution property of the classical indoor Saleh-Valenzuela (S-V) channel.

This dissertation also considers the problem of how to optimize the downlink capacity in a heterogeneous HAN with beamforming technique at the smart meter for Smart Grid application. The PDF of the smallest allocated transmit power is mathematically obtained from the properties of downlink indoor S-V channels. It is analytically shown that the allocated transmit power has a lower limit which is determined by the SINR threshold as well as the total number of active users in the HAN.

Traditionally, jamming to the wireless in-home system is a fatal threat for Smart Grid communications. To enhance HAN security for Smart Grid application, this dissertation incorporates the OFDM - based power line (PL) system into the HAN, and proposes two hybrid models of PL and wireless communications with transmit diversity and receive diversity, respectively. Finally, a hybrid wireless network with DBS is designed to improve the spectrum efficiency. It is analytically shown that compared to the traditional hybrid wireless network, the ergodic throughput capacity of hybrid wireless networks with DBS scales with gain with $N \times N_{BS}$.

Table of Contents

List of Illustrations

List of Tables

Chapter 1

Introduction and Preliminaries

1.1 Smart Grid Communications

Smart Grid is considered as a tight combination of wireless communication networks and power line communication systems with some new characteristics, such as energy saving, self-healing, high attack-resistance, etc. Communication networks play an important role in the realization of Smart Grid. The major challenge for developing Smart Grid communication solutions is to understand the architecture of the future Smart Grid system and its implications to communication solutions[1]. A typical smart grid communication system consists of an advanced metering infrastructure (AMI) with a multi-tier communication infrastructure that includes: home area network (HAN), which is used to gather sensor information from a variety of devices within the home, and optionally send control information to these devices to better control energy consumption, and provides access to in-home appliances, as shown in Figure 1.1; neighborhood area network (NAN) to connect the smart meters to the local access points; and a wide area network (WAN) to connect the grid to the core utility system [2] [3].

1.2 Preliminary to the Coexistence between IR-UWB and IEEE 802.11n

Ultra wideband (UWB) radio is a promising technology that can be applied at very low power for short-range high data-rates communications. In light of its main advantages of high data rates, low cost, and low power consumption, UWB systems tend to be short-range and indoor applications, examples of which are communica-

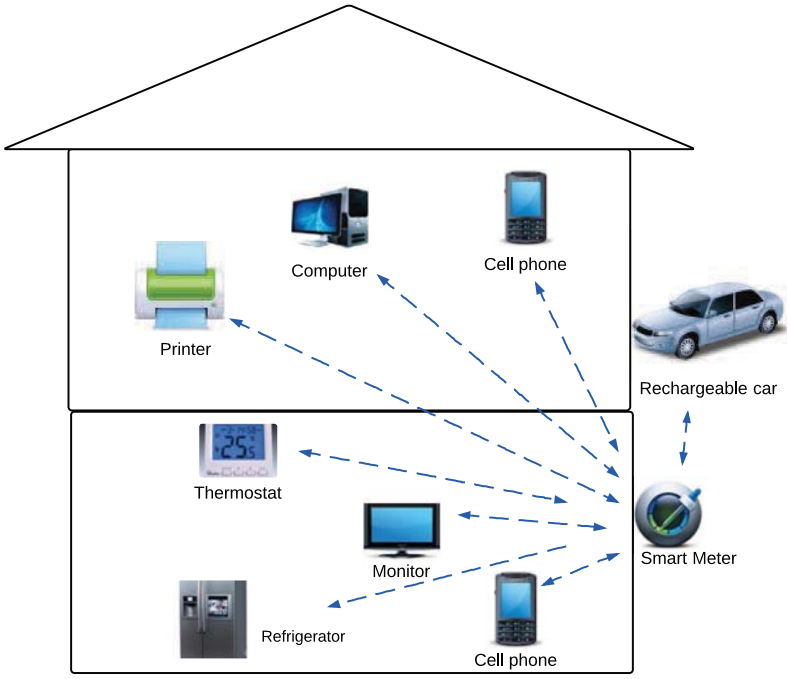

Figure 1.1. Communications of a HAN in Smart Grid.

tions between wireless monitors, digital camcorders, wireless printing, cell phones and personal computers[4]. Besides, owing to its precision capabilities combined with the extremely low power, UWB radio is ideal for certain frequency sensitive environments such as hospitals and healthcare. It was also used in military applications for covert communications. In this application, the military took advantage of the fact that UWB signals spread across a very wide bandwidth and could be made to appear as noise to most interception equipments [5]. UWB is part of "see-through-the-wall" precision radar imaging technology, precision locating and tracking. Moreover, UWB technology is an ideal candidate for future Wireless Personal Area Networks (WPAN) that requires processing information with low-power sources at very high speed across short distances [6].Short range communication systems could be applied to the fields

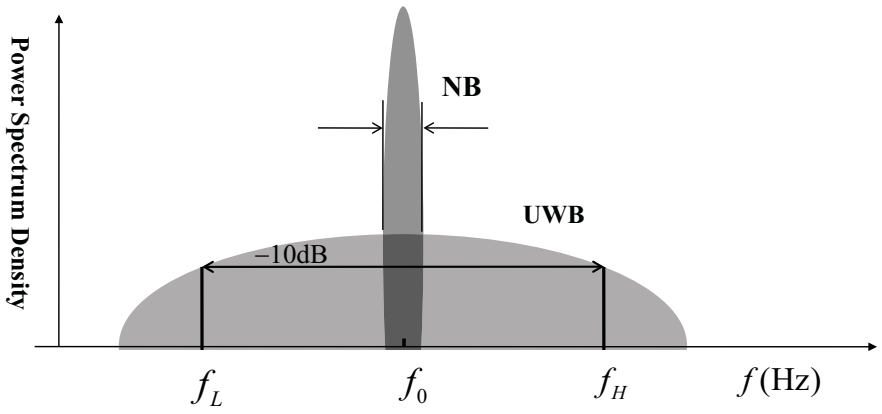

Figure 1.2. Spectrum Comparison of UWB and NB signals.

of Smart Grid[7], which includes an intelligent monitoring system that would keep track of electrical power distribution system[8].

In principle, any wireless communication technology that produces signals with a bandwidth wider than 500MHz or a fractional bandwidth greater than 0.2 can be considered as UWB[9], where the fractional bandwidth is defined as:

$$\eta = 2 \times \frac{f_H - f_L}{f_H + f_L} \tag{1.1}$$

f_L and f_H are the lower bond and upper bond of the spectral frequency of UWB radio.

The Federal Communication Commission (FCC) released a spectral mask with some restrictions for UWB. For indoor UWB systems, a maximum mean effective isotropic radiated power (EIRP) spectrum density of -41.3dBm/MHz is established over the 3.1∼10.6GHz operating bandwidth[10]. Different from the NB wireless com-

munications systems, i.e. Wireless Local Area Network (WLAN), Worldwide Interoperability for Microwave Access (WiMAX), and Long Time Evolution (LTE), UWB systems conventionally occupy a relatively large bandwidth in the frequency domain which is already allocated by these NB communication systems as illustrated in Fig. 1.2. Therefore, it is obvious that UWB systems would inevitably coexist with other NB wireless communication systems by sharing some operation bandwidth [11].

In the existing literatures, the coexistence issue of UWB system and other wireless communication systems, such as cellular systems and NB wireless systems, is widely studied. The investigation is mainly categorized into two parts: one is to study the the interference effect from other conventional systems on the UWB system, and the other one is to analyze how UWB signals could impact other coexisting systems. Particularly, previous literatures focus on the inference introduced by UWB signals to fixed wireless communications systems, for example, the global system for mobile communications (GSM), universal mobile telecommunication system (UMTS), and global positioning system (GPS) [12][13]. Later on, coexistence issue between UWB system and NB communication systems attracted researchers' attention due to the wide application of NB communication systems. Giogretti et.al [14] evaluated the performance of wideband communication systems in the presence of narrowband interference (NBI). In [14] closed-form bit-error probability expressions for spread-spectrum UWB systems were derived under the additive white Gaussian noise (AWGN) channels, flat-fading channels, and frequency-selective multipath fading channels respectively, where the NBI was considered as tone interferer. Furthermore, coexistence between UWB and Orthogonal-Frequency-Division-Multiplexing (OFDM)-based systems was thoroughly analyzed in [15].

Considering the operating frequencies of IEEE 802.11n, IEEE 802.11n system with either operating mode could be interference by UWB user, and the interference

of IEEE 802.11n system to UWB user is also unavoidable. The coexistence issue of UWB and IEEE 802.11n systems has been investigated since the standardization of IEEE 802.11n. [11] studied the maximum permissible emission power of UWB system under the coexistence with IEEE 802.11n by setting up the physical layer models of these two systems. The spectrum sensing performance of UWB-based Cognitive Radio (CR) systems with the primary user of IEEE 802.11n was presented in [16]. Based on these studies, the topic of how to optimize the capacity of UWB user while making sure that these two systems can still work simultaneously is seldom investigated. Therefore, study on the proper spectrum management of UWB system which optimizes its transmission rate, seems to be definitely necessary. Besides, this research will give a suggestion on the spectrum regulation of UWB system.

Capacity optimization for wireless communication systems has been widely studied. Some of them focus on the coexistence situation of two systems. [17] proposed a water-filling algorithm for direct-sequence (DS) UWB cognitive radio (CR) network that maximizes the sum capacity while enabling each transmitter to fit its power spectral density into, and thus to make the most of, the spectrum void. Bansal et.al investigated an optimal power loading algorithm for an OFDM-based cognitive radio system [18]. The downlink transmission capacity of the CR user is thereby maximized, while the interference introduced to the primary user (PU) remains within a tolerable range. The non-convex NP-hard problem of weighted sum rate maximization in a multiuser Gaussian channel that models a cognitive wireless network with affine power constrains was studied in [19]. The key technique is the use of nonnegative matrix theory, in particular the Perron-Frobenius Theorem and the Friedland-Karlin inequalities. Reference [19] also extends to a multiuser-multiple carrier model, where a common spectrum is divided into K frequency tones. [20] proposed a margin-based power allocation scheme that utilizes each UWB node's own position information,

and an exclusive region-based scheduling scheme that takes into consideration the interaction among simultaneous transmission links.

This dissertation investigates capacity optimization of IR-UWB user within the coexisting operating bandwidth with IEEE 802.11n user, while making sure that its cumulative interference to the coexisting IEEE 802.11n user is below a certain threshold. The optimal power allocation scheme is presented by using water-filling algorithm with Karush-Kuhn-Tucher (KKT) conditions, which is also compared with a traditional equal power allocation scheme.

1.3 Preliminaries to Dynamic HAN with WiFi Direct Technique

Nowadays WiFi Direct technology is attracting attentions for Smart Grid solutions, which are driven by the desire of more efficient energy usage worldwide. Different from the conventional WiFi infrastructure, WiFi Direct is a standard that allows WiFi devices to communicate with each other without the need for Wireless Access Point (AP). In this way, devices in the WiFi Direct network establish an ad-hoc peer-to-peer connectivity [21]. Moreover, a distinction from the well-known Wireless Mesh Network (WMN) is that the WiFi Direct devices could keep simultaneous connections within the network infrastructure. As a result, the configuration of WiFi Direct network could be either one-to-one, or one-to-many. The WiFi Direct devices in the Smart Grid application scenario could be smart phones, monitors, and smart meters, etc. An example of WiFi Direct network configuration for HAN in Smart Grid is as shown in Figure 1.3. The in-home appliances communicate with each other for file transmission, and the household devices send user information to the smart meter, while the smart meter conducts real-time monitoring to these in-home appliances.

WiFi is a mature, proven technology that implements many of the Smart Grid application scenarios in the HAN [22], with the following advantages:

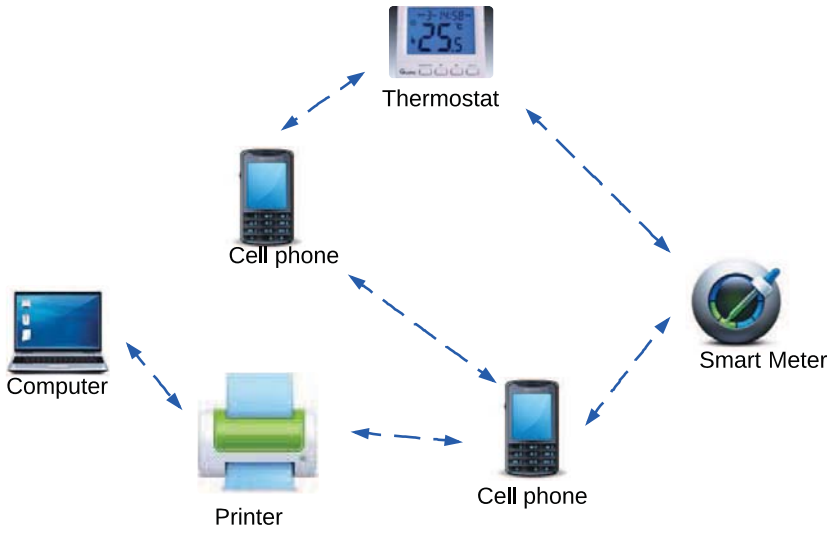

Figure 1.3. WiFi Direct HAN for Smart Grid.

1) an IP based-network for seamless connection;
2) satisfactory operational range across walls and other barriers;
3) high data throughput and low power consumption;
4) government-grade security for ensuring integrity of communications.

In the Smart Grid application, WiFi Direct devices are always battery-operated and thus power-sensitive. Consequently, an efficient power consumption scheme is highly demanded. The WiFi Direct devices can support the Power Save feature certified under the WMM (Wireless Multimedia) program [23]. As opposed to the traditional *Continuous Active Mode* (*CAM*) in which the devices remain awake all the time even no data transmission is required, the *Power Saving Mechanism* (*PSM*) attempts to conserve energy on idle devices by powering off their wireless interfaces for specific period of time [24]. A device in the HAN can power down the transceiver

to save energy. When the transceiver is on, it is said to be *awake* or *active*. When the transceiver is off, it is said to be *sleeping*, *dozing*, or in the *power-saving mode* [25].

In the existing literature, an experimental study of the IEEE 802.11 power saving mechanism on PDA in a wireless local area network was presented in [24], which provides guidance to the design of future power saving mechanisms. Lee et al. [26] proposed a cross layer power saving technique by utilizing the correlation based carrier sensing indicator to improve the power efficiency for wireless receivers. A scheduling algorithm to defer electric loads in Smart Grid is proposed by M. Alizadeh et al. [27]. Kim and Poor [28] considered the power consumption scheduling problem with future price uncertainty in Smart Grid applications, which is naturally cast as a Markov decision process. Reference [29] pointed out that one of the fundamental issues for the communication in a Smart Grid is the link capacity which should be able to convey the system state information with negligible error. Yang et al. [30] evaluates the outage probability of multisuer donwlink networks over Nakagami-m fading channels. Performance evaluation of outage probability over Rayleigh fading channels in distributed random access networks is presented in [31].

In this dissertation, we evaluate the advantages of a dynamic HAN for Smart Grid with the emerging WiFi Direct technique from two perspectives: power saving and communication reliability of the dynamic HAN. Since the power consumption of the HAN is directly related with the number as well as the working states of WiFi Direct devices, a Markov chain model is employed to represent a profile of the traffic intensity and the the number of WiFi Direct devices in active state. The steady state probability of the number of active users is derived from the Markov chain model, and thus the average power consumption is obtained. Furthermore, we investigate the downlink outage probability with multiple in-home users connected to the smart meter. For this indoor network, the classical S-V channel model is adopted. The

probability PDF of the signal to SINR for each user in the HAN is derived according to the distribution property of channel gain. The outage probability of the downlink scenario is analyzed with the characteristics of interference cancelation technique.

Multiuser selection scheme is applied to the uplink of a dynamic HAN for Smart Grid communication scenario. We evaluate the performance of the multiuser selection scheme in the absence of interference as well as in the presence of MUI. In the absence of interference, the PDF of received SNR for the selected user is derived from the amplitude distribution property of indoor S-V channel, and thus the closed-form outage probability is obtained for the scenario with dynamic number of active users. In addition, the BER of multiuser selection scheme is studied by numerical simulation. On the other hand, in the presence of MUI, we model the interference due to free space path loss and log-normal shadowing. Particularly, evaluation of the interference impact on multiuser selection scheme is improved by assuming the multiuser interference cancelation coefficient as a random variable between 0 and 1 for more reasonable analysis. To our best knowledge, this is the first study on performance analysis of multiuser selection scheme that is employed in dynamic HANs for Smart Grid communications.

1.4 Preliminaries to Capacity Optimization in a Heterogeneous HAN

As shown in Figure 1.1, HAN of Smart Grid is a dedicated network connecting heterogeneous household wireless devices with the smart meter, which can monitor the power activities, report the power consumption and send necessary control information to all the active users. The users in the HAN of Smart Grid could be smart phones, smart sensors, monitors, and in-home appliances, etc. Thus, various communication technologies are adopted for these smart grid appliances. For example, WiFi are used for the communications between cell phones, computers, printers and the

smart meter; For monitors, Bluetooth is employed; as to the thermostat and refrigerators, ZigBee could be introduced. Heterogeneous wireless communication indicates various Quality of Service (QoS) requirements. QoS typically refers to the performance or reliability of a communication link, for example, channel capacity. From the prospective of information theory, the Shannon channel capacity C (in bits/s) is modeled as a monotonic function of signal to interference and noise ratio (SINR) η:

$$C = B \log_2(1 + \eta) \tag{1.2}$$

where B is the channel bandwidth. So it is obvious that SINR is a measure index of QoS for a communication link. We can claim that heterogeneous wireless communication in the HAN of Smart Grid indicates that each user may have different SINR requirements. One way to achieve this is to adjust the transmit power to each user when data like control information is transmitted from the smart meter to all the users. With the traditional channel inversion method, since the subchannels created to each user are independent, changing the transmit power to one user would change the interference for all other users. This necessitates beamforming solution where the beamforming vectors and power weights are jointly optimized [32].

The reliability and efficiency of smart grid depends directly on the performance of the communication infrastructure [44]. In this dissertation, we take an in-depth look at the total downlink capacity optimization and optimal power allocation of heterogeneous multiuser HAN for Smart Grid applications. In this HAN, we present that multiple transmit antennas are equipped at the smart meter with beamforming technique, and therefore, the downlink from the smart meter to each user is essentially a multiple input and single output (MISO) channel for spatial diversity. The smart meter simultaneously transmits signals to each user, and thus code-division-multiple-access (CDMA) technique is employed in this multi-user communication sce-

nario [34]. Different from the traditional cellular network, heterogeneous service in the HAN requires heterogeneous transmission bandwidths as well as heterogeneous SINR constraints for each user [35]. This optimization problem is mathematically proved to be a convex optimization problem. In this case, the optimal solution of power allocation for each user could be obtained by employing KKT condition, which is considered both necessary and sufficient for convex optimality [36]. An optimal transmit power allocation algorithm is thus proposed and illustrated with examples of totally three, five, eight and ten active home appliances in the HAN. In addition, the propagation environment of the HAN experiences scattering, where there are many small reflectors. In this dissertation, S-V channel model is adopted to profile the scattering mechanisms of the communication link between the smart meter and home appliances. With channel state information is known at the transmitter (CSIT), the transmit power from the smart meter to each user exhibits variation due to the fading of the indoor S-V channels. Considering that the lowest SINR requirement should be satisfied for each user and the allocated transmit power fluctuates with the S-V channel, by investigating the PDF property of the allocated transmit power to each user, a theorem is presented that each user has a lower bound which is determined by both the total number of active users in the HAN and the required minimum SINR for the user. The lower bound of the transmit power to each user can be considered as a useful benchmark to guarantee reliable communications for real system design.

1.5 Preliminaries to Hybrid Models of Power Line and Wireless Communications in HAN

As to the security issue of HANs for Smart Grid communications, Lee et. al [37] reviewed fundamentals of wireless communication, investigated PHY attack models,

and thus proposed a spread-spectrum wireless communication scheme for robust data communication. In [37], the merits and drawbacks of both the wireless communication and the PL communication are discussed in depth. Moreover, the PHY attacks to the wireless medium are categorized into four classes: eavesdropping, jamming, restricting access, and injecting. The PL communication was validated as a good candidate for Smart Grid application in [38]. Home Plug Green PHY^{TM} has emerged as the leading Specification for implementing Smart Grid functionality across HAN PL-based networks [39]. Korki pointed out that the performance of the PL system are affected by noise and multipath propagation in the PL channel [40]. In addition, the Middleton's Class A model was employed as the noise in the simulation to evaluate the performance of the PL communication network. A classic multipath model for the PL channel was presented by Zimmermann, which was based on fundamental physical effects, and was analyzed by numerical measurements [41]. Furthermore, it was concluded that the average channel gain for PL communication is lognormally distributed [42]. Lai and Messier evaluated the performance of the wireless and PL diversity channel by applying MRC at the receiver part [43], but multipath propagation and attenuation were not considered in the evaluation, and the PL channel was only supposed as static.

Based on the above considerations, we evaluate the advantages of a dynamic HAN for Smart Grid with the emerging WiFi Direct technique from two perspective: power saving and communication reliability of the dynamic HAN. Since the power consumption of the HAN is directly related with the number as well as the working states of WiFi Direct devices, a Markov chain model is employed to represent a profile of the traffic intensity and the the number of WiFi Direct devices in active state. The steady state probability of the number of active users is derived from the Markov chain model, and thus the average power consumption is obtained. Furthermore, we

investigate the downlink as well as uplink outage probability with multiple in-home users connected to the smart meter. For this indoor network, the classical S-V channel model is adopted. The PDF of the SNR/SINR for each user in the HAN is derived according to the distribution property of channel gain. The outage probability of the downlink scenario is analyzed with the characteristics of interference cancelation technique.

In addition, we take an in-depth look at the characteristics of wireless and PL communications of in-home system for Smart Grid application, and propose two hybrid models with transmit diversity and receive diversity, under the environment of a potential jamming attack to the wireless channel. Since the reliability of Smart Grid directly relies on the performance on the communication infrastructure [44], which could be evaluated by BER, the BERs of the proposed hybrid models are evaluated and compared.

1.6 Preliminaries to Hybrid Wireless Networks with Distributed Base Stations

In recent years, a hybrid wireless network model is proposed to improve network connectivity, in which sparse base stations are connected by wires between ad-hoc networks [45]. But with the advance of users, network traffic is being proliferated and thus spectrum resource is getting scare for wireless hybrid networks. One potential solution to address this issue is to improve both the network topology and the traffic pattern as a means to provide higher network capacity, which is considered as an indicator of spectrum efficiency in $Mbps/Hz$.

The concept of distributed antenna systems (DAS) was originally introduced to the interference-limited cellular networks to shorten access distance, reduce transmit power and OCI, and thus enhance the system capacity [46]. It can be treated as a macroscopic multiple-antenna system [47]. Heath et al. [48] proposed a downlink

virtual MIMO architecture and analyzed its per-node capacity. In the context of the 3GPP LTE-Advanced standard, distributed MIMO technique is known as coordinated multi-point (CoMP) transmission or reception [49]. The performance gain of CoMP was studied in [50], but only when the large-scale fading information is known at the transmitter.

The capacity of a hybrid wireless network has been widely studied in the literature. Gupta and Kumar [51] initiated the study of scaling laws in large ad-hoc wireless networks. The ergodic throughput capacity of wireless hybrid networks using the SIC strategy and the frequency reuse scheme was investigated in [52].

Based on these considerations, how can the ergodic capacity scale if the concept of *distributed base stations* is employed in hybrid wireless networks? A thorough understanding of the information-theoretic capacity of multi-cell virtual MIMO system accounting for fading and path loss effects, even with and ideal backhaul, is yet to be obtained. In this dissertation, an analytical framework of the hyrbird wireless network with distributed base stations is proposed. Based on the developed macroscopic multiple antenna system, the scaling law of the ergodic throughout capacity under infrastructure mode is investigated over the independent but not identically distributed composite fast fading channels, in which both large-scale path loss and small-scale Rayleigh fading count, and the channel coherence time is much smaller than the delay requirement of the application [53].

1.7 Organization of Dissertation

The reminder of this dissertation is organized as follows.

- Chapter 2 presents an optimal power allocation scheme to optimize the capacity of IR-UWB user within the coexisting operating bandwidth with IEEE 802.11n

user, while making sure that its cumulative interference to the coexisting IEEE 802.11n user is below a certain threshold.

- Chapter 3 introduces WiFi Direct technique into HANs for Smart Gird, evaluates the power consumption of a dynamic HAN, and analyzes the downlink outage probability of a dynamic HAN.
- Chapter 4 evaluates the performance evaluation of the uplink scenario of the dynamic HAN, in which multiuser selection scheme is employed at the smart meter. It is numerically shown that show that WiFi Direct technique not only improves the power saving in the HAN for Smart Grid, but also enhances the reliability of HAN communications for Smart Grid.
- Chapter 5 presents an optimal power allocation scheme for heterogeneous HAN to optimize its downlink capacity. In addition, a theorem is presented that each user has a lower transmit power bound which is determined by both the total number of active users in the HAN and the required minimum SINR for the user. The lower bound of the transmit power to each user can be considered as a useful benchmark to guarantee reliable communications for real system design.
- Chapter 6 proposes two types of hybrid models of OFDM-based wireless and PL communication systems with transmit diversity and receive diversity, under the environment of a potential jamming attack to the wireless channel.
- Chapter 7 designs an analytical framework of the hyrbird wireless network with distributed base stations. The ergodic throughput capacity, which is an indicator of spectrum efficiency, is investigated over the independent but not identically distributed composite fast fading channels. It is analytically shown that compared to the traditional hybrid wireless network, the ergodic throughput capacity of hybrid wireless networks with DBS scales with gain with $N \times N_{BS}$.

- Chapter 8 provides the conclusion. It summarizes the main achievements of this dissertation and outlines future research directions.

Chapter 2

Coexistence of UWB and IEEE 802.11n: Capacity Optimization for IR-UWB

Due to the unique properties, such as low complexity and low cost, good resistance to severe multipath and jamming, and high time domain resolution for localization and tracking, Impulse Radio (IR) UWB is well suited to sensor network applications. This chapter investigates the coexistence issue between IR UWB system and narrowband (NB) OFDM-based wireless communications system, particularly the capacity optimization of Impulse Radio (IR) UWB user within the coexisting operating bandwidth with IEEE 802.11n user, while making sure that its cumulative interference to the coexisting IEEE 802.11n user is below a certain permissible threshold. The optimal power allocation scheme is presented by using water-filling algorithm with Karush-Kuhn-Tucher (KKT) conditions, which is also compared with a traditional equal power allocation scheme.

2.1 UWB Radio

Two types of UWB technologies are commonly used: impulse radio UWB (IR-UWB) and multiband OFDM UWB (MB-OFDM UWB). In this chapter, we adopt IR-UWB as the objective. IR-UWB uses a short pulse in the time domain that occupies a large bandwidth in the frequency domain to modulate the information[54]. The most commonly used pulse is Gaussian pulse and its derivatives, i.e., first and second derivatives of Gaussian pulse. The normalized Gaussian pulse is represented as:

$$p(t) = \frac{1}{\sqrt{2\pi}\sigma} \exp\left(-\frac{(t-\mu)^2}{(2\sigma)^2}\right) \tag{2.1}$$

where μ is the mean value the Gaussian random variable, and σ is its standard deviation. let $\sigma^2 = \alpha^2/(4\pi)$, where α is an index correlated to the width of pulse, indicating the shape of pulse, namely the shaping factor. Fig. 2.1 Shows the normalized Gaussian Impulse with $\mu = 0$, and $\sigma = 0.1$.

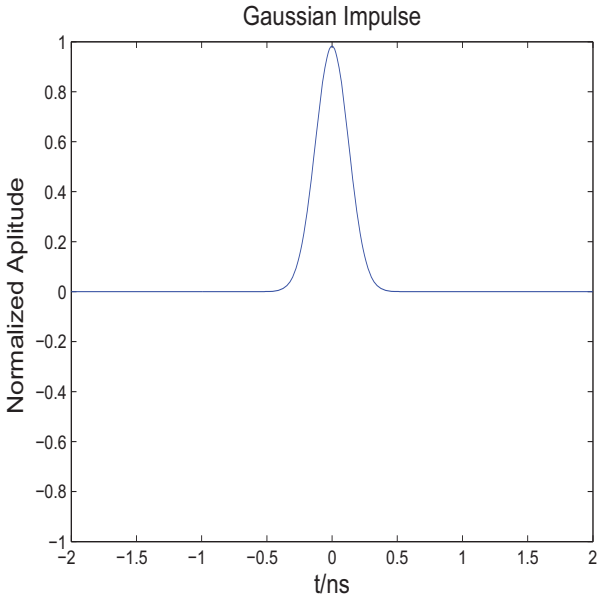

Figure 2.1. Normalized Gaussian Impulse.

2.2 IEEE 802.11n

Orthogonal Frequency Division Multiplexing (OFDM) technique is adopted in IEEE 802.11n system, which is essentially a multi-carrier modulation (MCM) method. The basic idea is to carry data in a large number of closely-spaced orthogonal subcarriers at a relatively low symbol rate. OFDM is used to cope with severe channel conditions (for example, frequency selective fading due to multipath), effectively eliminate inter-symbol interference (ISI), and also reduce the overall amount of required spectrum due to the overlapping of the tones[55]. For the traditional FDM multicar-

rier modulation technique, as shown in Fig. 2.2(a), each subcarrier in the frequency domain does not overlap each other. At the same time, in order to reduce mutual interference between the various subcarriers, subcarriers need to retain sufficient frequency spacing which results in low spectrum efficiency; But for OFDM technique, due to the orthogonal overlapping between subcarries, the protection bandwidth is greatly reduced and the spectrum efficiency is also highly improved as shown in Fig. 2.2(b).

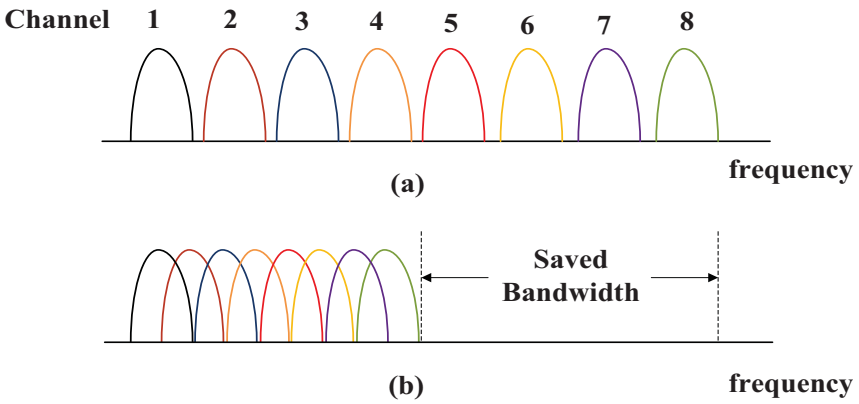

Figure 2.2. Traditional FDM and OFDM Techniques.

A typical OFDM system model is shown in Fig. 2.3. In the transmitter, the input serial data stream is shifted into a parallel format. The parallel data in each carrier is then separately modulated by the traditional modulation methods, such as QPSK and QAM. After the required spectrum is worked out, an inverse fast fourier transform (IFFT) is performed, and the guard period, also called the cyclic

prefix (CP) is added to the start of each symbol. The receiver basically does the reverse operation to the transmitter. CP is removed and fast fourier transform (FFT) of each OFDM symbol is then taken to obtain the original transmitted spectrum. Demodulation is performed in each carrier, which is followed by a parallel to serial conversion [56].

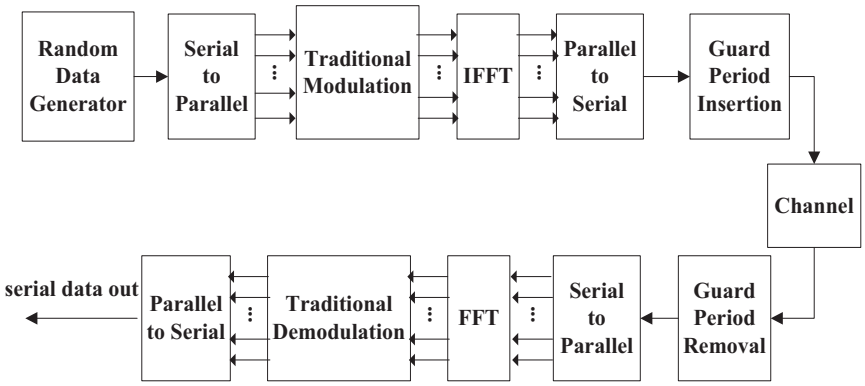

Figure 2.3. A Typical OFDM System Model.

The new Wireless Local Area Network (WLAN) standard, IEEE 802.11n, was finalized as standard in 2009. This standard aims at improving network throughput over previous standard, such as 802.11b and 802.11g with to the combination of OFDM and Multiple Input and Multiple Output (MIMO) techniques. Moreover, either 2.4GHz or 5GHz frequency band could be used for IEEE 802.11n. In the 5GHz band, a high throughput (HT) OFDM system with 40MHz bandwidth is specified[57].

The products with IEEE 802.11n technology, such as wireless LAN card, and wireless routers, have been widely applied in personal computers, notebook computers and other digital terminals prior to the finalization of the official standard.

Since OFDM technique is used in IEEE 802.11n signals, based on an ideal Nyquist pulse, the PSD of the l^{th} subcarrier in the IEEE 802.11n user is represented as

$$\Phi_l(f) = Q_l T_s (\frac{\sin \pi(f - f_l)T_s}{\pi(f - f_l)T_s})^2 \tag{2.2}$$

where Q_l is the transmit power in the l^{th} subcarrier, and T_s is the symbol duration.

2.3 Coexistence System Model

2.3.1 Distribution Model in Spatial Domain

Before we study the capacity optimization issue of UWB system under the coexistence with IEEE 802.11n system, the coexistence model of these two systems in the spatial domain is set up. In the downlink transmission scenario, as shown in Fig. 2.4, the receiver of IEEE 802.11n user could get the desired signal from its transmitter, and also get the interference signal from the coexisting UWB transmitter. For the same reason, not only the useful information from UWB transmitter, but also the jammer from IEEE 802.11n transmitter is obtained at the receiving part of UWB user. In this scenario, h_{ii} is denoted as the channel gain from IEEE 802.11n transmitter to its receiver, h_{iu} is the channel gain from IEEE 802.11n transmitter to UWB receiver, h_{ui} represents the channel gain from UWB transmitter to IEEE 802.11n receiver, and h_{uu} is the channel gain from UWB transmitter to its receiver. We assume these channel gains are perfectly known at the transmitters.

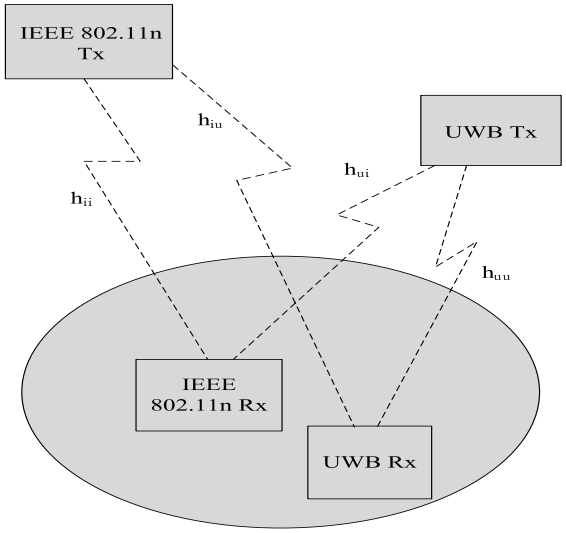

Figure 2.4. Distribution of IEEE 802.11n and UWB users in the spatial domain.

2.3.2 Distribution Model in Frequency Domain

In the frequency domain, the available bandwidth of IEEE 802.11n user can be divided into N subcarriers. It is assumed that the bandwidth of each subcarrier is Δf Hz. For band 1, band 2,...,band N, the bandwidths are correspondingly B_1, B_2,...,B_N. As shown in Fig. 2.5, UWB user and IEEE 802.11n user share the same spectrum in certain frequency part. In this case, we can study the capacity issue of UWB user within each subcarrier domain of IEEE 802.11n user, and then sum them up to get the optimized capacity.

The frequency spectrum of Time Domain Inc PulsON 220 UWB transceiver via Agilent Spectrum Analyzer as shown in Fig. 2.6. It is obvious to see that the frequency spectrum of UWB transceiver spans in a large range with center frequency 4.28GHz. And the power is relatively low.

The frequency spectrum in the Max Hold mode of OFDM-based NB signal is obtained from the WiFi-equipped cell phone. As shown in Fig. 2.7, the center frequency is 2.4GHz with 20MHz operating bandwidth.

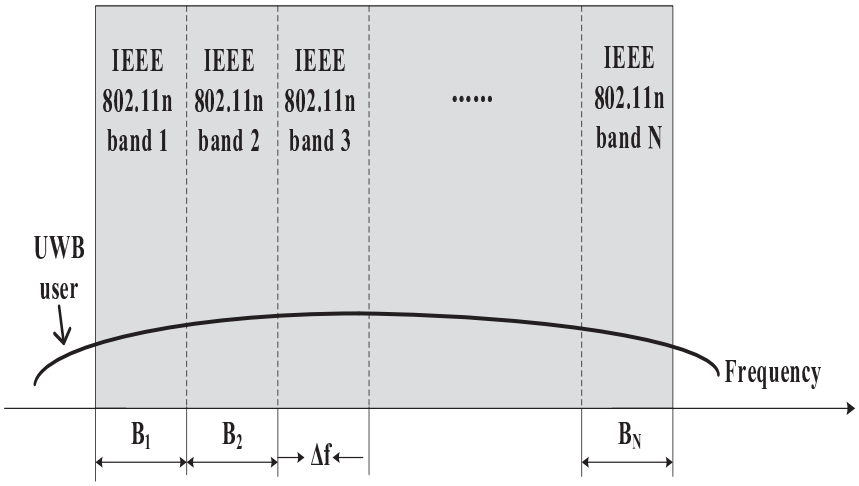

Figure 2.5. Distribution of IEEE 802.11n and UWB users in the frequency domain.

2.4 Interference Model

Our objective is to optimize the capacity of UWB user within the coexisting operating bandwidth with IEEE 802.11n user, under the constraint that its interference to IEEE 802.11n user is under an acceptable threshold. Meanwhile, studying the capacity of UWB user, the interference at the receiver part of UWB user should be considered. For simplicity, we study the scenario that UWB system coexists with only one NB wireless communication system, which is the IEEE 802.11n system. In this way, the received interference of UWB user includes the additive white Gaussian noise (AWGN) and interference from the coexisting IEEE 802.11n user.

We suppose $\mu = 0$ in 4.1, so the Power Spectrum Density (PSD) of the UWB user within the n^{th} subcarrier of IEEE 802.11n is[58]:

$$\Psi_n(f) = P_n \exp\left(-(2\pi f\sigma)^2\right) \tag{2.3}$$

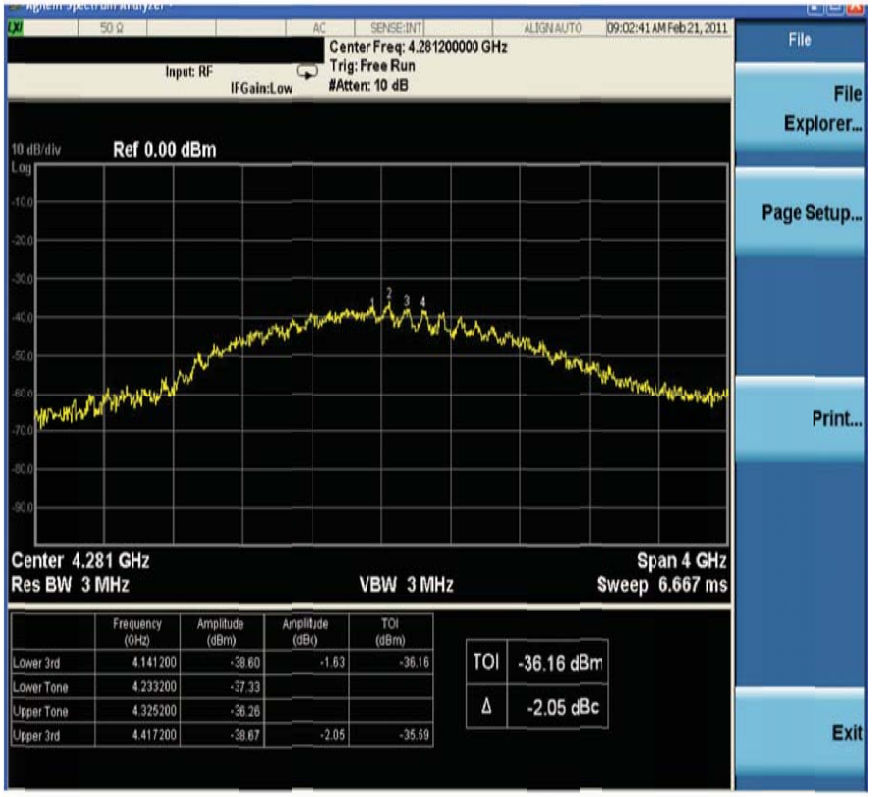

Figure 2.6. Frequency spectrum of UWB transceiver.

where P_n is the transmission power of UWB user within the subcarrier B_n of IEEE 802.11n. In this way, the interference of UWB user within the n^{th} subcarrier to the l^{th} subcarrier of IEEE 802.11n user can be represented as:

$$I_l^{(n)} = |h_{ui}|^2 \int_{d_{nl}-\Delta f/2}^{d_{nl}+\Delta f/2} \Psi_n(f) df \tag{2.4}$$

where d_{nl} is the frequency separation between the n^{th} subcarrier of and the l^{th} subcarrier of IEEE 802.11n user, and h_{ui} is the downlink channel gain from UWB transmitter to IEEE 802.11n receiver as mentioned in Section 2.3.

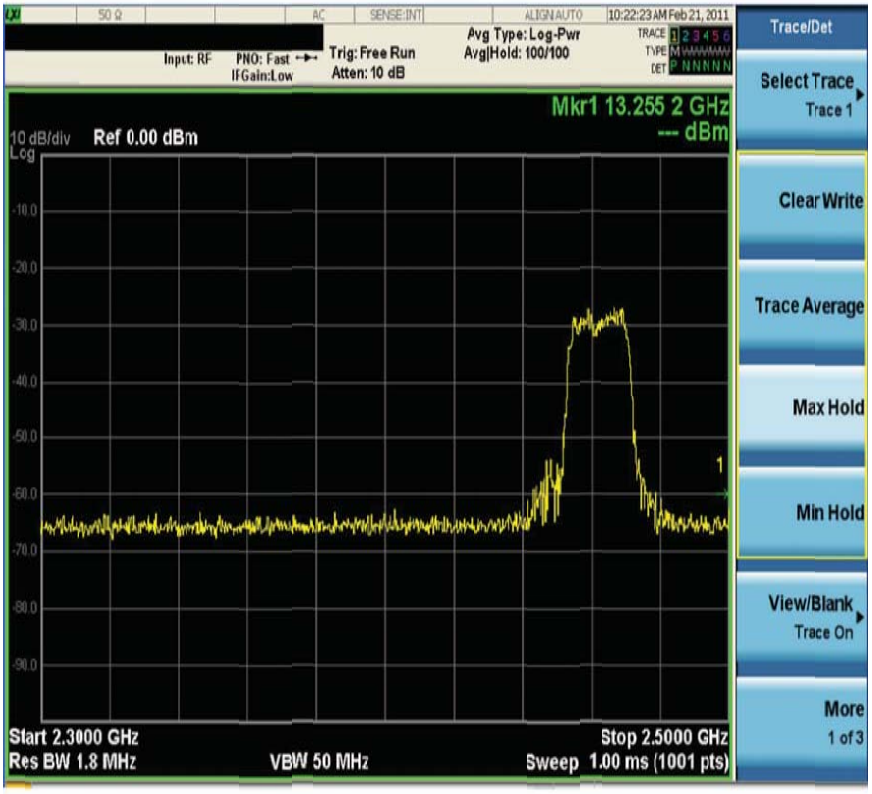

Figure 2.7. Frequency spectrum of OFDM-based WiFi user.

The interference to UWB user within the n^{th} subcarrier introduced by the l^{th} subcarrier of IEEE 802.11n can be written as

$$J_n^{(l)} = |h_{iu}|^2 \int_{d_{nl}-\Delta f/2}^{d_{nl}+\Delta f/2} \Phi_l(f) df \tag{2.5}$$

where h_{iu} is the downlink channel gain from IEEE 802.11n transmitter to UWB receiver as mentioned in Section 2.3, and $\Phi_l(f)$ is the PSD of IEEE 802.11n signals within the l^{th} subcarrier as represented in 4.4.

Table 2.1 lists the numerical values of IEEE 802.11n interference within the n^{th} subcarrier bandwidth of UWB user, namely $\sum_{l=1}^{N} J_n^{(l)}$, when the range of transmit power of IEEE 802.11n user varies.

Table 2.1. Interference of IEEE 802.11n user $\sum_{l=1}^{N} J_n^{(l)}$

Operating frequency of IEEE 802.11n	**Bandwidth of IEEE 802.11n**	**Range of Transmit Power (dBm)**	**Maximum $\sum_{l=1}^{N} J_n^{(l)}$ (dB)**	**Minimum $\sum_{l=1}^{N} J_n^{(l)}$ (dB)**
2.417-2.437GHz	20MHz	18-21	-78.5308	-78.6660
2.417-2.437GHz	20MHz	15-18	-81.5167	-81.6516
5.170-5.190GHz	20MHz	18-21	-84.9494	-85.1046
5.170-5.190GHz	20MHz	15-18	-87.9597	-88.1149
5.160-5.200GHz	40MHz	18-21	-82.0331	-82.1809
5.160-5.200GHz	40MHz	15-18	-85.1469	-85.2966

2.5 Interference Evaluation based on I/N criteria

The interference to noise ratio (I/N), which is defined as the power ratio of received interference and receiver noise floor, is a widely used interference evaluation method. This method is originally adopted by FCC to regulate the UWB emission limits [10], and provides a simplified model for the calculation of the maximum permissible interference level at the receiver input IEEE 802.11n user I_{MAX}. The normalized I_{MAX} in dBm[59], can be represented as

$$I_{th} = I/N + N \tag{2.6}$$

where I/N is the maximum permissible average or peak interference-to-noise ratio at the receiver IF output necessary to maintain the acceptable performance criteria, dB; N is the receiver's inherent noise level at the receiver IF output referred to the receiver input, dBm.

$$N = 10\log K + 10\log T + 10\log B + NF \tag{2.7}$$

where K is Boltzmann's constant, normally 1.38×10^{-20}, in milliwatts/K/Hz, T is the system noise temperature, in degrees Kelvin, B is the receiver IF bandwidth, in Hz, and NF is the noise coefficient, in dB.

According to (3.21) and (2.7), Table 2.2 lists the calculated maximum acceptable interference at the receiver part of IEEE 802.11n user in three different operating modes.

Table 2.2. Maximum permissible interference at the receiver part of IEEE 802.11n user

Operating frequency of IEEE 802.11n	**Bandwidth of IEEE 802.11n**	I_{th}
2.417-2.437GHz	20MHz	-105.62dBm
5.170-5.190GHz	20MHz	-105.62dBm
5.160-5.200GHz	40MHz	-102.61dBm

It is obvious that the maximum acceptable interference at the receiver part of IEEE 802.11n is mainly determined by the bandwidth of the receiver, no matter on which center frequency it operates. Moreover, for the interfered system with larger operating bandwidth, higher interference are tolerable than that with smaller operating bandwidth.

2.6 Optimal Power Allocation Scheme

We firstly study the capacity of UWB user within each operating bandwidth shared with IEEE 802.11n subcarrier. The transmission power of UWB user within the subcarrier B_n is represented as P_n, h_{uu} is the channel gain of the n^{th} subcarrier from UWB transmitter to its receiver, $J_n^{(l)}$ denotes the interference introduced by the l^{th} subcarrier of IEEE 802.11n user to the UWB receiver within the n^{th} subcarrier.

According to the Shannon capacity formula, the transmission rate of UWB user within the n^{th} subcarrier can be represented as[60]:

$$R_n = \Delta f \log_2 (1 + \frac{|h_{uu}|^2 P_n}{\sigma^2_{awgn} + \sum_{l=1}^{N} J_n^{(l)}}) \tag{2.8}$$

where σ^2_{awgn} is the power of additive white Gaussian noise.

As we know the capacity of UWB user within each subcarrier, the cumulative capacity of UWB user within the whole coexisting operating bandwidth with IEEE 802.11n user is essentially the summation of these subcarrier-capacities. Our objective is to maximize the capacity of UWB user while keeping its interference to IEEE 802.11n user below a certain threshold.

$$C = \max_{P_n} \sum_{n=1}^{N} \Delta f \log_2 (1 + \frac{|h_{uu}|^2 P_n}{\sigma^2_{awgn} + \sum_{l=1}^{N} J_n^{(l)}}) \tag{2.9}$$

subject to

$$\sum_{l=1}^{N} \sum_{n=1}^{N} I_l^{(n)} \leq I_{th} \tag{2.10}$$

and

$$P_i \geq 0, \forall n = 1, 2, \ldots, N \tag{2.11}$$

Since $\log(\cdot)$ is a concave function, and the sum of the concave functions is still a concave functions, to maximize a concave function is equivalent to minimizing the negative of the concave function, namely a convex function. Obviously it is a problem of convex optimization. In this case, by introducing a Lagrange multiplier ν to the in-

equality constraint in (2.10) and Lagrange multipliers λ_n to the inequality constraints in (4.8), we can get the following Karush-Kuhn-Tucher (KKT) condition[61]:

$$\begin{aligned}
\sum_{l=1}^{N}\sum_{n=1}^{N} I_l^{(n)} &\leq I_{th} \\
P_n^* &\geq 0, \forall n = 1, 2, \ldots, N \\
\lambda_n &\geq 0, \forall n = 1, 2, \ldots, N \\
\lambda_n P_n^* &= 0, \forall n = 1, 2, \ldots, N \\
-\frac{1}{\frac{\sigma_{awgn}^2+\sum_{l=1}^{N} J_n^{(l)}}{|h_{uu}|^2} + P_n^*} & \\
-\lambda_n + \nu \sum_{l=1}^{N} \frac{\partial I_l^{(n)}}{\partial P_n^*} &= 0, \forall n = 1, 2, \ldots, N
\end{aligned} \tag{2.12}$$

From the last condition in (4.9), we know that

$$\lambda_n = \nu \sum_{l=1}^{N} \frac{\partial I_l^{(n)}}{\partial P_n^*} - \frac{1}{\frac{\sigma_{awgn}^2+\sum_{l=1}^{N} J_n^{(l)}}{|h_{uu}|^2} + P_n^*} \tag{2.13}$$

So we can eliminate the slack variable λ_n firstly and get:

$$\begin{aligned}
\sum_{l=1}^{N}\sum_{n=1}^{N} I_l^{(n)} &\leq I_{th} \\
P_n^* &\geq 0, \forall n = 1, 2, \ldots, N \\
\nu P_n^* \sum_{l=1}^{N} \frac{\partial I_l^{(n)}}{P_n^*} - \frac{P_n^*}{\frac{\sigma_{awgn}^2+\sum_{l=1}^{N} J_n^{(l)}}{|h_{uu}|^2} + P_n^*} &= 0, \forall n = 1, 2, \ldots, N \\
\frac{1}{(\frac{\sigma_{awgn}^2+\sum_{l=1}^{N} J_n^{(l)}}{|h_{uu}|^2} + P_n^*)\frac{\partial I_l^{(n)}}{P_n^*}} &\leq \upsilon, \forall n = 1, 2, \ldots, N
\end{aligned} \tag{2.14}$$

We can denote $\frac{\partial J_n^{(l)}}{\partial P_n^*}$ as $K_l^{(n)}$ for simplicity, which is

$$K_l^{(n)} = |h_{ui}|^2 \int_{d_{nl}-\Delta f/2}^{d_{nl}+\Delta f/2} \exp\left(-(2\pi f\sigma)^2\right) df \tag{2.15}$$

From the last condition in (4.11), we can see that if

$$\nu < \frac{1}{(\frac{\sigma_{awgn}^2+\sum_{l=1}^{N} J_n^{(l)}}{|h_{uu}|^2}) \sum_{l=1}^{N} K_l^{(n)}} \tag{2.16}$$

then, $P_n^* > 0$. From the third condition, we can get P_n^* as

$$P_n^* = \frac{1}{\nu \sum_{l=1}^{N} K_l^{(n)}} - \frac{\sigma_{awgn}^2 + \sum_{l=1}^{N} J_n^{(l)}}{|h_{uu}|^2} \tag{2.17}$$

Otherwise, $P_n^* = 0$ if

$$\nu \geq \frac{1}{(\frac{\sigma_{awgn}^2 + \sum_{l=1}^{N} J_n^{(l)}}{|h_{uu}|^2}) \sum_{l=1}^{N} K_l^{(n)}} \tag{2.18}$$

To summarize, the allocated power of UWB user can be written as

$$P_n^* = \max\{0, \frac{1}{(\frac{\sigma_{awgn}^2 + \sum_{l=1}^{N} J_n^{(l)}}{|h_{uu}|^2}) \sum_{l=1}^{N} K_l^{(n)}}\} \tag{2.19}$$

Substituting (4.16) into (2.10), we can get

$$\sum_{l=1}^{N} \sum_{n=1}^{N} K_l^{(n)} \max\{0, \frac{1}{(\frac{\sigma_{awgn}^2 + \sum_{l=1}^{N} J_n^{(l)}}{|h_{uu}|^2}) \sum_{l=1}^{N} K_l^{(n)}}\} \leq I_{th} \tag{2.20}$$

From (4.17), we can see that when the left side is equal to the right side, the left side can reach its maximum value, namely, the allocated power is maximized. In order to maximize the capacity of UWB user, (4.17) can be written as

$$\sum_{l=1}^{N} \sum_{n=1}^{N} K_l^{(n)} \max\{0, \frac{1}{(\frac{\sigma_{awgn}^2 + \sum_{l=1}^{N} J_n^{(l)}}{|h_{uu}|^2}) \sum_{l=1}^{N} K_l^{(n)}}\} = I_{th} \tag{2.21}$$

We compare the proposed optimized capacity of UWB user with the capacity by using equal power allocation scheme[53] in three scenarios mentioned above. For the equal power allocation scheme, the allocated power for UWB user within each subcarrier shared with subcarriers of IEEE 802.11n user P_{eq} can be represented as:

$$P_{eq} = \frac{I_{th}}{\sum_{l=1}^{N} \sum_{n=1}^{N} K_l^{(n)}} \tag{2.22}$$

And the capacity of UWB user with equal power allocation $C_{eq}$is:

$$C_{eq} = \sum_{n=1}^{N} \Delta f \log_2 (1 + \frac{|h_{uu}|^2 P_{eq}}{\sigma_{awgn}^2 + \sum_{l=1}^{N} J_n^{(l)}}) \tag{2.23}$$

2.7 Conclusion

The maximum transmit power of IEEE 802.11n user is 200mW, namely 23dBm both in 20MHz and 40MHz [57]. We can assume the transmit power of IEEE 802.11n user Q is within the range of 64∼128mW (18∼21dBm) for indoor application. There are 64 OFDM subcarriers in the mode of 20MHz and 128 subcarriers with 40MHz bandwidth. Dividing the number of subcarriers by the total bandwidth, we can get the subcarrier frequency spacing 312.5 KHz. The symbol duration of IEEE 802.11n signal is $4\mu s$. According to the ITU-R requirements, the interference power due to unwanted emissions from sources sharing the same band on primary bases can be partitioned as the intraservice interference, the coprimary services interference, and other interfering aggregation. UWB systems are commonly classified as secondary services. For calculating the maximum permissible interference at the receiver of IEEE 802.11n user, system noise temperature is 293 K, noise coefficient of IEEE 802.11n receiver is 5.3dB, and the interference to noise ratio is -10dBm[13].

In this chapter, we select the operating frequency range of IEEE 802.11n user as 2417∼2437MHz with 20MHz bandwidth, 5170∼5190MHz with 20MHz bandwidth, and 5160∼5200MHz with 40MHz bandwidth. σ^2_{awgn} is assumed to be 1×10^{-3}. The shaping factor of Gaussian pulse is chosen as 0.2×10^{-9}. The channel gains between IEEE 802.11n user and UWB user h_{ii}, h_{iu}, h_{ui}, and h_{uu} are assumed to be Rayleigh flat fading with an average power gain of 10dB. The detailed parameter settings are shown in Table 6.2.3.

Fig. 2.8 is the interference introduced by the l^{th} subcarrier of IEEE 802.11n to UWB user within the n^{th} subcarrier spectrum domain, where the operating frequency of IEEE 80.211n is 2.417-2.437GHz and the operating bandwidth is 20MHz. We can see that the interference to UWB changes periodically due to the OFDM characteristic

Table 2.3. Parameter settings

Parameter	**Symbol**	**Value**
Transmit power of IEEE 802.11n user	Q	$64 \sim 128$mW ($18 \sim 21$dBm)
Number of subcarriers	N	64/128
Subcarrier frequency spacing	Δf	312.5KHz
Symbol duration of IEEE 802.11n signal	T_s	4×10^{-6}s
Power of AWGN	σ^2_{awgn}	4×1^{-3}s
Shaping factor of Gaussian pulse	α	0.2×1^{-9}s
Channel gains	h	10dB
Boltzmann's constant	K	1.38×10^{-20} mW/K/Hz
System noise temperature	T	293 K
Noise coefficient	NF	5.3dB
Interference to noise ratio	I/N	-10dB

for different distance between the l^{th} subcarrier of IEEE 802.11n and the n^{th} subcarrier of UWB user in the spectrum domain.

From the numerical results are shown in Table 2.4 we can see that: 1) the capacities of UWB user within the coexisting frequencies shared with IEEE 802.11n user, using the proposed optimal power allocation scheme, are significantly larger than those with equal power allocation scheme. 2) For the IEEE 802.11n user working on a certain frequency, i.e. the 5GHz band, UWB user could achieve larger capacity when coexisting with higher-bandwidth IEEE 802.11n user. This could be explained according to (3.21), (2.7) and Table 2.2. Since the interfered system with larger operating bandwidth can tolerate higher interference, the transmitting power of the interfering system, namely the UWB user, will be larger, which means higher capacity is achievable. 3) Compared with higher operating frequency of IEEE 802.11n user, the capacity of UWB user under the coexisting IEEE 802.11n user with lower operating frequency is larger. 4)When the range of transmit power of IEEE 802.11n varies,

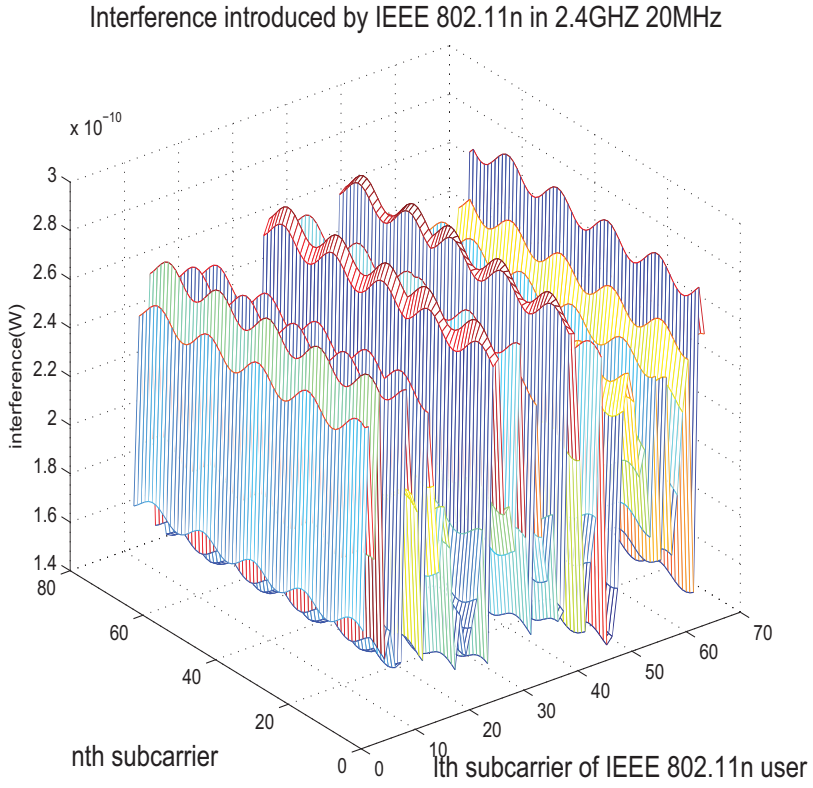

Figure 2.8. Interference Introduced by the l^{th} Subcarrier of IEEE 802.11n to UWB User (in 2.4GHZ with 20MHz bandwidth).

the capacity of UWB user changes. When the range decreases, the corresponding interference introduced by IEEE 802.11n user to UWB user gets smaller, that means UWB user could reach higher capacities.

Table 2.4. Optimal capacity and capacity with equal power allocation scheme

Operating frequency of IEEE 802.11n	Bandwidth of IEEE 802.11n	Range of Transmit power of IEEE 802.11n (dBm)	Optimal Capacity (bps)	Capacity with equal power allocation scheme (bps)
2.417-2.437GHz	20MHz	18-21	1.22837×10^9	1.8420×10^8
2.417-2.437GHz	20MHz	15-18	1.22845×10^9	1.8427×10^8
5.170-5.190GHz	20MHz	18-21	1.13294×10^9	1.3815×10^8
5.170-5.190GHz	20MHz	15-18	1.13300×10^9	1.3819×10^8
5.160-5.200GHz	40MHz	18-21	1.86853×10^9	2.7631×10^8
5.160-5.200GHz	40MHz	15-18	1.86873×10^9	2.7648×10^8

Chapter 3

Power Consumption and Downlink Outage Probability in a Dynamic HAN

3.1 Power Consumption of a Dynamic HAN

In this section, a Markov chain model is employed to represent the profile of a dynamic HAN for Smart Grid with the total number of WiFi Direct devices as M, in which the number of connections to the HAN varies from 0 to M as shown in Figure 3.1.

Before the presentation of the profile for this type of HAN, we propose the definition of a dynamic HAN in the first place: Definition 1: *A dynamic HAN* is a HAN in which WiFi Direct technique is employed for the communication between the devices that alternate between active states and doze states for power saving, so that the number of active users dynamically changes with the following assumptions:

1) the overall number of devices in the HAN is known ahead;
2) as to the WiFi Direct devices, the events of connecting to the HAN and disconnecting to the HAN are independent with each other;
3) the possibility of the simultaneous occurrence of two or more events is excluded.

In Figure 3.1, the states of Markov Chain denote different numbers of connections to the dynamic HAN. For example, N_m means that there are currently m WiFi Direct devices in the active state. Particularly, N_0 indicates that none of the devices is connected to the HAN, and N_M shows that all of the M devices are actively connected. When a new device joins in, the process goes from state N_m to state N_{m+1}. Similarly, when a working device disconnects from the HAN, the process goes from state N_m to state N_{m-1}. Basically, only one event can occur in a very small interval

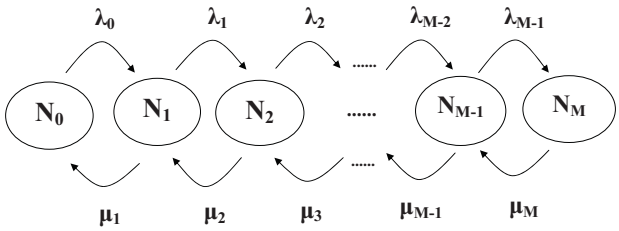

Figure 3.1. Markov Chain Model for the Number of Connections to a Dynamic HAN .

of time. And even though the probability of more than one event is non-zero, it is negligible[62].

In this Markov chain model, it is postulated that the number of devices that are connected to the dynamic HAN follows poisson distribution with rate λ and the holding time of the connection follows exponential distribution with average of T_H and rate of service $\mu = \frac{1}{T_H}$[63]. Therefore, we obtain the transition rates of λ_m and μ_m as the following expressions,

$$\lambda = \lambda_0 = \lambda_1 = \ldots = \lambda_m = \ldots = \lambda_{M-1} \tag{3.1}$$

$$\mu_m = m\mu, \quad m = 1, 2, \ldots, M \tag{3.2}$$

Given λ_m and μ_m, the global equilibrium equations for this Markov chain is written as[64],

$$\begin{cases} \lambda\pi_0 = \mu\pi_1 \\ \lambda\pi_0 + 2\mu\pi_2 = (\lambda+\mu)\pi_1 \\ \lambda\pi_1 + 3\mu\pi_3 = (\lambda+2\mu)\pi_2 \\ \vdots \\ \lambda\pi_m + (m+2)\mu\pi_{m+2} = (\lambda+(m+1)\mu)\pi_{m+1} \\ \vdots \\ \lambda\pi_{M-2} + M\mu\pi_{M-1} = (\lambda+(M-1)\mu)\pi_{M-1} \\ \lambda\pi_{M-1} = M\mu\pi_M \end{cases} \tag{3.3}$$

where π_m is the steady-state probability of the m_{th} state of the Markov Chain, which determines the probability of m devices connected to the HAN. After Simplifying (3.3), the general form of the state probability can be expressed as,

$$\pi_m = \frac{\rho}{m}\pi_{m-1}, m = 1, 2, \ldots, M \tag{3.4}$$

where $\rho = \lambda/\mu$ is defined as the *traffic intensity* of the HAN [65].

Since,

$$\sum_{m=0}^{M-1} \pi_m = 1 \tag{3.5}$$

by substituting (3.4) into (3.5), the probability of the initial state π_0 can be obtained as,

$$\pi_0 = \frac{1}{\sum_{m=0}^{M} \frac{1}{m!}\rho^m} \tag{3.6}$$

Thus, the steady-state probability of the states in the Markov Chain is written as,

$$\pi_m = \frac{\frac{1}{m!}\rho^m}{\sum_{i=0}^{M} \frac{1}{i!}\rho^i}, m = 0, 1, \ldots, M \tag{3.7}$$

Remark 1: It is noteworthy that the denominator in (3.7) is the Taylor Series expansions of the exponential function e^{ρ} for large M. In this way, (3.7) can be further simplified as,

$$\pi_m = \frac{\frac{1}{m!}\rho^m}{e^{\rho}}, m = 0, 1, \ldots, M \tag{3.8}$$

The WiFi Direct PSM aims at conserving energy on doze devices by turning off their radio transceivers, and thus consumes less energy than that in active state. For each PSM-equipped WiFi Direct device, it alternates between active state and doze state. We denote the power consumption of each device in these two states and the switching power consumption as $\mathcal{P}_a$, $\mathcal{P}_d$, and $\mathcal{P}_{sw}$. respectively.

In order to calculate the power consumption of the dynamic HAN, a new term is defined as follows:

Defination 2: In a dynamic HAN with totally M devices, *the power consumption with m active devices* $\mathcal{P}_M(m)$ is equal to:

$$\mathcal{P}_M(m) = m\mathcal{P}_a + (M - m)\mathcal{P}_d + \mathcal{P}_{sw} \tag{3.9}$$

Based on the Markov chain model presented above, the power consumption $\mathcal{P}_M$ in the dynamic HAN with totally M devices is essentially the expectation of $\mathcal{P}_M(m)$ expressed as:

$$\begin{aligned} \mathcal{P}_M &= \mathbb{E}[\mathcal{P}_M(m)] \\ &= \sum_{m=0}^{M} \pi_m \mathcal{P}_M(m) \\ &= \sum_{m=0}^{M} \pi_m [m\mathcal{P}_a + (M - m)\mathcal{P}_d + \mathcal{P}_{sw}] \end{aligned} \tag{3.10}$$

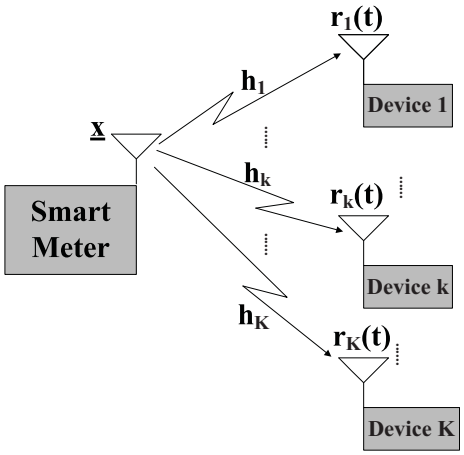

Figure 3.2. Downlink with K active users connected with a Smart Meter.

3.2 Downlink Outage Performance

3.2.1 Downlink Model

In the dynamic HAN for Smart Grid, the most frequently connected device is the smart meter, which is in charge of gathering power usage data and status from the utilities within the home, and also distributing power information like prices and control signals to the household appliances. In this section, we investigate the downlink outage performance in the HAN with K active users connected to the smart meter, as shown in Figure 3.2. Assume that the independent signal matrix $\underline{\mathbf{X}} = [x_1, x_2, \ldots, x_k, \ldots, x_K]$ are transmitted, with transmitted power matrix $\underline{\mathcal{P}} = [\mathcal{P}_1, \mathcal{P}_2, \ldots, \mathcal{P}_k, \ldots, \mathcal{P}_K]$, where x_k is the signal transmitted from the smart meter to the k_{th} user, and $\mathcal{P}_k$ is correspondingly the power of x_k. The channel matrix is $\underline{\mathbf{H}} = [h_1, h_2, \ldots, h_k, \ldots, h_K]$, where h_k denotes the channel gain between the smart

meter and the k_{th} user, and is independent S-V indoor channel. After normalization, $E\{h_k^2\} = 1, \forall k$.

By applying interference cancelation technique, the interference cancelation coefficient is added to each user, which is multiplied to the interference introduced by other users. The interference cancelation coefficient matrix is $\underline{\alpha} = [\underline{\alpha_1}, \underline{\alpha_2}, \ldots, \underline{\alpha_K}]$, where $\underline{\alpha_k} = [\alpha_{k1}, \alpha_{k2}, \ldots, \alpha_{kK}]^T$, and α_{ki} is the interference cancelation coefficient for the interference introduced by the i_{th} transmitted signal to the k_{th} user, which is a random variable ranges from 0 to 1, for $i = 1, 2, \ldots, K$.

Remark 2: As to the interference cancelation coefficient, it has the following properties:

1) Specifically, $\alpha_{ki} = 0$ denotes that the interference is fully canceled, while $\alpha_{ki} = 1$ means that the interference is entirely present;
2) it is easy to see that $\alpha_{kk} = 1$;
3) without interference cancelation, $\underline{\alpha}$ is a unit matrix since all the interferences are fully present.

3.2.2 Statistics of SINR

In practical multiuser scenarios, each user would experience multiuser interference (MUI) from other users. Considering the effect of MUI, the SINR that evaluates the ratio between the desired signal power and the amount of noise and interference generated by all the other users, should be used in the performance evaluation [72]. Thus the SINR γ_k at the k_{th} user is written as:

$$\gamma_k = \frac{|h_k|^2 \mathcal{P}_k}{\sum_{j \neq k} \alpha_{kj} |h_k|^2 \mathcal{P}_j + \sigma^2} \tag{3.11}$$

where σ^2 is the power of Addictive White Gaussian Noise (AWGN).

Theorem 1: For the HAN downlink scenario with indoor S-V channels, in which K active household users are connected to the smart meter, assume that the smart meter transmits signals to all the active users with equal power, that is, $\mathcal{P}_1 = \mathcal{P}_2 = \ldots = \mathcal{P}_k = \ldots = \mathcal{P}_K$, the probability density function (PDF) of the SINR γ_k at the k_{th} user is:

$$f_K(\gamma_k) = \frac{1}{\gamma_k^2[(1+\frac{1}{\gamma_k}) - \sum_{k=1}^{K}\alpha_k]^2\eta} e^{(-\frac{1}{[(1+\frac{1}{\gamma_k})-\sum_{k=1}^{K}\alpha_k]\eta})} \tag{3.12}$$

where $\eta = \mathcal{P}_k/\sigma^2$.

Proof: According to (3.11), γ_k is mathematically reformatted as:

$$\begin{aligned}\gamma_k &= \frac{|h_k|^2\mathcal{P}_k}{\sum_{j\neq k}\alpha_{kj}|h_k|^2\mathcal{P}_j + \sigma^2} \\ &= \frac{|h_k|^2\mathcal{P}_k}{\sum_{j=1}^{K}\alpha_{kj}|h_k|^2\mathcal{P}_j - \alpha_{kk}|h_k|^2\mathcal{P}_k + \sigma^2} \\ &= \frac{|h_k|^2\mathcal{P}_k}{|h_k|^2\underline{\alpha_{\mathbf{k}}\mathcal{P}} - |h_k|^2\mathcal{P}_k + \sigma^2}\end{aligned} \tag{3.13}$$

So that $|h_k|^2$ can be represented by γ_k according to (3.13) as:

$$|h_k|^2 = \frac{\sigma^2}{(1+\frac{1}{\gamma_k})\mathcal{P}_k - \underline{\alpha_{\mathbf{k}}\mathcal{P}}} \tag{3.14}$$

For the indoor S-V channel, since the amplitude of the channel gain follows Rayleigh distribution [69], $|h_k|^2$ follows exponential distribution as [67]:

$$f_{|h_k|^2}(|h_k|^2) = \frac{1}{\overline{|h_k|}^2}\exp(-\frac{|h_k|^2}{\overline{|h_k|}^2}) \tag{3.15}$$

where $\overline{|h_k|}^2$ is the mean of $|h_k|^2$.

Thus, the pdf of γ_k is obtained based on (3.15):

$$f_{\gamma_k}(\gamma_k) = \frac{\sigma^2\mathcal{P}_k}{\overline{|h_k|}^2\gamma_k^2[(1+\frac{1}{\gamma_k})\mathcal{P}_k - \underline{\alpha_{\mathbf{k}}\mathcal{P}}]^2} e^{(-\frac{\sigma^2}{\overline{|h_k|}^2[(1+\frac{1}{\gamma_k})\mathcal{P}_k - \underline{\alpha_{\mathbf{k}}\mathcal{P}}]})} \tag{3.16}$$

For tractable analysis, the pdf of γ_k with K active users in (3.16) is represented as $f_K(\gamma_k)$. After normalization of the channel, $\overline{|h_k|}^2 = 1$. We can simplify (3.16) as:

$$f_K(\gamma_k) = \frac{\sigma^2}{\gamma_k^2[(1+\frac{1}{\gamma_k}) - \sum_{k=1}^{K}\alpha_k]^2\mathcal{P}_k} e(-\frac{\sigma^2}{[(1+\frac{1}{\gamma_k}) - \sum_{k=1}^{K}\alpha_k]\mathcal{P}_k}) \tag{3.17}$$

Since $\mathcal{P}_k/\sigma^2 = \eta$, (3.17) can be further simplified as:

$$f_K(\gamma_k) = \frac{1}{\gamma_k^2[(1+\frac{1}{\gamma_k}) - \sum_{k=1}^{K}\alpha_k]^2\eta} e^{(-\frac{1}{[(1+\frac{1}{\gamma_k}) - \sum_{k=1}^{K}\alpha_k]\eta})} \tag{3.18}$$

3.2.3 Statistics of Outage Probability

Data transmission is considered successful if the transmission rate is below the the channel capacity. Otherwise, the link is said to be in *outage*. Thus the average downlink outage probability of the dynamic HAN with totally M users is expressed as [53][60]:

$$\begin{aligned} \mathbb{P}_{out} &= \sum_{m=1}^{M-1} \pi_m P_r[\log_2(1+\gamma_m) \leq R_{req}] \\ &= \sum_{m=1}^{M-1} \pi_m P_r[\gamma_m \leq 2^{R_{req}} - 1] \\ &= \sum_{m=1}^{M-1} \pi_m \int_0^{2^{R_{req}-1}} f_m(\gamma_k) d\gamma_k \end{aligned} \tag{3.19}$$

On the other hand, without WiFi Direct technique for the HAN, the outage probability is just written as:

$$\begin{aligned} \mathbb{P}_{out}^{M} &= P_r[\log_2(1+\gamma_k) \leq R_{req}] \\ &= \int_0^{2^{R_{req}-1}} f_{M-1}(\gamma_k) d\gamma_k \end{aligned} \tag{3.20}$$

Table 3.1. Parameter settings for Power Consumption

Symbol	**Value**
ρ	1$\sim$10
M	5, 10, and 15
$\mathcal{P}_a$	0.660watt
$\mathcal{P}_d$	0.296watt
$\mathcal{P}_{sw}$	0.001watt
σ^2	1×10^{-4}watt

3.3 Numerical Results

3.3.1 Power Consumption

The parameter settings for the calculation of power consumption are shown in Table 2.1, the traffic intensity ρ varies within the range from 1 to 10. The total number of WiFi Direct devices are 5, 10, and 15 respectively. The consumed energy for each device is set to be 0.660 watt in active state, 0.296 watt in doze state, and 0.001watt while switching between active state and doze state[68]. The power of AWGN is $1 \times 10^{-4} watt$. The average power of Rayleigh fading channel is normalized as 1.

The steady state probability π_m in (3.7) is listed in Table 2.2. We can see that the probability that large number of users connected to the HAN is extremely small, for example, $\pi_{11} = 6.41 \times 10^{-4}$ with $M = 15$. This phenomenon indicates the behavior similarity of two dynamic HANs with $M = 10$ and $M = 15$.

In order to investigate the power saving property of the dynamic HAN with the emerging WiFi Direct technique, a term *power saving ratio* κ is given:

Table 3.2. The steady state probability π_m

π_m	**M=5**	**M=10**	**M=15**
π_0	0.0233	0.0184	0.0183
π_1	0.0933	0.0735	0.0733
π_2	0.1866	0.1469	0.1465
π_3	0.2488	0.1949	0.1954
π_4	0.2488	0.1959	0.1954
π_5	0.1991	0.1567	0.1563
π_6	NA	0.1045	0.1042
π_7	NA	0.0597	0.0595
π_8	NA	0.0299	0.0298
π_9	NA	0.0133	0.0132
π_{10}	NA	0.0053	0.0053
π_{11}	NA	NA	0.0019
π_{12}	NA	NA	6.41×10^{-4}
π_{13}	NA	NA	1.97×10^{-4}
π_{14}	NA	NA	5.64×10^{-5}
π_{15}	NA	NA	1.50×10^{-5}

Definition 3: The *power saving ratio* of a dynamic HAN compared to a static HAN with overall M users is defines as:

$$\kappa = \frac{M\mathcal{P}_a - \mathcal{P}_M}{M\mathcal{P}_a} 100\% \tag{3.21}$$

The comparison of the power consumption of a dynamic HAN with PSM and a static HAN with CAM is shown in Figure 3.3. Figure 3.4 is the power saving ratio of the dynamic HAN with PSM for different total number of WiFi Direct devices. The power saving ratio for each traffic intensity is listed in Table 2.3.

Remark 3: From Figures 3.3 and 3.4, we could see that:

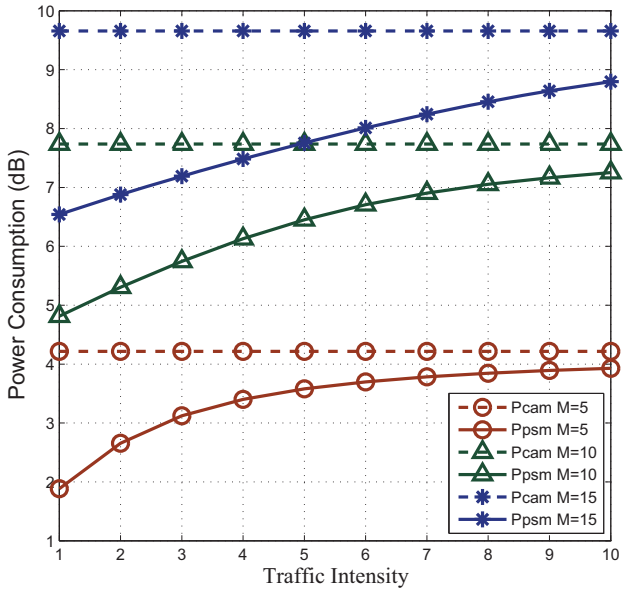

Figure 3.3. Power Consumption of the Dynamic HAN and Static HAN.

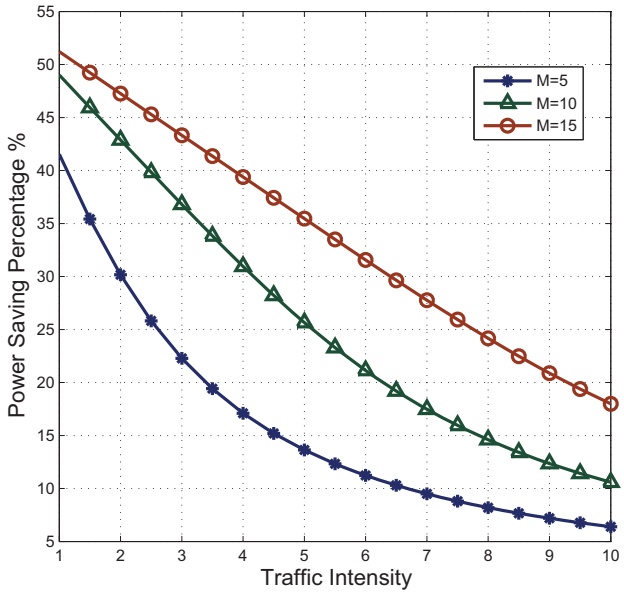

Figure 3.4. Power Saving Ratio of PSM Compared with CAM.

Table 3.3. Power Saving ratio for various traffic intensities

ρ	**M=5**	**M=10**	**M=15**
1	41.54%	49.01%	51.20%
2	30.16%	42.88%	47.26%
3	22.28%	36.80%	43.32%
4	17.10%	30.95%	39.38%
5	13.64%	25.64%	35.45%
6	11.23%	21.13%	31.56%
7	9.50%	17.48%	27.76%
8	8.20%	14.20%	24.17%
9	7.19%	12.35%	20.88%
10	6.40%	10.60%	17.99%

1) since the power consumption of a static HAN with CAM is not related to the traffic intensity, no matter how the traffic intensity changes, the static HAN maintains a constantly high power consumption;
2) even for a certain total number of WiFi Direct devices in the dynamic HAN, the power consumption with PSM increases along with the increment of the traffic intensity, and PSM saves less power consumption compared with CAM as the traffic intensity grows. This could be explained that intensive traffic intensity indicates frequent switching between active states and doze states, and thus the switching power consumption becomes considerate overhead. Moreover, switching cost has more obvious effect on the power saving ratio with larger total number of WiFi Direct devices in the HAN.

3.3.2 Downlink Outage Performance

By taking (3.17) into (3.19) and (3.20), we can get the numerical results of the outage probability for each user using Monte-carlo Simulation. Figure 3.5 illustrates

the comparison of outage probability between dynamic downlink HAN and static downlink HAN when $\rho = 4$, $M = 5$ and 10. The solid lines are the outage probability without WiFi Direct technique, and the dash lines are the one with WiFi Direct. Figure 3.6 illustrates the comparison of downlink outage probability in a dynamic HAN when $\rho = 4$, $M = 5$ and 10. The solid lines are the outage probability without interference cancelation (IC), and the dash lines are the one with interference cancelation.

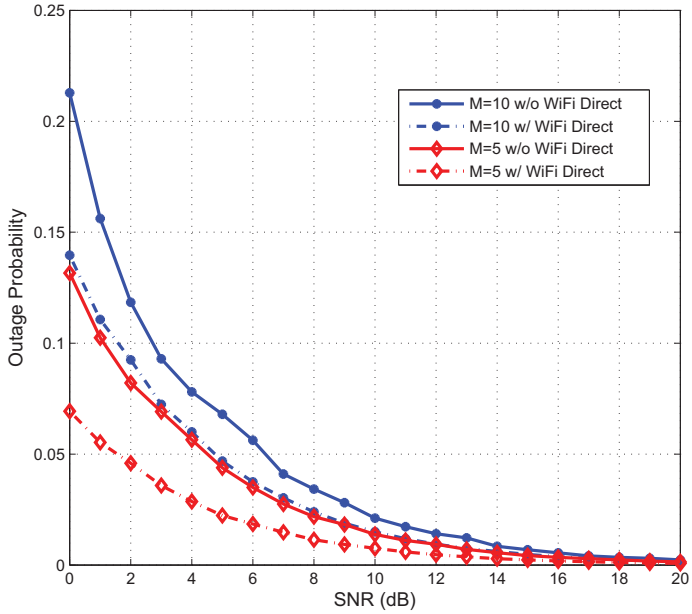

Figure 3.5. Downlink Outage Probability with IC, $\rho = 4$.

Remark 4: From Figures 3.5 and 3.6, it is concluded that:

1) with more users, the outage probability exhibits dramatically higher values due to a potentially worse SINR for each user;
2) the downlink outage probability performance of a HAN is greatly improved with WiFi Direct technique, especially at low SNR region, which indicates that WiFi

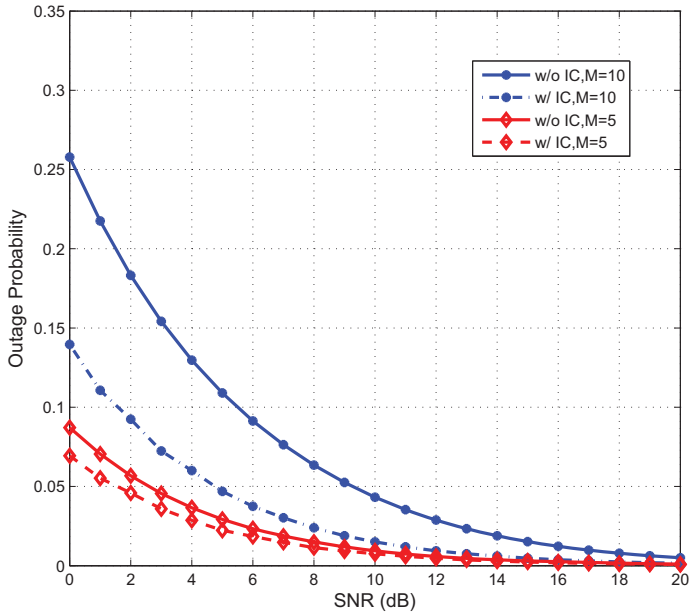

Figure 3.6. Downlink Outage Probability of a Dynamic HAN, $\rho = 4$.

Direct technique not only improves the power saving in Smart Grid, but also enhances the reliability of communications in Smart Grid; item[3)] the downlink HAN exhibits better outage performance with interference cancelation, which reduces SINR effectively, especially with large total number of WiFi-Direct users in the HAN.

3.4 Conclusion

In this chapter, we study the performance of dynamic HANs with the emerging WiFi Direct technique for Smart Grid communications from two aspects: power consumption and downlink outage performance. Particularly, we evaluate and compare the power consumption of the dynamic HAN with power saving scheme and the traditional HAN with continuous active mode. For the power saving scheme, since the WiFi Direct devices switch between active state and doze state, the power consump-

tion of the WiFi Direct network with PSM is highly correlated with the number of communication connections in the network. A Markov chain model is introduced to model the traffic intensity and the number of connections with a specific WiFi Direct device in a HAN, and thus based on this Markov chain model the power consumption of the dynamic HAN is calculated. Furthermore, the downlink outage probability of dynamic HANs for Smart Grid is evaluated with interference cancelation technique. The numerical results show that WiFi Direct technique not only improves the power saving in Smart Grid, but also enhances the reliability of communications in Smart Grid.

Chapter 4

Uplink Multiuser Selection in A Dynamic HAN

4.1 Uplink Multiuser Selection Scheme

4.1.1 Statistics of SNR in the Absence of Interference

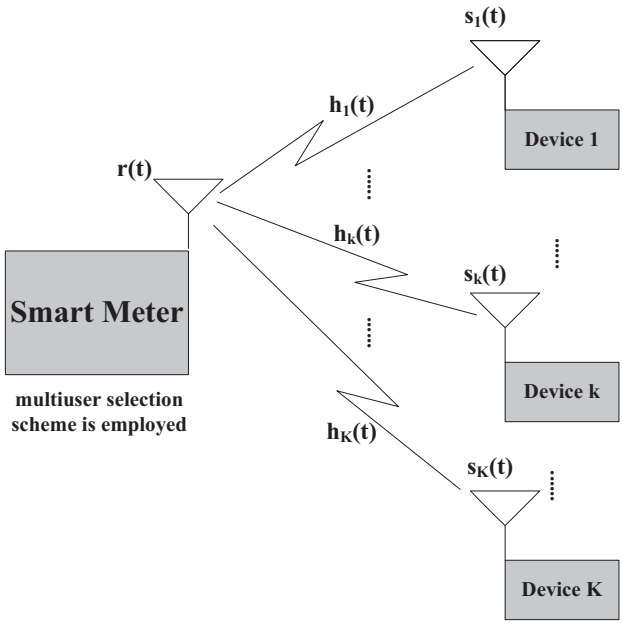

Figure 4.1. Principle of an Uplink Multiuser Communication Scenario in a HAN.

In a typical uplink multiuser communication scenario of a HAN for Smart Grid as shown in Figure 4.1, the signal $r_k^{up}(t)$ at the smart meter from the k_{th} device through the channel at symbol time t can be expressed as:

$$r_k^{up}(t) = h_k^{up}(t)s_k^{up}(t) + n_k(t), k = 1, 2, \ldots, K \tag{4.1}$$

where $s_k^{up}(t)$ is the transmitted signal at symbol time t from the k_{th} device, $h_k^{up}(t)$ is the uplink channel gain of link k from device k to the smart meter at symbol time t, $n_k(t)$ is an independent and identically distributed (i.i.d.) sequence of zero-mean complex Gaussian noise with variance σ^2, and K is the total number of active devices.

Thus the received SNR per symbol from the k_{th} device η_k^{up} in the absence of interference is:

$$\eta_k^{up} = \frac{\mathcal{P}_k^t |h_k^{up}|^2}{\sigma^2} \tag{4.2}$$

where $\mathcal{P}_k^t$ is the average power of the transmitted signal from the k_{th} device. Saleh-Valenzuela (S-V) channel model is adopted for indoor HAN communication scenarios. Since the amplitude of S-V channel gain follows Rayleigh distribution [69] [70], η_k^{up} follows exponential distribution, where $\mathcal{P}_k^t$ and σ^2 are assumed to be constant for tractable analysis. The PDF of η_k^{up} is written as [67][71]:

$$f_{\eta_k^{up}}(\eta) = \frac{1}{\overline{\eta}_k} \exp(-\frac{\eta}{\overline{\eta}_k}) \tag{4.3}$$

where $\overline{\eta}_k$ is the average SNR from device k. Thus the cumulative density function (CDF) of η_k^{up} is:

$$F_{\eta_k^{up}}(\eta) = 1 - \exp(-\frac{\eta}{\overline{\eta}_k}) \tag{4.4}$$

By employing multiuser selection scheme at the smart meter, the link with the maximum SNR among all the K active links is selected at each symbol time. So the received SNR per symbol at the smart meter is

$$\eta_s = \max \eta_k^{up}, k = 1, 2, \ldots, K \tag{4.5}$$

For i.i.d. random variable η_k^{up}, $k = 1, 2, \ldots, K$, the CDF of η_s with K active devices can be calculated as:

$$\begin{aligned} F_{\eta_s}^K(\eta) = Pr[\eta_s \leq \eta] &= \prod_{k=1}^{K} P_r[\eta_k^{up} \leq \eta] \\ &= \prod_{k=1}^{K} F_{\eta_k^{up}}(\eta) = [F_{\eta_k^{up}}(\eta)]^K \\ &= [1 - \exp(-\frac{\eta}{\overline{\eta}})]^K \end{aligned} \tag{4.6}$$

where $\overline{\eta} = \overline{\eta}_k, k = 1, 2, \ldots, K$, which denotes that all the links have the same average received SNR. The PDF of η_s with K active devices is obtained by taking the derivative of $F_{\eta_s}^K(\eta)$ as to η:

$$\begin{aligned} f_{\eta_s}^K(\eta) = \frac{dF_{\eta_s}^K(\eta)}{d\eta} &= K[1 - \exp(-\frac{\eta}{\overline{\eta}})]^{(K-1)} f_{\eta_k^{up}}(\eta) \\ &= \frac{K}{\overline{\eta}}[1 - \exp(-\frac{\eta}{\overline{\eta}})]^{(K-1)} \exp(-\frac{\eta}{\overline{\eta}}) \end{aligned} \tag{4.7}$$

Considering that each device with WiFi Direct technique in HANs of Smart grid alternates between active state and doze state, the average PDF of η_s is consequently written as:

$$\begin{aligned} \overline{f}_{\eta_s}(\eta) &= \mathbb{E}[f_{\eta_s}^K(\eta)] \\ &= \sum_{K=0}^{M} \pi_K f_{\eta_s}^K(\eta) \\ &= \sum_{K=0}^{M} \pi_K \frac{K}{\overline{\eta}}[1 - \exp(-\frac{\eta}{\overline{\eta}})]^{(K-1)} \exp(-\frac{\eta}{\overline{\eta}}) \end{aligned} \tag{4.8}$$

where π_K is the steady state probability when K users are in active state, as derived in Chapter 2.

4.1.2 Statistics of SINR in the Presence of MUI

In practical systems, once the link with the best SNR is selected at the receiver part of the smart meter at one symbol time, the selected signal would experience MUI

from other unselected users. Considering the effect of MUI, the SINR that evaluates the ratio between the desired signal power and the amount of noise and interference generated by all the other unselected users, should be used in performance evaluation [72]. Thus the SINR η_K with totally K active users can be expressed as:

$$\gamma_K^{up} = \frac{\mathcal{P}_i^r}{\mathcal{I}_K + \sigma^2} = \frac{\mathcal{P}_i^r}{\sum_{k \neq i} \mathcal{I}_k + \sigma^2} \tag{4.9}$$

where $\mathcal{P}_i^r$ is the received power of the selected device i, $\mathcal{I}_k$ is the MUI from the unselected device k, and K is the total number of active users that is modeled as a Markov chain, with the steady state probability π_K. For more reasonable analysis compared with [72], a multiuser interference cancelation coefficient α_k that varies between 0 and 1 is multiplied to each received power $\mathcal{P}_k^r$. Consequently, $\mathcal{I}_k$ can be expressed as:

$$\mathcal{I}_k = \alpha_k \mathcal{P}_k^r \tag{4.10}$$

In free space, the received power by a receiver antenna due to path loss $\mathcal{P}_k^r$ can be described according to Friis transmission equation [73]:

$$\frac{\mathcal{P}_k^r}{\mathcal{P}_k^t} = G_t G_r [\frac{\lambda}{4\pi d_k}]^2 \tag{4.11}$$

where G_t and G_r are the antenna gains of the transmitter and receiver antennas respectively, dBi. λ is the wavelength of the transmitting signal, which can be calculated by $\lambda = c/f_c$ ($c = 3 \times 10^8 m/s$ is the speed of light, f_c is the operating frequency of the transmitting signal). d_k is the distance between the transmitter and receiver antennas.

The path loss model can also be expressed in dB form as follows:

$$\mathcal{P}_k^r(dB) = \mathcal{P}_k^t(dB) + G_t(dBi) + G_r(dBi) + 20\log(\frac{\lambda}{4\pi d_k}), \tag{4.12}$$

A signal transmitted through a wireless channel will typically experience random variation due to blockage from objects in the signal path, giving rise to random variations of the received power at a given distance. Such variations are also caused by changes in reflecting surfaces and scattering objects. The most common model for the additional random attenuation due to this effects is log-normal shadowing [74]. Models for path loss and log-normal shadowing can be superimposed to capture power falloff versus distance along with the random attenuation about this path loss from shadowing. The received power $\mathcal{P}_k^r(dB)$ by a receiver antenna from user k according the superimposed model is:

$$\mathcal{P}_k^r(dB) = \mathcal{P}_k^t(dB) + G_t(dBi) + G_r(dBi) + 20\log(\frac{\lambda}{4\pi d_k}) - X_{\sigma_k} \tag{4.13}$$

where X_{σ_k} is Gaussian-distributed random variable with mean zero and variance σ_k^2.

The interference from unselected users is thus expressed as follows:

$$\begin{aligned} \mathcal{I}_k(dB) &= \mathcal{P}_k^r(dB) + \alpha_k(dB) \\ &= \mathcal{P}_k^t(dB) + G_t(dBi) + G_r(dBi) \\ &+ 20\log(\frac{\lambda}{4\pi d_k}) - X_{\sigma_k} + \alpha_k(dB) \end{aligned} \tag{4.14}$$

It is obvious that the interference $\mathcal{I}_k$ from the unselected user k follows log-normal distribution with mean μ_k as:

$$\mu_k = \mathcal{P}_k^t(dB) + G_t(dBi) + G_r(dBi) + 20\log(\frac{\lambda}{4\pi d_k}) + \alpha_k(dB) \tag{4.15}$$

and variance σ_k^2.

Applying the central limit theorem, the sum of a series of random variables that follow log-normal distribution can be approximately considered as another log-normal-distributed random variable. By assuming that $\sigma_k^2 = \sigma_I^2$, the sum of interference from all the unselected users $\mathcal{I}_K$ in (4.9) also follows log-normal distribution

with variance $\sigma^2_{I_K}$ and mean μ_{I_K}, which are derived from the known parameters μ_k and σ^2 as shown below [75]:

$$\begin{cases} \sigma^2_{I_K} = \ln[(\exp(\sigma^2_I) - 1)\frac{\sum_{k\neq i}\exp(2\mu_k)}{\sum_{k\neq i}\exp^2(\mu_k)} + 1] \\ \mu_{I_K} = \frac{\sigma^2_I - \sigma^2_{I_K}}{2} + \ln(\sum_{k\neq i}\exp(\mu_k)) \end{cases} \tag{4.16}$$

4.2 Performance Analysis

In this section, the performance of multiuser selection scheme applied to a dynamic HAN in Smart Grid with the emerging WiFi Direct technique is measured in terms of uplink capacity outage probability and BER.

4.2.1 Outage Probability

4.2.1.1 In the Absence of Interference

The capacity of multi-device HAN with received SNR η_s in the absence of interference by employing multiuser selection scheme is:

$$C(\eta_s) = \log_2(1 + \eta_s) \tag{4.17}$$

The HAN is said to be in *outage* when when the required data transmission rate R_{req} is higher than the achievable capacity of the selected uplink. Thus the closed-form uplink outage probability is expressed as [53] [60]:

$$\begin{aligned} \mathbb{P}^{up}_{out} &= Pr[C(\eta_s) \leq R_{req}] \\ &= Pr[\log_2(1 + \eta_s) \leq R_{req}] \\ &= \sum_{K=0}^{M} \pi_K [1 - \exp(-\frac{2^{R_{req}} - 1}{\overline{\eta}})]^K \end{aligned} \tag{4.18}$$

The deduction of the closed-form uplink outage probability in the absence of interference is shown in Appendix A.

4.2.1.2 In the Presence of MUI

In the presence of MUI, the uplink capacity outage probability of the dynamic HAN can be written as:

$$\mathbb{P}_{Iout}^{up} = Pr[\pi_K log_2(1+\gamma_K^{up}) \leq R_{req}] \tag{4.19}$$

By taking (4.9),(4.13) (4.16) into (4.19), we can obtain the closed-form outage probability as below:

$$\mathbb{P}_{Iout}^{up} = \pi_K Q(\frac{\mu_i - \mu_{I_K} - (2^{R_{req}}-1)(dB) - \sigma^2(dB)}{\sqrt{\sigma_i^2 + \sigma_{I_K}^2}}) \tag{4.20}$$

where the Q-function is defined as the probability that a Gaussian random variable is greater than x. The deduction of the closed-form uplink outage probability in the presence of MUI is illustrated in Appendix B.

4.2.2 Bit Error Rate (BER)

For M-ary signaling, the SNR per bit η_b could be approximately expressed as:

$$\eta_b \approx \frac{\eta_s}{\log_2 M} \tag{4.21}$$

Combining with (4.8), we can get the average PDF of η_b as:

$$\overline{f}_{\eta_b}(\eta) = \sum_{K=0}^{M} \pi_K \frac{K}{\overline{\eta_b}} [1 - \exp(-\frac{\eta}{\overline{\eta_b}})]^{(K-1)} \exp(-\frac{\eta}{\overline{\eta_b}}) \tag{4.22}$$

where $\overline{\eta_b}$ is the average $\frac{E_b}{N_0}$, namely the average SNR per bit.

Assuming η_b is roughly constant over each bit time, the average BER in the absence of interference is:

$$P_b = \int_0^\infty p_b(\eta) \overline{f}_{\eta_b}(\eta) d\eta \tag{4.23}$$

where $p_b(\eta)$ is the BER for a certain modulation scheme under AWGN channel [74]. For WiFi technique, the High Throughput (HT) physical(PHY) data subcarriers are

modulated using BPSK, QPSK, 16-QAM or 64-QAM [76]. The BER of these four modulation schemes over AWGN channel could be easily obtained from [74].

The numerical results of BER can be evaluated by Mathematica, where the Q-function which is used for the calculation of the BER of the four modulation schemes over AWGN channel, can be represented by alternative Q-function as:

$$Q(x) = \frac{1}{\pi}\int_0^{\frac{\pi}{2}} \exp\left[-\frac{x^2}{2\sin^2\phi}\right]d\phi, x > 0 \tag{4.24}$$

4.3 Numerical Results and Discussion

4.3.1 Outage Probability

4.3.1.1 In the Absence of Interference

Figure 4.2 shows the uplink outage probability of multiuser selection scheme in the absence of interference of a dynamic HAN due to different traffic intensities when the total number of WiFi Direct devices is 10. Meanwhile, for a fixed traffic intensity $\rho = 8$ but different total number of WiFi-Direct devices in a HAN, the uplink outage probability based on the multiuser selection scheme is illustrated in Figure 4.3.

Remark 5: From Figures 4.2 and 4.3 we can see that:

1) the uplink outage probability changes dramatically at low average SNR but has a constant tendency when the average SNR is relatively high.
2) The traffic intensity of a certain HAN in smart grid has considerate impact on the uplink outage probability of multiuser selection scheme. Intensive traffic intensity indicates frequent switching between active state and doze state, and high probability that more devices are involved in the uplink communication with the smart meter. Consequently, a lower outage probability is achieved by selecting the link with maximum SNR among all the active links.

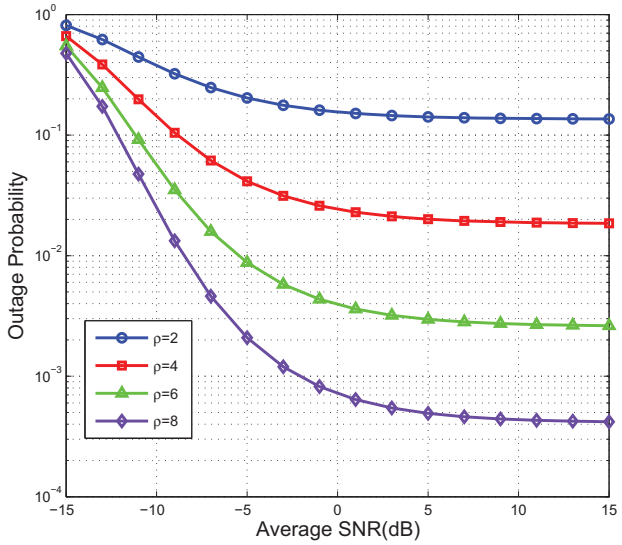

Figure 4.2. Uplink Outage Probability without MUI when $M = 10$.

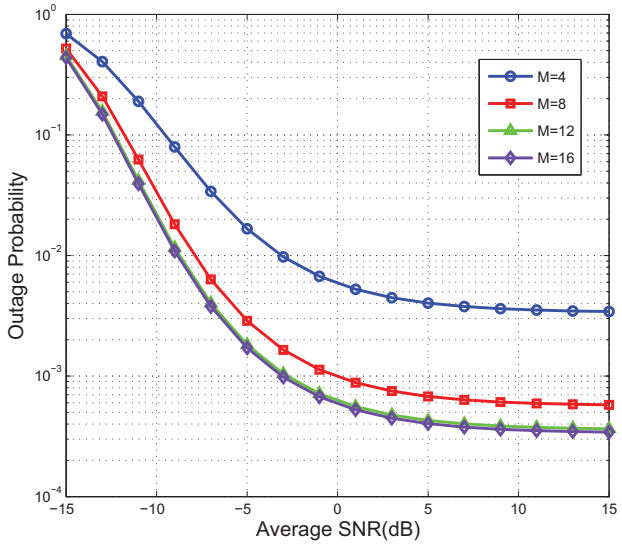

Figure 4.3. Uplink Outage Probability without MUI when $\rho = 8$.

3) It is figured out that the values of steady state probability P_K for K larger than 13 are extremely small with $M = 16$, so that the HANs with $M = 12$ and $M = 16$ exhibit similar characteristics, which could explain the approximate

overlap between the curves of outage probability with $M = 12$ and $M = 16$ in Figure 4.3.

4.3.1.2 In the Presence of MUI

With MUI, the simulation parameters are set as listed in Table 3.1. The transmit power of each device $\mathcal{P}_k^t$ varies within the range from 64 to 128mW. The distance from each device to the smart meter d_k is between 1 and 1.5m. And the multiuser interference cancelation coefficient α_k takes values between 0 and 1. For two extreme cases, $\alpha_k = 0$ denotes that the MUI is fully canceled and SINR reverts to SNR, which is the same case as that in the absence of interference; $\alpha_k = 1$ means that the desired signal experiences heavy MUI with no interference cancelation. By taking monte-carlo simulation of 100000 times, we obtain the numerical results of outage probability for $\alpha_k = 1$ and α_k as a random variable, which are shown in Figures 4.4 and 4.5 respectively.

Table 4.1. Parameter Settings with MUI

Parameter	Value
ρ	4,6,and 8
G_t	1dBi
G_r	1dBi
f_c	2.4×10^9Hz
σ_I^2	3dB
$\sigma^2(dB)$	-40dB
d_k	$1 \sim 1.5m$
$\mathcal{P}_k^t$	$64 \sim 128mW$
α_k	$0 \sim 1$

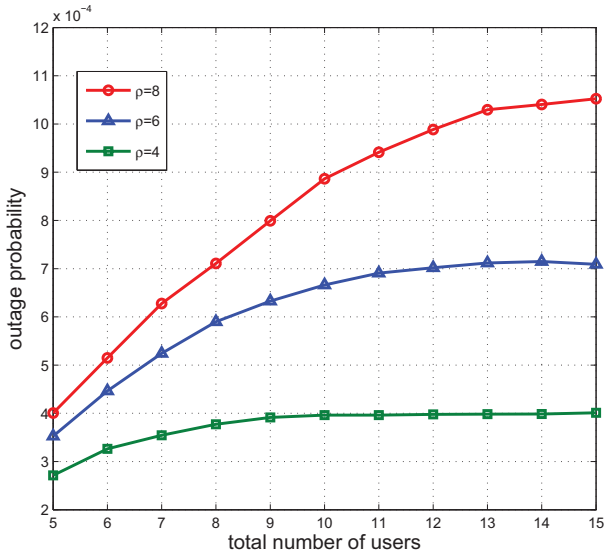

Figure 4.4. Uplink Outage Probability with Full MUI when $\rho = 8$.

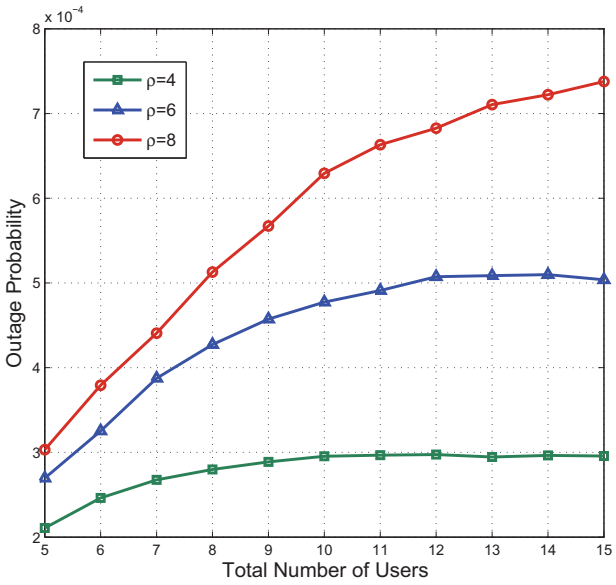

Figure 4.5. Uplink Outage Probability with MUI when $\rho = 8$.

From Figures 4.4 and 4.5, the following conclusion is drawn that in the presence of MUI, the dramatic impact of MUI on the outage performance of multiuser selection scheme mainly depends on increasing unselected users, heavy traffic intensity, as well

as the level of MUI. Particularly, when MUI is fully present ($\alpha_k = 1$), multiuser selection scheme exhibits worse outage performance.

4.3.2 Bit Error Rate

The numerical values of BER are determined by mainly three factors: the total number of WiFi-Direct devices in a HAN, the traffic intensity and the modulation scheme of symbols. The numerical results of BER are compared with two fixed factors and the other changing parameter. Particularly, the BER with BPSK due to different traffic intensity when $M = 5$ is shown in Figure 4.6. Figure 4.7 illustrates the BER with four kinds of modulation scheme: BPSK, QPSK, 16-QAM and 64-QAM when $\rho = 8, M = 10$. For a certain traffic intensity of $\rho = 8$ and BPSK modulation scheme, Figure 4.8 plots the BER with different total number of WiFi-Direct devices in a HAN.

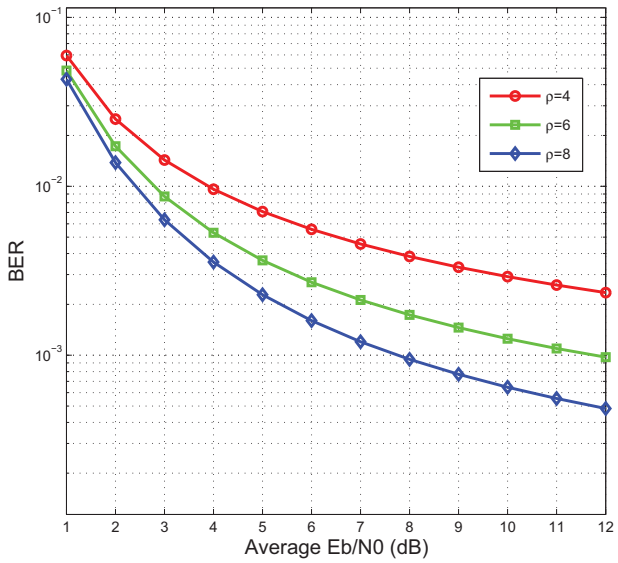

Figure 4.6. BER of Multiuser Selection Scheme in a HAN with BPSK when $M = 5$.

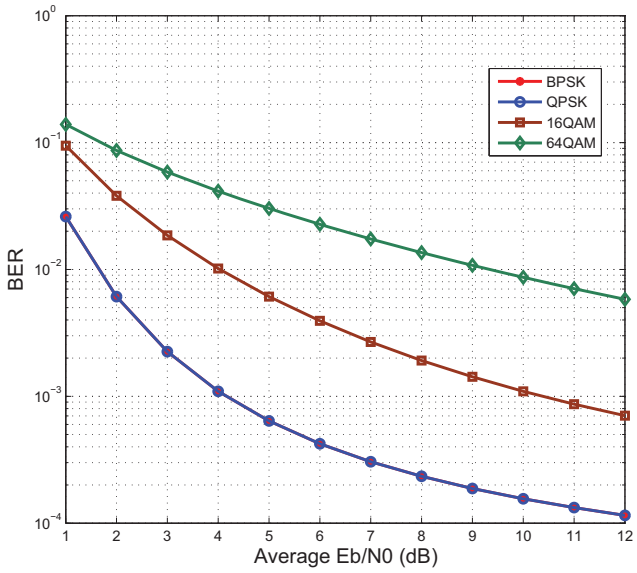

Figure 4.7. BER of Multiuser Selection Scheme in a HAN with $\rho = 8, M = 10$.

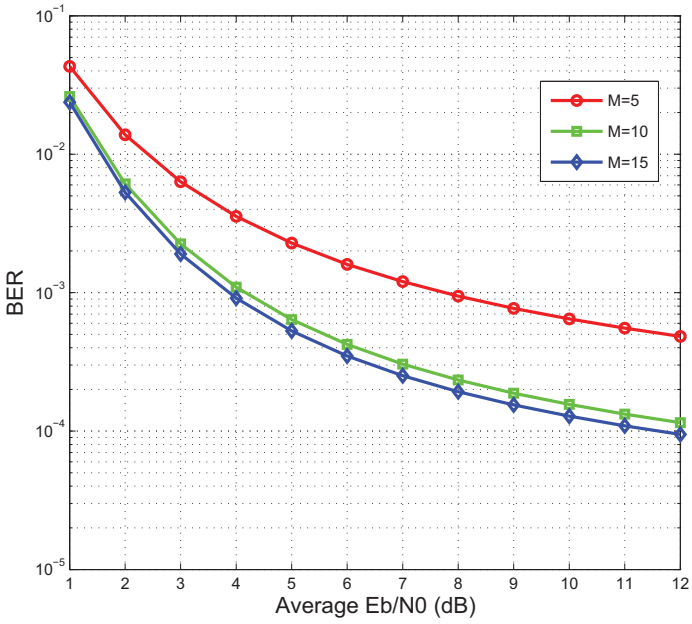

Figure 4.8. BER of Multiuser Selection Scheme in a HAN with BPSK when $\rho = 8$.

Remark 6: According to Figures 4.6-4.8, it is obvious to see that:

1) for a certain HAN in smart grid, larger traffic intensity results in better BER performance with fixed modulation scheme and average SNR.
2) Different modulation schemes have obviously different impact on the BER performance. Particularly, data modulated by 64-QAM has the highest BER, which are due to the different BER performance of these modulation schemes under AWGN channel. It is noteworthy that BPSK and QPSK exhibit the same BER performance even over the fading channel.
3) when the total number of WiFi-Direct devices in a HAN of smart grid in considerately large, as shown in Figure 4.8, the BER plots of multiuser selection scheme are similar with $M = 10$ and $M = 15$. This also could be explained by the property of numerical values of P_K as mentioned in the last subsection.

4.4 Conclusions

In this chapter, the performance of multiuser selection scheme that is employed in dynamic HANs for Smart Grid communications with WiFi Direct technique is evaluated from two aspects: outage probability and BER. The closed-form capacity outage probability is calculated in two cases: in the absence of interference and in the presence of MUI. In the first case, the PDF of received SNR is derived from the amplitude distribution property of indoor S-V channel gain. A random variable that quantifies the level of MUI cancelation-multiuser interference cancelation coefficient is added for the calculation of SINR when MUI is present. In addition, the BER expressions of different modulation schemes under AWGN channel are included in the calculation of BER of the multiuser selection scheme. Numerical results show that the performance of multiuser selection scheme in dynamic HANs of for Smart Grid communications is related with several factors, i.e. total number of devices in

HANs, traffic intensity, modulation scheme, and multiuser interference cancelation coefficient, etc.

Chapter 5

Capacity Optimization in Heterogeneous HAN

5.1 Heterogeneous HAN for Smart Grid

For explicit expression, two definitions are given as follows:

Definition 4: *A Heterogeneous HAN for Smart Grid* is the HAN in which various wireless communication technologies, including Wi-Fi, ZigBee, and Bluetooth, etc., are used for the communications between household wireless devices and the smart meter. And the properties of the heterogeneous HAN is:

1) various SINRs are required for different users;
2) various bandwidths are used for the communications between the smart meter and different users.

Definition 5: The *downlink* of a HAN in Smart Grid is defined as the communication link when the smart meter transmits signals to the users.

We consider a HAN with one smart meter installed outside the door, and K heterogeneous active in-home wireless devices that obtain control and monitor information from the smart meter. The independent signal matrix $\underline{X} = [x_1, x_2, \ldots, x_k, \ldots, x_K]^T$ is transmitted in the downlink, with transmit power matrix $\underline{P} = [P_1, P_2, \ldots, P_k, \ldots, P_K]^T$, where x_k is the signal transmitted to the k_{th} user, and P_k is correspondingly the power of x_k.

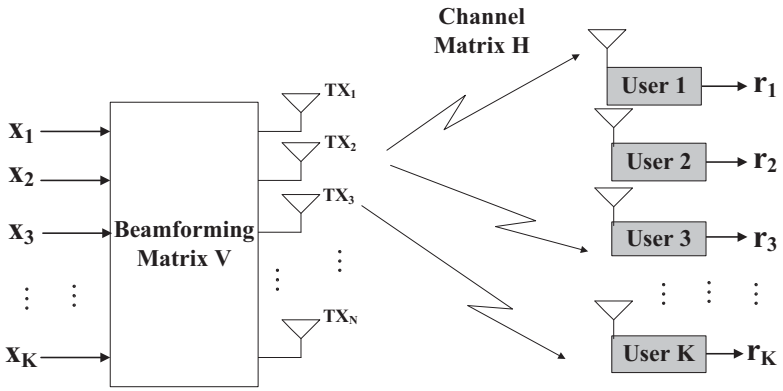

Figure 5.1. Multiuser Downlink Model with Beamforming at Smart Meter.

Beamforming is employed at the transmit part of the smart meter, with N transmit antennas, and each user has single receive antenna, as shown in Figure 5.1. $\underline{V}$ is an $N \times K$ beamforming matrix expressed as:

$$\begin{aligned} \underline{V} &= \begin{bmatrix} \underline{V_1} & \underline{V_2} & \dots & \underline{V_k} & \dots & \underline{V_K} \end{bmatrix} \\ &= \begin{bmatrix} v_{11} & v_{12} & \dots & v_{1k} & \dots & v_{1K} \\ v_{21} & v_{22} & \dots & v_{2k} & \dots & v_{2K} \\ \vdots & \vdots & \ddots & \vdots & \ddots & \vdots \\ v_{N1} & v_{N2} & \dots & v_{Nk} & \dots & v_{NK} \end{bmatrix} \end{aligned} \tag{5.1}$$

where $\underline{V_k}$ is the beamforming vector corresponding to the k_{th} user.

The downlink channel matrix is $\underline{H} = [\underline{H_1}, \underline{H_2}, \dots, \underline{H_k}, \dots, \underline{H_K}]$, where $\underline{H_k}$ denotes the channel vector corresponding to the k_{th} user, which also indicates the downlink from the smart meter to each user is MISO channel for spatial diversity. All the

downlink channels are independent and identically distributed (i.i.d.) Rayleigh flat fading channels with unit variance[77].

$$\begin{aligned}\underline{H} &= \begin{bmatrix} \underline{H_1} & \underline{H_2} & \dots & \underline{H_k} & \dots & \underline{H_K} \end{bmatrix} \\ &= \begin{bmatrix} h_{11} & h_{12} & \dots & h_{1k} & \dots & h_{1K} \\ h_{21} & h_{22} & \dots & h_{2k} & \dots & h_{2K} \\ \vdots & \vdots & \ddots & \vdots & \ddots & \vdots \\ h_{N1} & h_{N2} & \dots & h_{Nk} & \dots & h_{NK} \end{bmatrix}\end{aligned} \tag{5.2}$$

5.2 Downlink Capacity Optimization

In this section, total downlink capacity optimization is investigated for a heterogeneous HAN. According to the model of a heterogeneous HAN with the smart meter equipped with beamforming and K active users as illustrated in section 6.1, we can see that the received signal r_k of the k_{th} user from the smart meter is:

$$\begin{aligned} r_k &= \underline{H_k}^T \underline{V_k} x_k + \underline{H_k}^T \sum_{j \neq k} \underline{V_j} x_j + n_k \\ &= \underline{H_k}^T \underline{VX} + n_k \end{aligned} \tag{5.3}$$

where n_k is the thermal noise at the users modeled as additive white Gaussian noise (AWGN) with one-sided power spectral density (PSD) of N_0.

For this multiuser downlink scenario, each user experiences interference which stems from the transmitted signals to all other users. The SINR at the k_{th} user is written as:

$$\eta_k = \frac{|\underline{H_k}^T \underline{V_k}|^2 P_k}{\sum_{j \neq k} |\underline{H_k}^T \underline{V_j}|^2 P_j + \mathcal{W}_k N_0} \tag{5.4}$$

where $\mathcal{W}_k$ is the transmission bandwidth assigned to the k_{th} user.

Applying singular value decomposition (SVD) theorem to $|\underline{H_k}^T \underline{V_j}|^2$, the detail of which is in Appendix C, η_k in (5.2) can be mathematically reformatted as [78] [53]:

$$\begin{aligned}\eta_k &= \frac{\lambda_k^2 \sum_{n=1}^{N} |\beta_{n,k}|^2 P_k}{\sum_{j\neq k} \lambda_j^2 \sum_{n=1}^{N} |\beta_{n,k}|^2 P_j + \mathcal{W}_k N_0} \\ &= \frac{\lambda_k^2 \sum_{n=1}^{N} |\beta_{n,k}|^2 P_k}{\sum_{j=1}^{K} (\lambda_j^2 \sum_{n=1}^{N} |\beta_{n,k}|^2 P_j) + \mathcal{W}_k N_0 - \lambda_k^2 \sum_{n=1}^{N} |\beta_{n,k}|^2 P_k} \\ &= \frac{\lambda_k^2 \sum_{n=1}^{N} |\beta_{n,k}|^2 P_k}{\sum_{n=1}^{N} |\beta_{n,k}|^2 \cdot \sum_{j=1}^{K} \lambda_j^2 P_j + \mathcal{W}_k N_0 - \lambda_k^2 \sum_{n=1}^{N} |\beta_{n,k}|^2 P_k}\end{aligned} \tag{5.5}$$

where $\beta_{n,k}$ is the channel gain from the n_{th} transmit antenna at the smart meter to the k_{th} user, λ_j is the singular value of the matrix $\underline{V_j}$.

Without loss of generality, $\lambda_j = 1$ for transmit beamforming. Therefore, the total downlink capacity of the multiuser downlink system with K active users is expressed as:

$$\begin{aligned}&C_{tot} \\ &= \sum_{k=1}^{K} \mathcal{W}_k \log_2(1+\eta_k) \\ &= \sum_{k=1}^{K} \mathcal{W}_k \log_2(1 + \frac{\sum_{n=1}^{N} |\beta_{n,k}|^2 P_k}{\sum_{n=1}^{N} |\beta_{n,k}|^2 \sum_{j=1}^{K} P_j + \mathcal{W}_k N_0 - \sum_{n=1}^{N} |\beta_{n,k}|^2 P_k}) \\ &= \sum_{k=1}^{K} \mathcal{W}_k \log_2(\frac{\sum_{n=1}^{N} |\beta_{n,k}|^2 \sum_{j=1}^{K} P_j + \mathcal{W}_k N_0}{\sum_{n=1}^{N} |\beta_{n,k}|^2 \cdot \sum_{j=1}^{K} P_j + \mathcal{W}_k N_0 - \sum_{n=1}^{N} |\beta_{n,k}|^2 P_k})\end{aligned} \tag{5.6}$$

For heterogenous communications, all the K users are required to achieve individual SINR requirements $\eta_k^{th}, k = 1, 2, \ldots, K$ for successful communication. That is:

$$\eta_k = \frac{\sum_{n=1}^{N} |\beta_{n,k}|^2 P_k}{\sum_{n=1}^{N} |\beta_{n,k}|^2 \cdot \sum_{j=1}^{K} P_j + \mathcal{W}_k N_0 - \sum_{n=1}^{N} |\beta_{n,k}|^2 P_k} \geq \eta_k^{th} \tag{5.7}$$

The downlink capacity optimization of the heterogeneous HAN is expressed as:

$$\begin{aligned}
\max_{P_k} \quad & \sum_{k=1}^{K} \mathcal{W}_k \log_2\left(\frac{\sum_{n=1}^{N} |\beta_{n,k}|^2 \cdot \sum_{j=1}^{K} P_j + \mathcal{W}_k N_0}{\sum_{n=1}^{N} |\beta_{n,k}|^2 \cdot \sum_{j=1}^{K} P_j + \mathcal{W}_k N_0 - \sum_{n=1}^{N} |\beta_{n,k}|^2 P_k}\right) \\
s.t. \quad & \frac{\sum_{n=1}^{N} |\beta_{n,k}|^2 P_k}{\sum_{n=1}^{N} |\beta_{n,k}|^2 \cdot \sum_{j=1}^{K} P_j + \mathcal{W}_k N_0 - \sum_{n=1}^{N} |\beta_{n,k}|^2 P_k} \geq \eta_k^{th}, \\
& \sum_{k=1}^{K} P_k = P_{tot}, \\
& P_k \geq 0, \quad k = 1, 2, \ldots, K
\end{aligned} \tag{5.8}$$

Remark 7: The objective of this optimization problem is to maximize the total downlink capacity with the constraints that:

1) all the K users must achieve individual SINR requirements for successful communication;
2) the sum of allocated transmit power to each user is equal to the permissible total transmit power at the smart meter.
3) the transmit power to each user is feasible.

This is interesting from a network operator's perspective since it minimizes inter-user interference and improves the throughput as well as the power efficiency of the network at the same time.

In the following, an optimal transmit power allocation scheme is presented based on (5.8).

For notation brevity, denote $\sum_{n=1}^{N} |\beta_{n,k}|^2 \cdot P_{tot} + \mathcal{W}_k N_0$ as $\mathcal{A}_k^N$, $\sum_{n=1}^{N} |\beta_{n,k}|^2$ as $\mathcal{B}_k^N$, which are both independent from P_k:

$$\begin{aligned}
\mathcal{A}_k^N &= \sum_{n=1}^{N} |\beta_{n,k}|^2 \cdot P_{tot} + \mathcal{W}_k N_0 \\
\mathcal{B}_k^N &= \sum_{n=1}^{N} |\beta_{n,k}|^2
\end{aligned} \tag{5.9}$$

Thus, taking (5.9) into (5.8), the optimization problem can be written as:

$$\begin{aligned} \max_{P_k} \quad & \sum_{k=1}^{K} \mathcal{W}_k \log_2\left(\frac{\mathcal{A}_k^N}{\mathcal{A}_k^N - \mathcal{B}_k^N \cdot P_k}\right) \\ s.t. \quad & P_k \geq \frac{\mathcal{A}_k^N \eta_k^{th}}{\mathcal{B}_k^N (1+\eta_k^{th})}, \quad k = 1, 2, \ldots, K \\ & \sum_{k=1}^{K} P_k = P_{tot} \end{aligned} \tag{5.10}$$

It is easy to see that (5.10) is a convex optimization problem. Since $\log(\cdot)$ is a concave function, and $\log_2(\frac{\mathcal{A}_k^N}{\mathcal{A}_k^N - \mathcal{B}_k^N \cdot P_k})$ is concave as to P_k. In addition, the sum of concave functions is still a concave function. To maximize a concave function is equivalent to minimizing the negative of the concave function, namely a convex function:

$$\begin{aligned} \min_{P_k} \quad & -\sum_{k=1}^{K} \mathcal{W}_k \log_2\left(\frac{\mathcal{A}_k^N}{\mathcal{A}_k^N - \mathcal{B}_k^N \cdot P_k}\right) \\ s.t. \quad & \frac{\mathcal{A}_k^N \eta_k^{th}}{\mathcal{B}_k^N (1+\eta_k^{th})} - P_k \leq 0, \quad k = 1, 2, \ldots, K \\ & \sum_{k=1}^{K} P_k = P_{tot} \end{aligned} \tag{5.11}$$

In this case, by introducing Lagrange multipliers λ and μ_k, $k = 1, 2, \ldots, K$, we can get the Lagrangian dual function of the optimization problem in (5.11) as [61]:

$$\begin{aligned} L(P_k, \lambda, \mu_k) = \quad & -\sum_{k=1}^{K} \mathcal{W}_k \log_2\left(\frac{\mathcal{A}_k^N}{\mathcal{A}_k^N - \mathcal{B}_k^N \cdot P_k}\right) \\ & + \lambda\left(\sum_{k=1}^{K} P_k - P_{tot}\right) \\ & + \sum_{k=1}^{K} \mu_k [\mathcal{A}_k^N \eta_k^{th} - \mathcal{B}_k^N (1+\eta_k^{th}) P_k] \end{aligned} \tag{5.12}$$

Applying KKT condition, the optimal solution of transmit power allocation to each user P_k^* satisfies the following equations:

$$\begin{aligned} &\frac{\partial L(P_k^*, \lambda, \mu_k)}{\partial P_k^*} = 0 \\ &\mu_k \geq 0, \quad k = 1, 2, \ldots, K \\ &\mu_k[\mathcal{A}_k^N \eta_k^{th} - \mathcal{B}_k^N (1 + \eta_k^{th}) P_k^*] = 0, \quad k = 1, 2, \ldots, K \end{aligned} \tag{5.13}$$

The first equation in (5.13) is taking the derivative of $L(P_k, \lambda, \mu_k)$ with respect to P_k^* and let it equal zero:

$$-\frac{\mathcal{B}_k^N}{\ln 2(\mathcal{A}_k^N - \mathcal{B}_k^N P_k^*)} + \lambda - \mu_k \mathcal{B}_k^N (1 + \eta_k^{th}) = 0 \tag{5.14}$$

Thus, μ_k is obtained as:

$$\mu_k = \frac{\lambda - \frac{\mathcal{B}_k^N}{\ln 2(\mathcal{A}_k^N - \mathcal{B}_k^N P_K^*)}}{\mathcal{B}_k^N (1 + \eta_k^{th})} \tag{5.15}$$

The second condition in (5.13) holds iff:

$$\lambda \geq \frac{1}{\ln 2(\frac{\mathcal{A}_k^N}{\mathcal{B}_k^N} - P_k^*)} \tag{5.16}$$

Taking (5.15) into the third equation of (5.13), we can get:

$$[\lambda - \frac{\mathcal{B}_k^N}{\ln 2(\mathcal{A}_k^N - \mathcal{B}_k^N P_K^*)}][\mathcal{A}_k^N \eta_k^{th} - \mathcal{B}_k^N (1 + \eta_k^{th}) P_k^*] = 0 \tag{5.17}$$

When (5.16) takes equality, $P_k^* = \frac{\mathcal{A}_k^N}{\mathcal{B}_k^N} - \frac{1}{\ln 2\lambda}$; otherwise, $P_k^* = \frac{\mathcal{A}_k^N \eta_k^{th}}{\mathcal{B}_k^N (1+\eta_k^{th})}$. Combining with (5.9), we can get the optimal transmit power profile as:

$$P_k^* = \begin{cases} P_{tot} + \frac{\mathcal{W}_k N_0}{\sum_{n=1}^N |\beta_{n,k}|^2} - \frac{1}{\ln 2\lambda}, & equality \quad in \quad (5.16), \\ (P_{tot} + \frac{\mathcal{W}_k N_0}{\sum_{n=1}^N |\beta_{n,k}|^2}) \frac{\eta_k^{th}}{(1 + \eta_k^{th})}, & else. \end{cases} \tag{5.18}$$

Substituting (5.18) into (5.6), the optimized total downlink capacity is easily obtained.

5.3 Lower Bound of the Transmit Power

From the first constraint condition in (5.11), we can see that the transmit power of each user has a minimum value for reliable communication which is related by its SINR requirement:

$$P^*_{k\,min} = (P_{tot} + \frac{\mathcal{W}_k N_0}{\sum_{n=1}^{N} |\beta_{n,k}|^2}) \frac{\eta_k^{th}}{(1+\eta_k^{th})}, \quad k = 1, 2, \cdots, K \tag{5.19}$$

In this section, the property of the minimum transmit power $P^*_{k\,min}$ in (5.19) is investigated with the following theorem.

Theorem 2: The minimum transmit power to the k_{th} user $P^*_{k\,min}$ fluctuates due to the downlink S-V channel $\beta_{n,k}, n = 1, 2, \cdots, N$. And $P^*_{k\,min}$ has a lower bound which is determined by the required minimum SINR η_k^{th}:

$$P^*_{k\,L} = \frac{P_{tot}\eta_k^{th}}{(1+\eta_k^{th})} \tag{5.20}$$

Proof: For the indoor S-V channel, the amplitude of S-V channel gain preserves Rayleigh distribution [69] [70],

$$f_{|\beta_{n,k}|}(|\beta_{n,k}|) = 2|\beta_{n,k}| \exp(-|\beta_{n,k}|^2) \tag{5.21}$$

So that the power for each link $|\beta_{n,k}|^2$ follows exponential distribution as:

$$f_{|\beta_{n,k}|^2}(|\beta_{n,k}|^2) = \frac{1}{\overline{|\beta_{n,k}|^2}} \exp(-\frac{|\beta_{n,k}|^2}{\overline{|\beta_{n,k}|^2}}) \tag{5.22}$$

where $\overline{|\beta_{n,k}|^2}$ is the average power for each downlink. Without loss of generality, $\overline{|\beta_{n,k}|^2}$ is normalized as 1.

It is well known that the sum of K independent exponential variables follows Erlang distribution. Therefore, $\sum_{n=1}^{N} |\beta_{n,k}|^2$ in (5.19) is Erlang distributed. According to (5.9), $\sum_{n=1}^{N} |\beta_{n,k}|^2$ is denoted as $\mathcal{B}_k^N$ for simplicity, so the PDF of $\mathcal{B}_k^N$ is expressed as:

$$f_{\mathcal{B}_k^N}(\mathcal{B}) = \frac{\mathcal{B}^{(N-1)} \exp(-\mathcal{B})}{(N-1)!}, \quad \mathcal{B} \geq 0 \tag{5.23}$$

From (5.19) we can see that:

$$\mathcal{B}_k^N = \frac{\mathcal{W}_k N_0}{(1+\frac{1}{\eta_k^{th}})P_{k\,min}^* - P_{tot}} \tag{5.24}$$

Combining (5.24) with (5.23), we can obtain the PDF of the minimum allocated transmit power to each user due to Rayleigh flat fading as:

$$\begin{aligned} f_{P_{k\,min}^*}(P_k) = & \frac{[\frac{\mathcal{W}_k N_0}{K(1+\frac{1}{\eta_k^{th}})P_k - P_{tot}}]^{(N-1)} \exp(-\frac{\mathcal{W}_k N_0}{K(1+\frac{1}{\eta_k^{th}})P_k - P_{tot}})}{(N-1)!} \\ & \times \frac{\mathcal{W}_k N_0}{(1+\frac{1}{\eta_k^{th}})P_k{}^2}, \quad P_{k\,min}^* \geq \frac{P_{tot}\eta_k^{th}}{(1+\eta_k^{th})} \end{aligned} \tag{5.25}$$

It is noteworthy that $P_{k\,min}^*$ has a lower bound of $\frac{P_{tot}\eta_k^{th}}{(1+\eta_k^{th})}$.

5.4 Numerical Results and Discussion

Example 1: To validate the properties of the proposed optimal power allocation scheme, we consider a HAN for Smart Grid consisting of one smart meter, one WiFi device, and one Bluetooth device. The SINR threshold for WiFi appliances is $22dB$ [79], and the SINR threshold for Bluetooth users is $18dB$ [80]. The transmission bandwiths are $20MHz$, and $1MHz$, respectively. The default transmit power at the smart meter to each user is $20dBm$, and the thermal noise at each receiver is $-95dBm$.

Figures 5.2 and 5.3 show the PDF of optimal allocated transmit power for a WiFi user and a Bluetooth user, respectively. The blue dashed lines are the PDF when two transmit antennas are equipped at the smart meter, the red double-dots dashed lines are the PDF with four transmit antennas at the smart meter, and the green solid lines are the PDF with eight transmit antennas. From Figures 5.2 and 5.3, we can see that with a certain total number of active users in the HAN, more transmit antennas at the smart meter render the PDF of the minimum allocated transmit power for a user concentrates on smaller values.

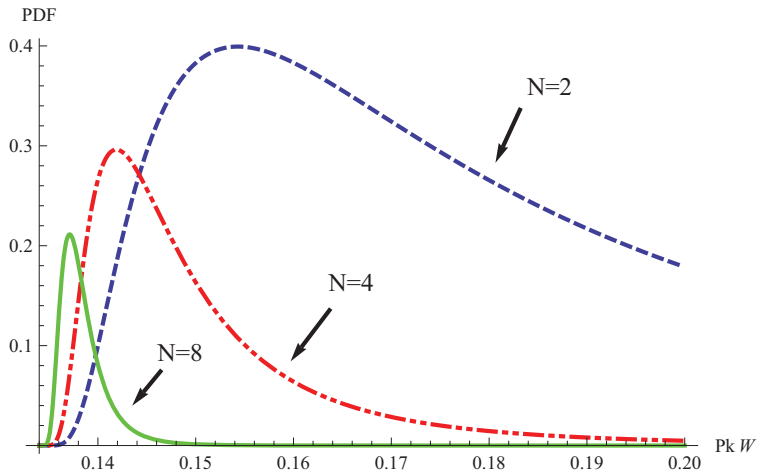

Figure 5.2. PDF of the Allocated Transmit Power for a Wi-Fi Appliance.

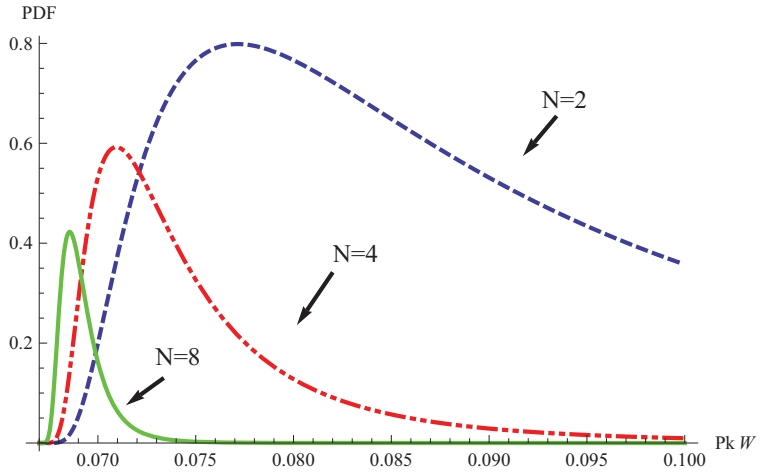

Figure 5.3. PDF of the Allocated Transmit Power for a Bluetooth User.

Figure 5.4 illustrates the comparison of the PDF of optimal allocated transmit power for a WiFi user and a Bluetooth user, when four transmit antennas are equipped at the smart meter. From Figure 5.4, it is obvious that a much higher transmit power is required for a WiFi user.

Example 2: The numerical results of total downlink capacity with optimal power allocation are obtained by Monte-Carlo simulation based on (5.6) and (5.18), which are also compared to the ones with equal power allocation scheme. In this HAN

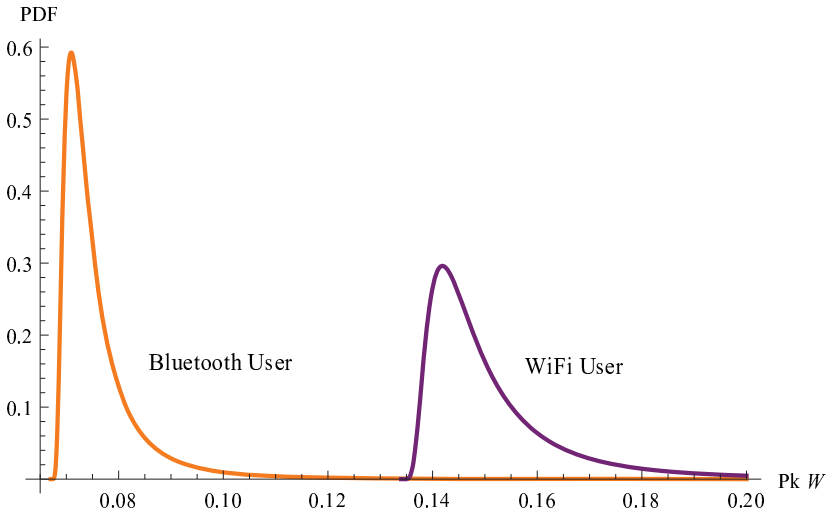

Figure 5.4. PDF of the Allocated Transmit Power for a Wi-Fi User and a Bluetooth User, $N = 4$.

scenario, the smart meter is equipped with 2,4,or 8 transmit antennas for beamforming technique. The SINR threshold for a WiFi appliance is $22dB$, while it is $18dB$ for a ZigBee or Bluetooth user. The transmission bandwidths for these three types of users are $20MHz$, $5MHz$, and $1MHz$, respectively. The total transmit power at the smart meter is $0.1 \times K(Watts)$, where K is the number of active users in the HAN, and the thermal noise at each receiver is $-95dBm$. Four scenarios with various number of active users are shown in Table 1, where N_w, N_z, and N_b are the numbers of WiFi users, ZigBee users, and Bluetooth users, respectively.

Table 5.1. Four Simulation Scenarios

Total No of active users	N_w	N_z	N_b
$K = 3$	1	1	1
$K = 5$	2	2	1
$K = 8$	3	2	3
$K = 10$	4	3	3

Tables $2 \sim 5$ list the downlink maximum capacity as well as the capacity with equal power allocation scheme for the four scenarios mentioned above. The optimal transmit power allocated to WiFi user(P_w), ZigBee user(P_z), and Bluetooth user(P_b) are also presented in the tables. From these results, we can see that:

1) the downlink capacity with the proposed optimal power allocation scheme based on (5.18) is significantly enhanced compared to the capacity with equal power allocation scheme. Particularly, with beamforming technique at the smart meter, the maximum capacity is slightly decreased as the number of antennas gets larger, while the equal-power capacity dramatically declines;
2) as the number of active users in the HAN increases, the downlink capacity with the proposed optimal power allocation scheme drops due to more interferers from other users existing in the HAN.

Table 5.2. Capacity Comparison and Optimal Power Allocation with Three Users

$K=3$	$C_{opt}(MHz)$	$C_{ave}(MHz)$	$P_w(W)$	$P_z(W)$	$P_b(W)$
$N=2$	18.634	16.655	0.1202	0.1174	0.0623
$N=4$	18.605	15.127	0.1197	0.1182	0.0622
$N=8$	18.586	12.892	0.1194	0.1182	0.0624

Table 5.3. Capacity Comparison and Optimal Power Allocation with Five Users

$K=5$	$C_{opt}(MHz)$	$C_{ave}(MHz)$	$P_w(W)$	$P_z(W)$	$P_b(W)$
$N=2$	18.175	14.551	0.1196	0.1182	0.0712
$N=4$	18.152	14.244	0.1194	0.1182	0.071
$N=8$	18.141	13.591	0.1193	0.1182	0.0712

Table 5.4. Capacity Comparison and Optimal Power Allocation with Eight Users

$K=8$	$C_{opt}(MHz)$	$C_{ave}(MHz)$	$P_w(W)$	$P_z(W)$	$P_b(W)$
$N=2$	17.720	13.641	0.1246	0.1195	0.0628
$N=4$	17.680	12.052	0.1213	0.1186	0.0683
$N=8$	17.661	9.985	0.1202	0.1184	0.0684

Table 5.5. Capacity Comparison and Optimal Power Allocation with Ten Users

$K=10$	$C_{opt}(MHz)$	$C_{ave}(MHz)$	$P_w(W)$	$P_z(W)$	$P_b(W)$
$N=2$	17.183	13.565	0.1199	0.1183	0.0534
$N=4$	16.904	11.615	0.1196	0.1182	0.0565
$N=8$	16.786	9.160	0.1194	0.1182	0.0558

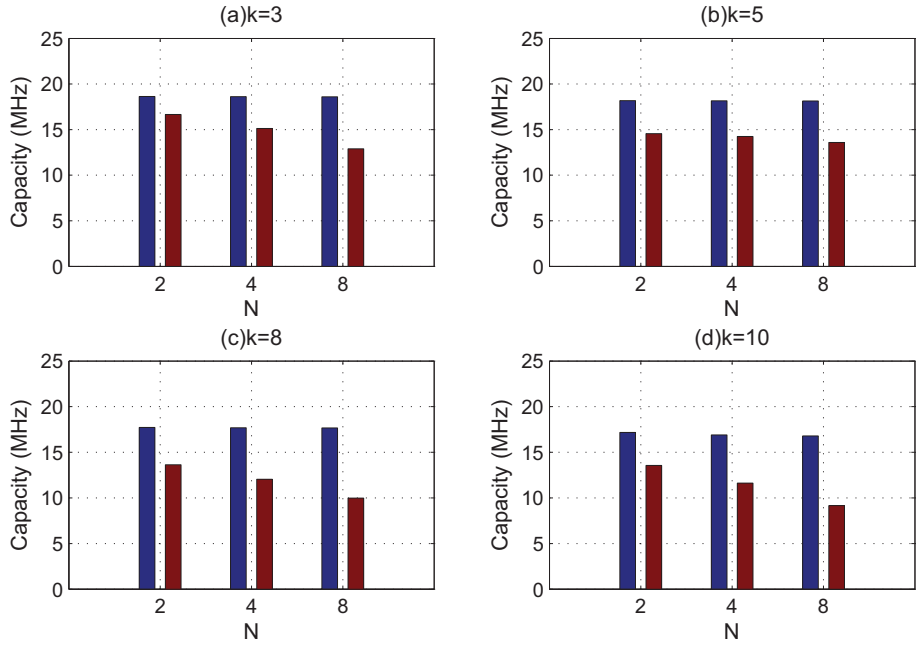

Figure 5.5. Capacity Comparisons.

Figure 5.5 shows the capacity comparisons between the optimal power allocation scheme and equal power allocation scheme for the four scenarios listed in Table 1.

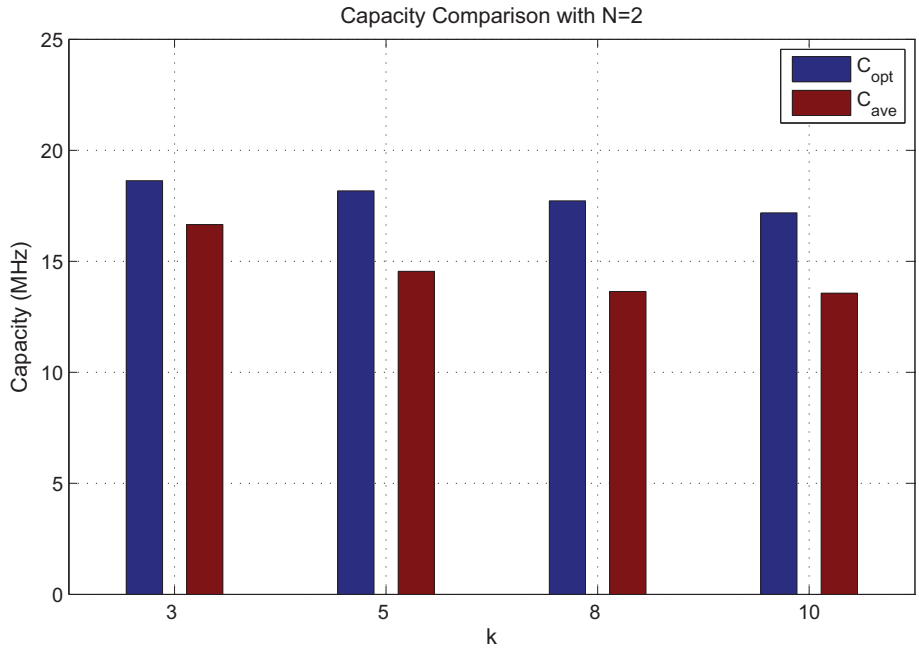

Figure 5.6. Capacity Comparison with N=2.

Figure 5.6 illustrates the comparisons when the number of transmit antennas at the smart meter is fixed ($N = 2$), where the blue bar is the capacity with optimal power allocation scheme, and the red bar is the one with equal power allocation scheme. It is obviously shown that the optimal power allocation scheme outperforms the equal power allocation scheme. Particularly, with more active users in the HAN, the gap between these two schemes is getting larger.

5.5 Conclusion

In this chapter, we proposed an optimal power allocation scheme for downlink capacity in a heterogeneous HAN with application to Smart Grid, in which beamforming technique is applied to the smart meter. The optimization problem of total downlink capacity for the HAN is mathematically a convex optimization problem, and KKT condition, both necessary and sufficient for convex optimization problem,

is thus introduced to derive the optimal solution for power allocation. The property of the minimum transmit power allocated to each user is also investigated by employing the theorem that the sum of independent exponentially distributed random variables follows Erlang distribution. Monte-carlo simulation is taken for total downlink capacity with the presented optimal power allocation scheme, which is also compared with equal power allocation scheme. Numerical results show the dramatic advantage of the proposed optimal power allocation scheme on the basis of the optimal total downlink capacity.

Chapter 6

Hybrid Models of OFDM-based Power Line and Wireless Communications For HAN Security

6.1 Hybrid Models of OFDM-based Power Line and Wireless Communications

This chapter presents two hybrid models of OFDM-based wireless and PL communications in HANs for Smart Grid security. Since OFDM technique is used in both wireless system and PL system, the same OFDM symbols are generated at the transmitter part, which are thus up-converted to the wireless channel ($2.4GHz$) and the PL channel ($2 \sim 30MHz$), separately. For the hybrid model with transmit diversity, Alamouti scheme is adopted as the space time block code (STBC), and the desired transmission data are decoded using maximum likelihood (ML) detector; for the hybrid model, SC scheme is employed to recover the transmission data over the wireless channel and the PL channel. The details of these two hybrid models are elaborated in subsections 6.1.1 and 6.1.2.

6.1.1 Alamouti-code Transmit Diversity

Figure 6.1 shows the hybrid model of OFDM-based wireless and PL communications with transmit diversity. At the transmitter part, the same OFDM symbols are generated, and thus transmitted through wireless channel and PL channel by Alamouti code. At the receiver part, only one receiver with ML detector is used to recover the transmitted OFDM symbols. The Alamouti code for this hybrid model is listed in Table 4.1. At a given OFDM symbol period t_{2k}, two generated OFDM symbols $s[2k]$ and $s[2k+1]$ are simultaneously transmitted to the wireless channel

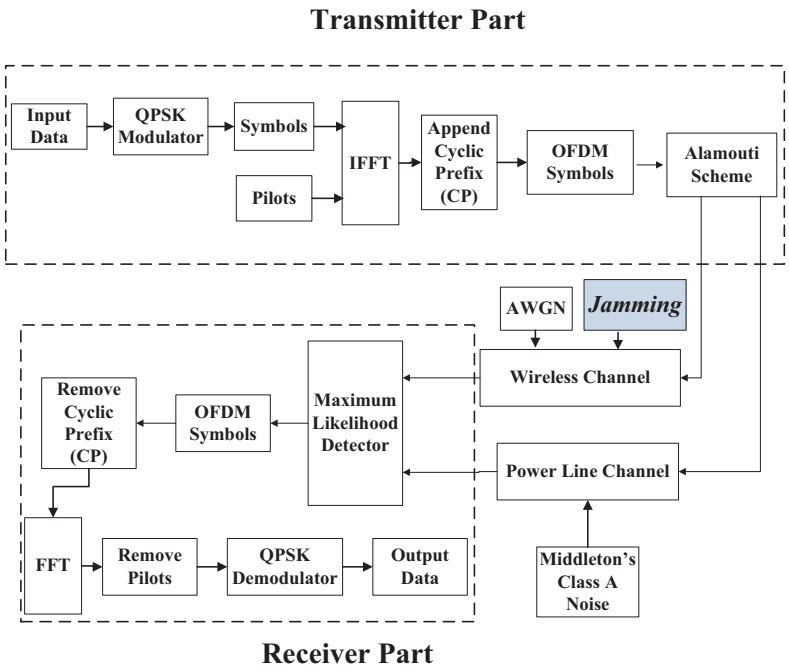

Figure 6.1. The Hybrid Model with Transmit Diversity.

and the PL channel. During the next OFDM symbol period t_{2k+1}, $-s^*[2k+1]$ is up-converted to the wireless channel while $s^*[2k]$ is up-converted to the PL channel. At the receiver, the received OFDM symbols from the wireless channel and the PL channel are combined to get:

$$\begin{aligned} r[2k] =& s[2k]h_{RF}[2k] + s[2k+1]h_{PL}[2k] \\ &+ j[2k] + n_{RF}[2k] + n_{PL}[2k] \end{aligned} \tag{6.1}$$

$$\begin{aligned} r[2k+1] =& -s^*[2k+1]h_{RF}[2k] + s^*[2k]h_{PL}[2k] \\ &+ j[2k+1] + n_{RF}[2k+1] + n_{PL}[2k+1] \end{aligned} \tag{6.2}$$

where h_{RF} and h_{PL} are the wireless channel and the PL channel respectively, and the fading across two adjacent OFDM symbols are assumed to be constant. j is the

jamming signal added to the wireless channel. n_{RF} and n_{PL} are the noise in the wireless channel and the PL channel.

Table 6.1. Alamouti Code for the Hybrid Model with Transmit Diversity

OFDM Symbol Time	**Wireless Channel**	**PL Channel**
t_{2k}	$s[2k]$	$s[2k+1]$
t_{2k+1}	$-s^*[2k+1]$	$s^*[2k]$

The received OFDM symbols in (6.1) and (6.2) are thus sent to ML detector, and the desired transmitted OFDM symbols are estimated as[81]:

$$\widetilde{s}[2k] = h^*_{RF}[2k]r[2k] + h_{PL}[2k]r^*[2k+1] \tag{6.3}$$

$$\widetilde{s}[2k+1] = h^*_{PL}[2k]r[2k] - h_{PF}[2k]r^*[2k+1] \tag{6.4}$$

6.1.2 SC Receive Diversity

As illustrated in Figure 6.2, in-home PL system is incorporated with the wireless communication system to enhance the reliability of HAN in case of a potential security threat from jamming. Channel diversity is realized at the receiver part of the hybrid model, so that a post processing is needed to recover the desired data information at receiver. The hybrid model with receive diversity employs SC scheme, in which the received OFDM symbols with higher signal to noise ratio (SNR)/signal to jamming and noise ratio (SJNR) is selected between the received signals propagated over the wireless channel and the PL channel:

$$r[k] = \begin{cases} s[k]h_{RF}[k] + j[k] + n_{RF}[k] & \text{if } \frac{s^2[k]h^2_{RF}[k]}{j^2[k]+n^2_{RF}[k]} \geq \frac{s^2[k]h^2_{PL}[k]}{n^2_{PL}[k]}, \\ s[k]h_{PL}[k] + n_{PL}[k] & \text{if } \frac{s^2[k]h^2_{RF}[k]}{j^2[k]+n^2_{RF}[k]} < \frac{s^2[k]h^2_{PL}[k]}{n^2_{PL}[k]}. \end{cases} \tag{6.5}$$

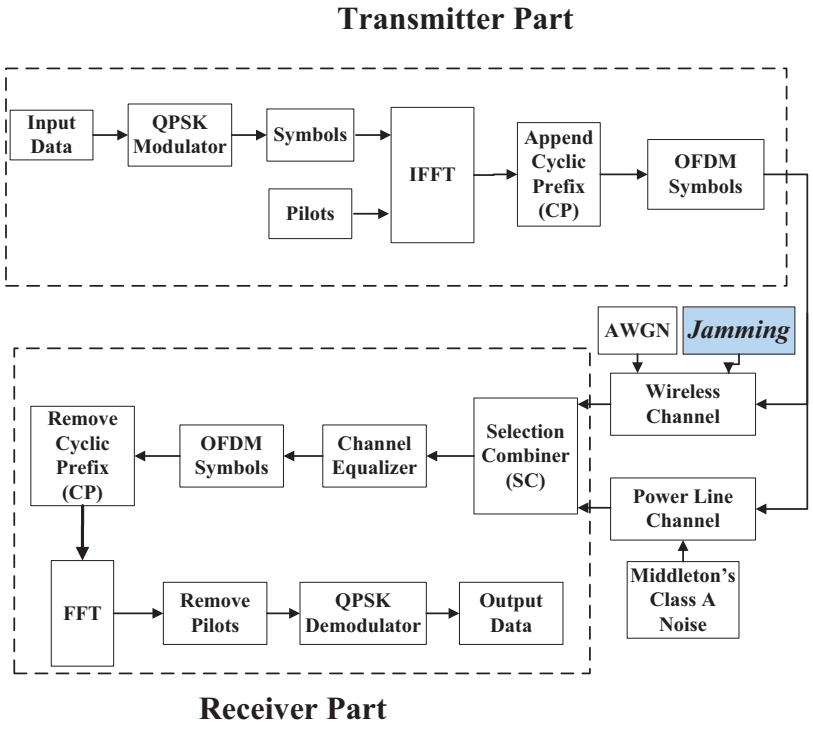

Figure 6.2. The Hybrid Model with Receive Diversity.

Remark 8: SC scheme is highly recommended in the proposed hybrid structure for the following two reasons:

1) it is easy to implement with low complexity;
2) once the wireless channel experiences jamming signals, and the transmitted data information over this radio frequency (RF) medium is severely distorted, to simply abandon the corrupted signal is preferred.

6.2 Hybrid Model Characteristics

This section renders an in-depth investigation of the properties of the hybrid models of OFDM-based wireless and PL communications, including the characteris-

tics of wireless and PL channels, noises in these two channels, as well as jamming to the wireless channel.

6.2.1 Channel Characteristics

Generally, Rayleigh fading is a statistical model to describe signal attenuation over a non-LOS wireless channel environment. In this chapter, Rayleigh flat fading channel is adopted as the wireless channel in the hybrid architectures, and the magnitude of the wireless channel follows Rayleigh distribution.

The PL channel differs from the wireless channel considerably in topology, structure, and physical properties. Zimmermann proposed a multipath model for the PL channel based on physical signal propagation effects including branches and impedance mismatching [41]. The complex frequency response that describes the typical transfer characteristics of PL channel ranging from $500kHz$ to $20MHz$ is:

$$H_{PL}(f) = \sum_{i=1}^{N_p} g_i \cdot e^{-(\alpha_0+\alpha_1 f^k)d_i} \cdot e^{-j2\pi f(d_i/v_p)} \tag{6.6}$$

where i is the number of the path, and the path with the shortest delay has index $i = 1$; N_p is the total number of paths of the PL channel; α_0 and α_1 are attenuation parameters; k is the exponent of the attenuation factor, and the typical values are between 0.5 and 1; f is the operating frequency of the PL channel; d_i is the distance for path i; v_p is the propagation velocity along the PL cable, and v_p is calculated by $v_p = c/e$, where c is the speed of light, and e is the dielectric constant of the PL cable, so that the term d_i/v_p can be denoted as the time delay for path i, namely τ_i; g_i the is the weighting factor for path i, and Galli [42] points out that the path amplitude of the PL channel is log-normally distributed;

6.2.2 Noise Characteristics

The wireless channel mainly experiences a thermal noise that is generally modeled as addictive white Gaussian noise (AWGN). But as to the PL channel, not only background noise, but also impulsive noise exist in power lines, so that AWGN is not suitable to represent the PL noise any more. The PDF of impulsive noise can be expressed as a sum of Gaussian functions with different variances [82]. The Middleton's Class A model is employed in this chapter to characterize the PL noise, and the probability density function (PDF) of Middleton's Class A model is given as:

$$p_{n_{PL}}(z) = \sum_{m=0}^{\infty} \frac{e^{-A} A^m}{m!} \frac{1}{\sqrt{2\pi\sigma_m^2}} \exp(-\frac{z^2}{2\sigma_m^2}) \tag{6.7}$$

where

$$\sigma_m^2 = (\sigma_g^2 + \sigma_i^2)\frac{m/A + \Gamma}{1 + \Gamma} \tag{6.8}$$

is the variance represented by a weighted sum of Gaussian distribution.

Remark 9: It is noteworthy that there are two important parameters used in Middleton's Class A model:

1) *impulsive index A*: it is defined as the average number of source emission per second multiplies the mean duration of a typical interfering source emission[83]. Small value of A means the statistics of noise is away from Gaussian distribution, but as A is made large, it approaches Gaussian distribution.
2) *Gaussian-to-Impulsive variance Ratio (GIR)* Γ: it is denoted as $\Gamma = \sigma_g^2/\sigma_i^2$, where σ_g^2 is Gaussian noise variance, and σ_i^2 is the impulsive noise variance. Therefore, small value of Γ indicates an impulsive noise with relatively large power.

6.2.3 Jamming Characteristics

Jamming is defined as the act of deliberately directing electromagnetic energy towards an RF communication system in an attempt to disrupt or prevent signal transmission, and is viewed as a special case of denial of service (DoS) attacks. The distinction between jamming and interference is that generally a jamming signal is intentionally generated to deteriorate the signal to noise ratio (SNR) over the wireless channel, whereas an interference signal comes from the transmitted radio of other coexisting wireless systems. In a PHY jamming attack, the jammer emits "useless" information to the designated RF channel, which could be be white noise or any signal that resembles network traffic [84].

In this chapter, a random complex Gaussian signal is selected as jamming inserted to the wireless channel with a certain probability in time domain as $P(Jam)$.

Table 6.2. Parameter Settings for Monte-Carlo Simulation

Parameters	**Symbols**	**Values**
Symbol duration	T_s	4×10^{-6}s
FFT size	N_{fft}	64
CP size	N_{cp}	16
Maximum Doppler shift	f_d	100Hz
Operating frequency of the PL channel	f_{PL}	3MHz
Attenuation parameters	α_0, α_1	-2.03×10^{-3}, 3.75×10^{-7}
Exponent of the attenuation factor	k	0.7
Total number of path in the PL channel	N_{path}	4
Distances of the paths	d_i	10m, 10.3m, 10.6m, and 11m
Dielectric constant of the PL cable	e	1.4
GIR	Γ	0.01

6.3 Simulation

Considering the vulnerability of the wireless system to the security threat from jamming, the in-home PLC system is incorporated into the HAN for Smart Grid. In this section, BER performance of the hybrid architectures presented in Section 6.1 is investigated by Monte-Carlo simulation. In the simulation scenarios, the parameter settings are listed in Table 4.2. At the transmitter part, QPSK is employed to constellate the input data bits into complex symbols, which are thus assembled into 52 OFDM subcarriers, and the symbol duration is 4×10^{-6}s. 12 pilots are inserted to mitigate intercarrier interference (ICI) and the FFT size is 64. The size of cyclic prefix (CP), which effectively eliminates intersymbol interference (ISI), is 16. In the simulation, Rayleigh flat fading channel is generated by Jake's model method, with the maximum Doppler shift as $100Hz$. For the signal propagation along PL cables, the OFDM symbols generated at the transmitter are up-converted to the $3MHz$ four-path PL channel, in which the attenuation parameters α_0 and α_1 are -2.03×10^{-3} and 3.75×10^{-7}; the exponent of the attenuation factor is 0.7; the lengths of the four paths are set as $10m$, $10.3m$, $10.6m$, and $11m$; the dielectric constant of the PL cable is 1.4. GIR of the Middleton's Class A noise is set as 0.01. In addition, the channel side information (CSI) is assumed to be known at the receiver. Thus in the simulation, the channel equalization is simply achieved by removing the channel information from the data after receive diversity processing.

The BER comparison is over single wireless channel and single PL channel is illustrated in Figure 6.3. Due to the harsh PL channel environment, the PLC exhibits worse BER performance compared to the wireless system.

The BER performance over single wireless system is shown in Figure 6.4. A potential jamming is added to the wireless channel with the probabilities of $Pr_J = 0.02$

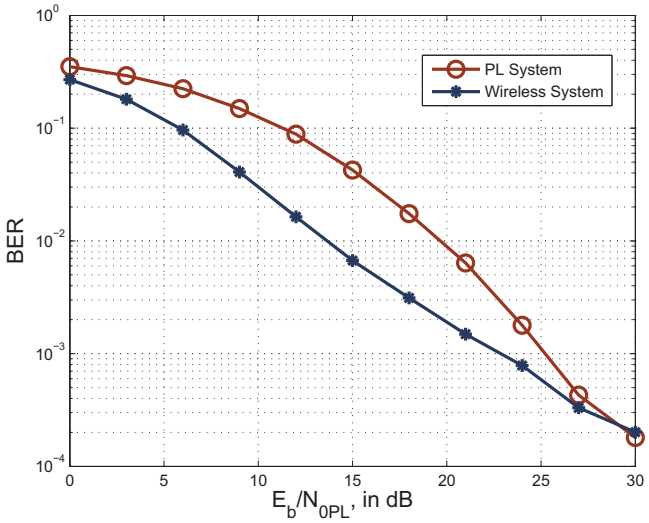

Figure 6.3. BER of Wireless System and PL System, no Jamming.

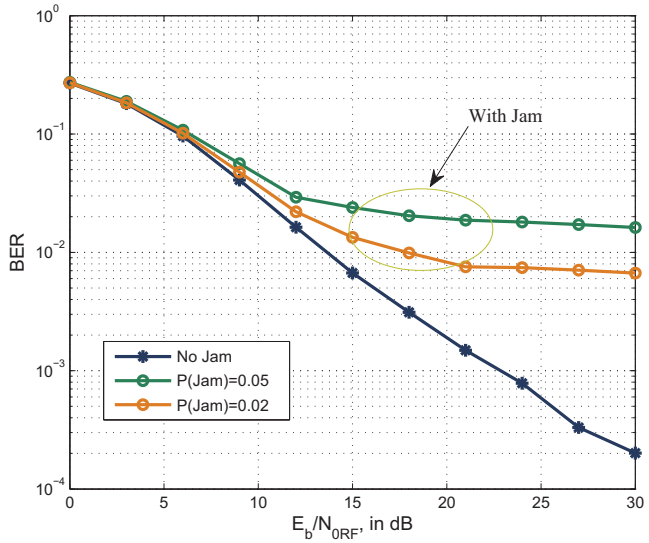

Figure 6.4. BER of Single Wireless System.

and 0.05. Once the wireless channel is contaminated by the jamming, the communication reliability is dramatically reduced.

Figures 6.5 and 6.6 illustrate the BER performance of the hybrid system with SC receive diversity. Figure 6.5 is the one with no jamming to the wireless channel,

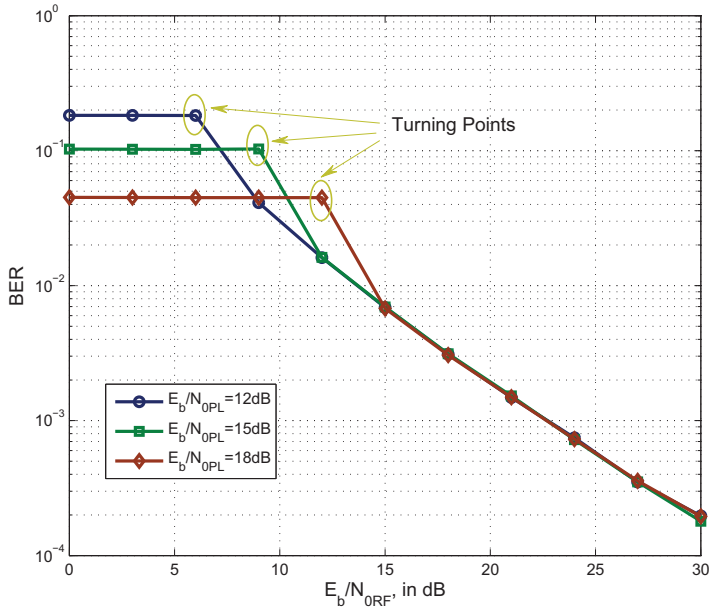

Figure 6.5. BER of the Hybrid Model with Receive Diversity, no Jamming.

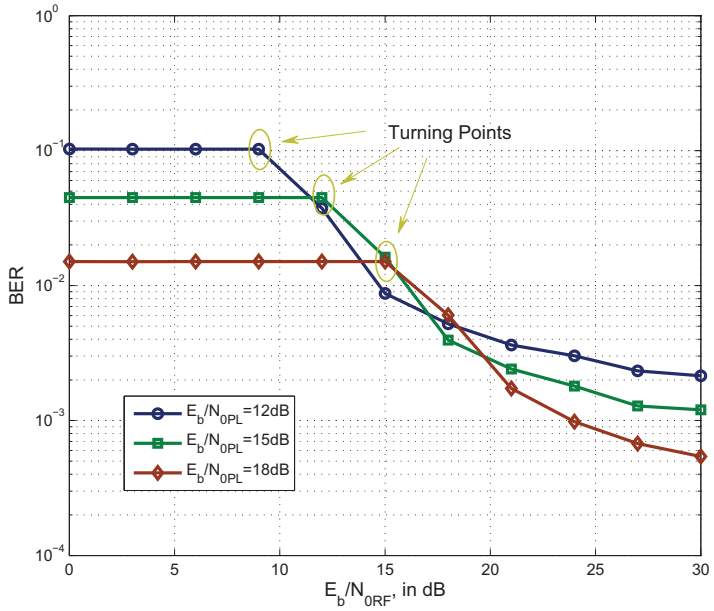

Figure 6.6. BER of the Hybrid Model with Receive Diversity, $P(Jam) = 2\%$, and $SJR = 5dB$.

while Figure 6.6 is the one with jamming of $P(Jam) = 2\%$ and signal to jamming ratio $SJR = 5dB$. The PL channel is under three different conditions, with $E_b/N_{0_{PL}}$ as 12dB, 15dB, and 18dB, and the impulsive index A is set as 0.3.

Remark 10: From Figures 6.5 and 6.6:

1) it is noteworthy that there is an apparent turning point in each plot, as circled. These turning points can be explained by exploring the receive diversity scheme used at the receiver part of the hybrid architecture. The SC scheme always chooses the branch with the higher SNR, so that when no jamming is added to the wireless channel, as $E_b/N_{0_{RF}}$ is getting larger, the transmitted signal over the wireless channel is selected at the receiver, and the three plots overlap in Figure 6.5.
2) By an intensive investigation on the positions of the turning points, we can see that the x-axis values of the turning points are all smaller than the corresponding $E_b/N_{0_{PL}}$. Taking the plot with $E_b/N_{0_{PL}} = 15dB$ in Figure 6.5 as an example, the turning point occurs when $E_b/N_{0_{RF}} = 9dB$. This phenomenon indicates the severer channel condition of the PL channel compared to the wireless channel. And once a potential jamming is added to the wireless channel, which deteriorates the wireless channel, the turning points appear rightwards, as shown in Figure 6.6.

For the combinational model with Alamouti-code transmit diversity, Figure 6.7 shows its BER performance with three different values of E_bN_{0PL}. The three solid lines are with no jamming to the wireless channel, and the three dashed plots are with a potential jamming of $P(Jam) = 2\%$ and $SJR = 5dB$. For the PL channel, the impulsive index A is still 0.3. Figure 6.8 illustrates the impact of Middleton's Class A noise in the PL channel on the BER performance of the hybrid model. The solid lines are the BER performance with no jamming added to the wireless channel, but

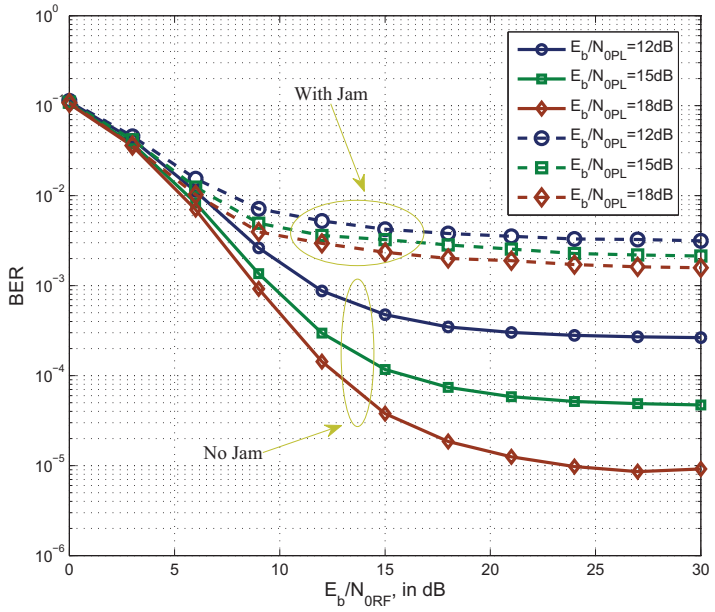

Figure 6.7. BER of the Hybrid Model with Transmit Diversity, $P(Jam) = 2\%$, $A = 0.3$, and $SJR = 5dB$.

for the PL channel, E_bN_{0PL} is set to be $15dB$, and A is selected as 1, 0.3, and 0.1, which indicate various probabilities of pulses overlapping in time. When the wireless channel experiences a jamming of $P(Jam) = 2\%$ and $SJR = 5dB$, the three BER plots totally overlap no matter what the value of A is.

Remark 11 An interesting observation from Figure 6.8 is that as A increases BER decreases. This could be explained by the property of the impulsive index A, which is mentioned in subsection 6.2.2. Large A indicates that the statistics of Middleton's Class A noise approaches Gaussian distribution, while small A means that the noise in the PL is more like impulsive noise. For $A = 1$, approximately $1dB$ gain is obtained at $BER = 2 \times 10^{-4}$ compared to $A = 0.3$, and $3dB$ gain compared with $A = 0.1$.

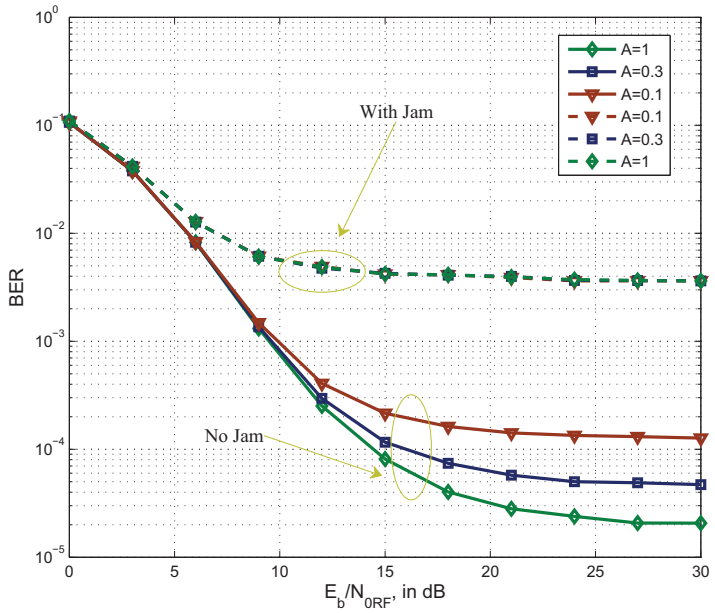

Figure 6.8. BER of the Hybrid Model with Transmit Diversity, $P(Jam) = 2\%$, $E_b N_{0PL} = 15dB$, and $SJR = 5dB$.

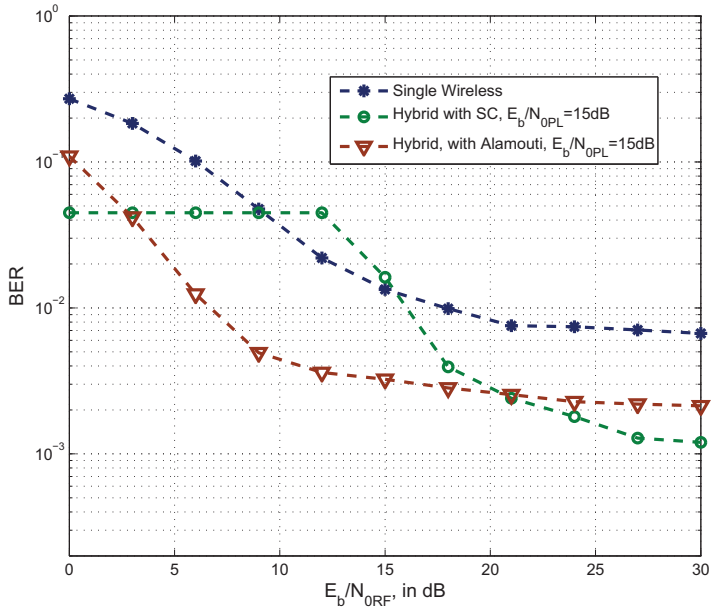

Figure 6.9. BER Comparison of Hybrid Models, $P(Jam) = 2\%$, and $SJR = 5dB$.

Figure 6.9 is the BER comparison of a single wireless communication system, and the two hybrid models of wireless and PL communication systems with transmit diversity and receive diversity. The wireless channels in the three systems are all threatened by a potential jamming of $P(Jam) = 2\%$ and $SJR = 5dB$. It is shown that the hybrid model with Alamouti-code transmit diversity maintains BER improvement over the single wireless system. But for the hybrid model with SC receive diversity, only when $E_b N_{0RF}$ is large enough after the turning point, BER performance could be guaranteed.

6.4 Conclusion

In this chapter, a combination of the OFDM-based wireless communication and the existing in-home PL system is proposed as a hybrid HAN for Smart Grid. Particularly, two hybrid model with Alamouti-code transmit diversity and SC receive diversity are presented. Monte-Carlo simulation results show that the proposed hybrid structures effectively enhance the BER performance of the HAN, even when the wireless channel experiences a potential jamming. The combination of wireless communication and PL communication provides a new concept of the reliable and secure HANs for Smart Grid, with the advantages as:

1) *low cost*: due to the ubiquity of power lines and wall outlets, the combinational structures of wireless communication and the existing PL networks in HANs for Smart Grid are cost-effective;
2) *easy to implement*: OFDM techniques could be used in both wireless communication and PL communications, so that for the hybrid model with Alamouti-code transmit diversity, only one receiver is required to recover the transmitted signals, and for the hybrid model with SC receive diversity, only one transmit-

ter is used to generate the same transmission OFDM signals, which are thus up-converted to wireless channel and PL channel separately;

3) *high security and reliability*: the hybrid models tolerate jamming to the wireless channel well, provide a reliable communication system, and thus the security is guaranteed in HANs for Smart Grid.

Chapter 7

Scaling Laws for the Ergodic Capacity of Hybrid Wireless Networks with Distributed Base Stations

7.1 Preliminaries

Similar to [85], we consider a two-tier hybrid wireless network on the surface a square area: the lower tier consists of n nodes, which are uniformly and independently distributed in a square area of $[0, \sqrt{n}] \times [0, \sqrt{n}]$; the upper tier is composed of b base stations, and the deployment of the base stations follows the *grid deployment* method [86], that is, the square area is divided into b smaller squares, which are also called *cells* and the base station locates at the center of each cell. Base stations do not serve as data sources or data destinations, but only forward traffic between cells in the infrastructure mode. Furthermore, we assume $b = o(\frac{n}{\log n})$ to make sure that b tends to infinity as $n \to \infty$, but at a much slower rate. When $n \to \infty$, the number of nodes, n_c, in each cell of side length $c = \sqrt{n/b}$ is bounded by $\Theta(\frac{n}{b})$ [52].

Since the throughput capacity of hybrid wireless networks is *interference-limited*, we introduce 1) opportunistic communication to eliminate *intra-cell* interference, 2) frequency reuse to reduce *other-cell* interference (OCI), and 3) distributed base station (DBS) to achieve transmit/receive *diversity*.

7.1.1 Opportunistic Communication

According to the protocol model presented in [51], every other node k simultaneously transmitting over the same channel as node s should satisfy $d_{kd} \geq (1+\Delta)d_{sd}$, where Δ is a positive constant to model a guard zone, d_{kd} and d_{sd} are the distances of

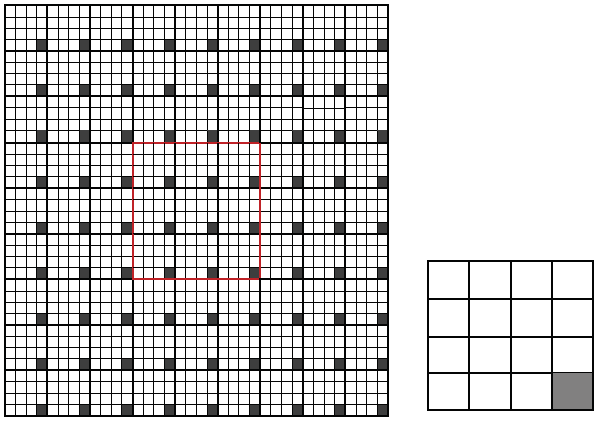

Figure 7.1. Frequency Reuse Scheme for $a = 1$..

the opportunistic source node k to the destination node d and the scheduled source node s away from the destination node d, respectively.

Assume, for any scheduled source s, there are K nodes within the same cell, whose Euclidean distance away from destination node d is greater than d_{sd}. without loss of generality, we have $d_{0d} \leq d_{1d} \leq \ldots d_{kd} \leq \ldots \leq d_{Kd}$, $(k = 0, 1, \ldots, K)$. Allowing these K nodes to be opportunistic sources and transmit data simultaneously to the destination node d, the channel now becomes a fading multiple-access channel. The optimal multiple access strategy now is for all these sources to spread their signal across the entire bandwidth, much like the the CDMA system [53]. However, rather than decoding every node treating the intra-cell interference from other nodes as noise, a SIC technique is employed at the receiver. That is, after one node is decoded, its signal is deducted from the aggregate received signal before the next node is decoded, which significantly limits the intra-cell interference. It allows the system to benefit

from *multiuser diversity*. The SIC strategy maximizes the sum rate and achieves a set of sum rate satisfying

$$\begin{aligned} R_0 &\leq \log\left(1+\frac{\underline{P}_0\cdot|h_{0d}|^2}{\sigma^2}\right) \\ &\vdots \\ \sum_{k=0}^{K} R_k &\leq \log\left(1+\frac{\sum_{k=0}^{K}\underline{P}_k\cdot|h_{kd}|^2}{\sigma^2}\right) \end{aligned} \tag{7.1}$$

where R_k denotes the kth node's achievable rate, $\underline{P}_k$ is the transmit power from the k_{th} source node, h_{kd} is and the composite channel between the k_{th} source node and the destination node, and σ^2 is the power of AWGN.

7.1.2 Frequency Reuse

Other-cell interference caused by simultaneous signal transmission in difference cells may still exist. Fortunately, such interference can be minimized by employing the *frequency reuse* concept as illustrated in [87]. Specifically, we first group the cells together to form a certain number of clusters. Then, we assign different frequency bands to cells within the same cluster; however, among different clusters, these frequency bands will be reused. Hence, the transmissions in the cells (in different clusters) with the same frequency can be carried out simultaneously without causing excessive inter-cell interference as long as the distance between these cells is large enough. The frequency reuse rule from [52] [88] is borrowed: for any integer $a > 0$, there exists a reuse policy with M^2 (*reuse factor*) frequency bands where $M = 2(a+1)$, such that all cells in the network can transmit simultaneously with bounded interferences.

Figure 7.1 shows an example of the frequency reuse scheme with $a = 1$. A reuse set of $M^2 = 4(a+1)^2 = 16$ frequency bands, $\{f_1, f_2, \cdots, f_{16}\}$, is assigned to the 16 cells of each cluster. Note that for a given cell, there is always one cell in every cluster

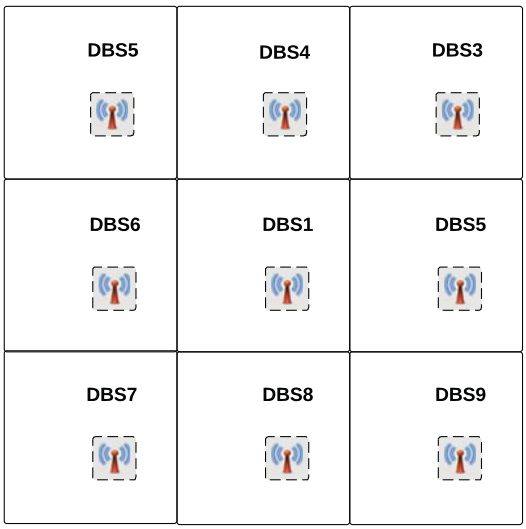

Figure 7.2. Hybrid Wireless Network with $N = 9$ Distributed Base Stations.

that shares the same frequency band. In the left subfigure of Figure 7.1, the shaded cells occupy the same frequency, and the right subfigure is a cluster including 16 cells.

7.1.3 Distributed Base Station

Traditionally, multiple antennas are used to provide *diversity gain* and increase the reliability of wireless links. In this subsection, we will present a new way to achieve transmit/receive diversity - distributed based stations (DBS). As introduced in the last subsection, the frequency resource is reused in each cluster. For a target cell, it can be served by not only the local base station, but also neighbor base stations from the cells of adjacent clusters sharing the same frequency band.

Next, we propose the definition of the hybrid wireless network with N DBS.

Definition 8: In the hybrid wireless network, N DBS can cooperatively serve N cells in which the N DBS are located. And each DBS is from the cells of N adjacent clusters sharing the same frequency band.

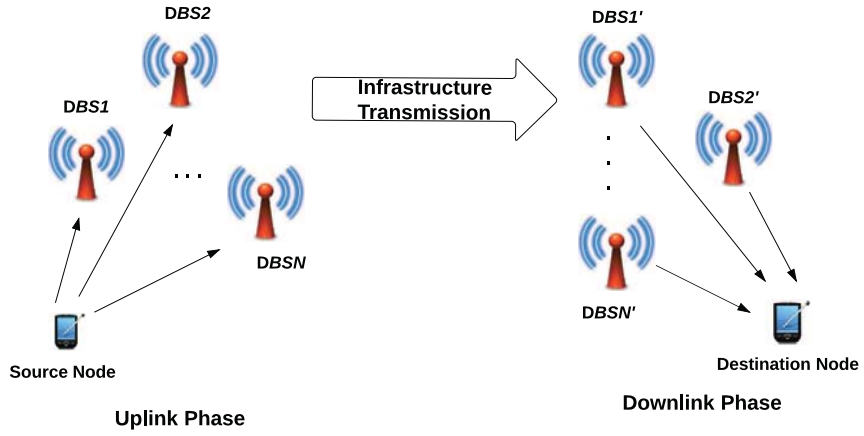

Figure 7.3. Infrastructure Mode with Distributed Base Stations.

Figure 7.2 illustrates an example of the hybrid wireless network with $N = 9$ DBS, in which each solid square area denotes a cluster, and the nine dashed squares are the cells sharing the same frequency.

7.2 Modeling of Hybrid Wireless Networks with Distributed Base Stations

In this chapter, we investigate the traffic transmission between the nodes which are located in different cells with the aid of cooperative DBS, and thus the infrastructure transmission mode is implemented as shown in Figure 7.3. N DBS are in charge of forwarding signals to/from the nodes in the shaded cells as illustrated in Figure 7.1. We assume N_{BS} antennas are equipped in the DBS, while the nodes has single antenna ($N_{nd} = 1$). The model of hybrid wireless networks with DBS has the following properties:

1) The whole transmission procedure is composed of three phases: during the *uplink phase*, the source node first transmit traffic to all the DBS under the existence of opportunistic nodes in the same cell; And then, in the *transport phase*, the co-working DBS decode the received data and send them to the DBS which are serving

the destination cell via the wired network; Furthermore, the data is transmitted to the destination node also by cooperative DBS during the *downlink phase*.

2) In uplink phase, the received signal at the DBS is described as:

$$\underline{y_u} = \sum_{k=0}^{\kappa} \sqrt{\underline{P_u}} \underline{H_k^H} x_k + \underline{i_u} + \underline{n} \tag{7.2}$$

where $\underline{P_u}$ is the transmit power at each source node or opportunistic nodes; κ is the number of opportunistic nodes which simultaneously generate traffic to N DBS; $\underline{H_k}$: $\underline{C}^{1\times N\cdot N_{BS}}$ is the composite channel matrix from the k_{th} node to N DBS; x_k represents the normalized transmit symbol from the k_{th} node; $\underline{i_d}$ denotes the uplink OCI, which is colored Gaussian distributed with covariance matrix $\underline{K_d}$; $\underline{n} \sim \underline{CN}(0, \sigma_n^2 I_{N\cdot N_{BS}})$ is the AWGN.

Particularly, $\underline{H_k}$ consists N independent subchannel matrices to each DBS:

$$\underline{H_k} = [\underline{H_1^k} \quad \underline{H_2^k} \ldots \underline{H_n^k} \ldots \underline{H_N^k}] \tag{7.3}$$

where $\underline{H_n^k} : \underline{C}^{1\times N_{BS}}$ represents the composite fast fading channel matrix from the k_{th} node to the n_{th} DBS:

$$\underline{H_n^k} = h_n^{ls} \underline{H_{n,k}^{ss}}, \quad n = 1, 2, \ldots N \tag{7.4}$$

where $h_n^{ls} = \frac{e^{-\gamma d_n/2}}{d_n^{\alpha/2}}$ denotes the large-scale path loss to the n_{th} DBS, in which the distance between the n_{th} DBS and the source node is d_n, and γ and α are the absorption constant of the attenuation and path-loss exponent. Here we assume all the nodes have approximately the same distance from the each DBS; $\underline{H_{n,k}^{ss}} : \underline{C}^{1\times N_{BS}}$ is the small-scale Rayleigh fading channel matrix, in which all the entries are standard normal distributed.

3) Similarly, in the downlink phase, the received signal at the destination node is expressed as:

$$y_d = \sqrt{\frac{P_d}{N_{BS}}} \underline{H}^H \underline{x} + i_d + n \tag{7.5}$$

where $\underline{P}_d$ the transmit power at each DBS; $\underline{H} : \underline{C}^{N \cdot N_{BS} \times 1}$ is the composite channel matrix from N DBS to the destination node; $\underline{x} : \underline{C}^{N \cdot N_{BS} \times 1}$ represents the normalized transmit symbol matrix from each transmit antenna; i_d denotes the OCI to the destination node.

Particularly, $\underline{H}$ consists N independent subchannel matrices from each DBS:

$$\underline{H} = [\underline{H}_1 \quad \underline{H}_2 \dots \underline{H}_n \dots \underline{H}_N]^T \tag{7.6}$$

where $\underline{H}_n : \underline{C}^{N_{BS} \times 1}$ represents the composite fast fading channel matrix from the n_{th} DBS to the destination code:

$$\underline{H}_n = h_n^{ls} \underline{H}_n^{ss}, \quad n = 1, 2, \dots N \tag{7.7}$$

where $h_n^{ls} = \frac{e^{-\gamma d_n/2}}{d_n^{\alpha/2}}$ denotes the large-scale path loss from the n_{th} DBS; $\underline{H}_n^{ss} : \underline{C}^{N_{BS} \times 1}$ is the small-scale Rayleigh fading channel matrix, in which all the entries are standard normal distributed.

4) The OCI is limited with the introduction of frequency resue strategy. The downlink OCI $I_d = \Theta((\frac{n}{b})^{-\frac{\alpha}{2}})$, and the uplink OCI $I_u = \Theta((\frac{n}{b})^{1-\frac{\alpha}{2}})$ [52]. For a certain target cell, the OCI is treated as *addictive colored Gaussian noise*.

5) From [52], we know that for a given source and destination pair in any cell, there are $\Theta(\frac{n}{b})$ nodes in the same cell that have greater distances from the destination than the source node. Therefore, with N DBS cooperatively serving the cells, given a source node communicating to the DBS, there exist *at most* $\kappa = \Theta(\frac{Nn}{b})$ nodes in the cells sharing the same frequency that can serve as *opportunistic nodes*.

6) We assume a total bandwidth of W Hz for data transmission under infrastructure mode, which is split into two bands: W_u Hz for uplink, and W_d Hz for downlink. Obviously, $W = W_u + W_d$. Taking into account the benefits of opportunistic sources and SIC decoding strategy, we found that the bandwidth allocated

to a scheduled source for uplink transmission is $\eta_u W_u = \frac{\kappa+1}{Nn_c}\frac{W_u}{M^2} = \Theta(W_u)$ Hz, where M^2 is the frequency reuse factor. While for downlink transmission, the bandwidth allocated to each destination node is limited to $\eta_d W_d = \frac{1}{Nn_c}\frac{W_d}{M^2} = \Theta(\frac{b}{Nn}W_d)$ Hz.

7.3 Ergodic Throughput Capacity

In this section, we pay our attention to the ergodic throughput capacity of the hybrid wireless network with DBS under infrastructure node. Given a source-destination pair (s, d) in the network, the transmission rate R from the source node s to the destination node d is upper-bounded by the capacity of the virtual MIMO channel. Specifically, during the uplink phase, the schedule source and the opportunistic nodes transmit all traffic to N DBS. And in the transport phase, the base stations are connected by high bandwidth long range links and thus it is assumed that there is no capacity constraint within the infrastructure transmission [89]. Subsequently, the data is retransmitted to the destination node during the downlink phase.

Lemma 1: Consider a wireless network with N DBS, for a certain time slot, if the information rate R is achievable between a node and N DBS, we have,

$$R \leq \frac{1}{2}\log\left(1 + \frac{\sum_{j=1}^{N} P_u \lambda_j^2}{I_u + \sigma_n^2}\right) + \epsilon \tag{7.8}$$

where each λ_j corresponds to an *eigenmode* of the channel, and $\epsilon \to 0$ as the probability of error tends to zero.

The detailed derivation of Lemma 1 is provided in Appendix. The channel is decomposed into N parallel sub-channels via singular value decomposition (SVD). Lemma 1 can serve as the essential principle in investigating the information transmission limits over general fading channels.

Definition 7: For a hybrid wireless network of n nodes, and b base stations, an ergodic throughput capacity of $T(n, b, N)$ bit/s for each node is feasible under the

infrastructure mode, if with N distributed base stations, there is a spatial and temporal scheme for scheduling transmissions such that every node can averagely receive $T(n, b, N)$ bit/s over all possible channel realizations. And the ergodic throughput capacity is determined by:

$$T(n, b, N) = \min\{T^u(n, b, N), T^d(n, b, N)\} \tag{7.9}$$

where $T^u(n, b, N)$ and $T^u(n, b, N)$ are the uplink ergodic throughput capacity and downlink ergodic throughput capacity, respectively.

7.3.1 Uplink Ergodic Throughput Capacity

In the fasting fading scenario, the ergodic capacity is defined as the ensemble average of channel capacity over all possible channel realizations [90]. If we assume the channel state information is known only at the receiver (CSIR), combining with the received signal model of the uplink phase in (7.2), the ergodic capacity with opportunistic communications and SCI scheme is expressed as:

$$C^u = \mathbb{E}[\log(1 + \frac{\sum_{k=0}^{\kappa} \underline{P}_u \|\underline{H}_k\|^2}{I_u + \sigma_n^2})] \tag{7.10}$$

Given the properties of the composite uplink channel matrix in (7.3) and (7.3), the ergodic capacity of the source node and opportunistic nodes is further derived as:

$$\begin{aligned} C^u &= \mathbb{E}[\log(1 + \frac{\underline{P}_u}{I_u + \sigma_n^2} \sum_{k=0}^{\kappa} \sum_{n=1}^{N} (h_n^{ls})^2 \|\underline{H}_{n,k}^{ss}\|^2)] \\ &\overset{(a)}{=} \mathbb{E}[\log(1 + sinr_u \sum_{n=1}^{N} \beta_n \sum_{k=0}^{\kappa} \|\underline{H}_{n,k}^{ss}\|^2)] \end{aligned} \tag{7.11}$$

At step (a), $\frac{\underline{P}_u}{I_u + \sigma_n^2}$ is denoted as $sinr_u$, and $(h_n^{ls})^2$ is denoted as β_n.

Since the entries of $\underline{H}_{n,k}^{ss}$ are independent identically distributed (*i.i.d.*) complex normal random variables (r.vs.), $\|\underline{H}_{n,k}^{ss}\|^2$ follows Chi-square distribution with $2N_{BS}$ degrees of freedom, which is also Gamma distributed: $\|\underline{H}_{n,k}^{ss}\|^2 \sim \Gamma(N_{BS}, 2)$.

Furthermore, denoting $\beta_n \sum_{k=0}^{\kappa} \|\underline{H}_{n,k}^{ss}\|^2$ as φ_n and thus denoting $\sum_{n=1}^{N} \varphi_n$ as φ, we can see that $\varphi_n \sim \Gamma(\kappa N_{BS}, 2\beta_n)$.

To this step, it is obvious that $\varphi_n, n = 1, 2, \ldots, N$ are independent but not identically distributed(*i.n.d*). Our concern is what kinds of properties φ has. One method called *second order moment matching* to obtain another reasonable Gamma approximation of the sum of a series independent but weighted Chi-square distributed r.vs. was proposed by R. W. Health *et al* [48].

Given $\varphi_n \sim \Gamma(\kappa N_{BS}, 2\beta_n)$, φ can be approximated as another Gamma distribution as $\Gamma(k_\varphi, \theta_\varphi)$, with the same first and second moments as:

$$k_\varphi = \frac{\kappa N_{BS}(\sum_{n=1}^{N} \beta_n)^2}{\sum_{n=1}^{N}(\beta_n)^2} \quad and \quad \theta_\varphi = \frac{2\sum_{n=1}^{N}(\beta_n)^2}{\sum_{n=1}^{N} \beta_n} \tag{7.12}$$

and the mean and variance are separately:

$$\mu_\varphi = 2\kappa N_{BS} \sum_{n=1}^{N} \beta_n \quad and \quad \sigma_\varphi^2 = 4\kappa N_{BS} \sum_{n=1}^{N} \beta_n^2 \tag{7.13}$$

Here, $\kappa + 1$ is approximated by κ.

Clearly, no closed-form solution exists for this ergordic capacity. However, approximating $\log(1 + sinr_u \cdot \varphi)$ by $\log(sinr_u \cdot \varphi)$ for large $sinr_u$, the ergodic capacity is expressed as:

$$\begin{aligned}
C^u &= \mathbb{E}[\log(1 + sinr_u \sum_{n=1}^{N} \beta_n \sum_{k=0}^{\kappa} \|\underline{H}_{n,k}^{ss}\|^2)] \\
&= \mathbb{E}[\log(1 + sinr_u \cdot \varphi)] \\
&\approx \mathbb{E}[\log(sinr_u \cdot \varphi)] \\
&\overset{(a)}{=} \log_2 sinr_u + \log_2 e \cdot \psi(k_\varphi) + \log_2(\theta_\varphi) \\
&\overset{(b)}{=} \log_2 sinr_u + \log_2 e[\ln k_\varphi + \frac{1}{k_\varphi} + O(\frac{1}{k_\varphi^2})] + \log_2(\theta_\varphi) \\
&\overset{(c)}{=} \log_2 sinr_u + \log_2 e\{\ln[\frac{\kappa N_{BS}(\sum_{n=1}^{N} \beta_n)^2}{\sum_{n=1}^{N}(\beta_n)^2}] + \frac{\sum_{n=1}^{N}(\beta_n)^2}{\kappa N_{BS}(\sum_{n=1}^{N} \beta_n)^2} \\
&+ O(\frac{[\sum_{n=1}^{N}(\beta_n)^2]^2}{\kappa^2 N_{BS}^2(\sum_{n=1}^{N} \beta_n)^4})\} + \log_2[\frac{2\sum_{n=1}^{N}(\beta_n)^2}{\sum_{n=1}^{N} \beta_n}]
\end{aligned} \tag{7.14}$$

where $\psi(k_\varphi)$ in step (a) is the digamma function, and its asymptotic approximation $\psi(k_\varphi) = \ln k_\varphi + \frac{1}{k_\varphi} + O\big(\frac{1}{k_\varphi^2}\big)$ is used to get step (b). Further, according to (7.12), step (c) is derived to obtain the final expression of C^u.

Since $I_u = \Theta((\frac{n}{b})^{1-\frac{\alpha}{2}})$, together with $\kappa = \Theta(\frac{Nn}{b})$, we can conclude that in the high SINR scenario, the uplink ergodic capacity is upper bounded by $\Theta(\log(\frac{NN_{BS}n}{b}))$, namely, $C^u = O\big(\log(\frac{NN_{BS}n}{b})\big)$.

Similarly, employing $\log(1 + sinr_u \cdot \varphi) \approx \log_2 e \cdot sinr_d \cdot \varphi$ for small $sinr_u$,

$$\begin{aligned} C^u &= \mathbb{E}[\log(1 + sinr_u \sum_{n=1}^{N} \beta_n \sum_{k=0}^{\kappa} \|\underline{H}_{n,k}^{ss}\|^2)] \\ &= \mathbb{E}[\log(1 + sinr_u \cdot \varphi)] \\ &\approx \mathbb{E}[\log_2 e \cdot sinr_u \cdot \varphi] \\ &\overset{(a)}{=} \log_2 e \cdot sinr_u \mathbb{E}[\varphi] \\ &= \log_2 e \cdot sinr_u \cdot 2\kappa N_{BS} \sum_{n=1}^{N} \beta_n \end{aligned} \tag{7.15}$$

And the uplink ergodic capacity is upper bounded by $\Theta(\frac{NN_{BS}n}{b})$, namely, $C^u = O\big(\frac{NN_{BS}n}{b}\big)$.

Theorem 3: For a hybrid wireless network of n nodes and N distributed base stations over *Rayleigh* fading channels, if the total number of base stations $b = o(\frac{n}{\log n})$, the *uplink ergodic throughput capacity* under the *infrasctructure* transmission mode at high SINR is

$$T^u(n, b, N) = O\big(\log(\frac{NN_{BS}n}{b})W_u\big) \quad bit/s \tag{7.16}$$

And at low SINR:

$$T_{infra}^d = O\big(\frac{NN_{BS}n}{b}W_u\big) \quad bit/s \tag{7.17}$$

where N_{BS} is the number of transmit antennas equipped at the base station.

Numerical simulations are presented to to validate the scaling laws of the ergodic capacity in the uplink phase. Figure 7.4 shows the ratio between ergodic capacity and

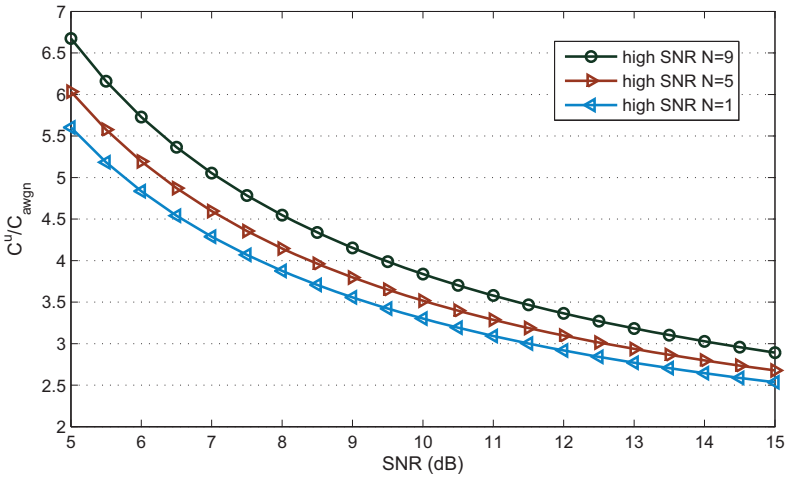

Figure 7.4. Ergodic Capacity in the uplink phase with $N_{BS} = 4$.

the capacity under AWGN at high SNR with $N_{BS} = 4$ antennas at DBS ($\kappa = 50$), in which $N = 1$ indicates no cooperation between base stations. By comparing the performance, one can attribute the capacity improvement to the number of DBS involved in (N). Similarly, Figure 7.5 illustrates uplink performance at high SNR with $N = 9$ DBS. It is obvious that the ergodic capacity scales in $O\big(N_{BS}\big)$.

7.3.2 Downlink Ergodic Throughput Capacity

Given the received signal model as in (7.5), the ergodic capacity of the downlink phase under infrastructure mode is:

$$\begin{aligned} C^d &= \mathbb{E}\left[\log\left(1+\frac{\underline{P}_d\|\underline{H}\|^2}{N_{BS}(I_d+\sigma_n^2)}\right)\right] \\ &\overset{(a)}{=} \mathbb{E}[\log(1+\frac{sinr_d}{N_{BS}}\cdot\|\underline{H}\|^2)] \\ &= \mathbb{E}[\log(1+\frac{sinr_d}{N_{BS}}\cdot\sum_{n=1}^{N}\|\underline{H}_n\|^2)] \\ &= \mathbb{E}[\log(1+\frac{sinr_d}{N_{BS}}\cdot\sum_{n=1}^{N}(h_n^{ls})^2\|\underline{H}_n^{ss}\|^2)] \end{aligned} \tag{7.18}$$

where step (a) is obtained by denoting $\frac{\underline{P}_d}{I_d+\sigma_n^2}$ as $sinr_d$.

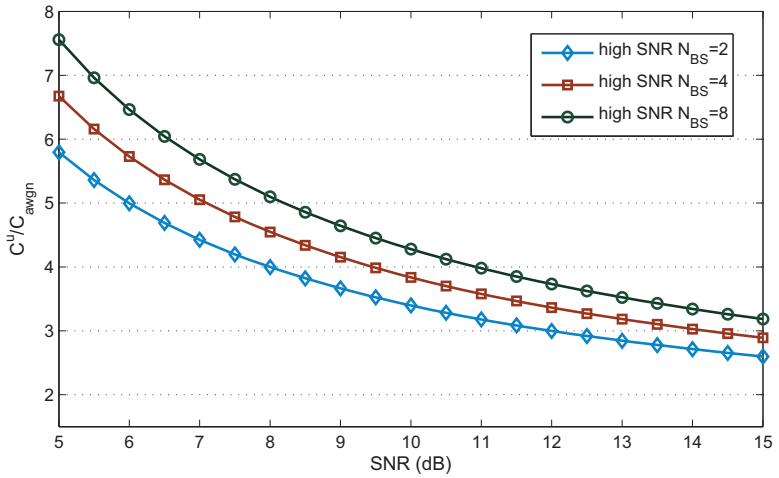

Figure 7.5. Ergodic Capacity in the uplink phase with $N = 9$.

Since the entries of $\underline{H}_n^{ss}$ are independent identically distributed (*i.i.d.*) complex normal random variables (r.vs.), $\|\underline{H}_n^{ss}\|^2$ follows Chi-square distribution with $2N_{BS}$ degrees of freedom, which is also Gamma distributed: $\|\underline{H}_n^{ss}\|^2 \sim \Gamma(N_{BS}, 2)$. Furthermore, we denote $(h_n^{ls})^2\|\underline{H}_n^{ss}\|^2$ and $\sum_{n=1}^{N}(h_n^{ls})^2\|\underline{H}_n^{ss}\|^2$ in (7.18) as χ_n and $\chi = \sum_{n=1}^{N}\chi_n$ for simplicity, respectively. With a scalar $\beta_n = (h_n^{ls})^2 = e^{-\gamma d_n} d_n^{-\alpha}$ added to $\|\underline{H}_n^{ss}\|^2$, $\chi_n \sim \Gamma(N_{BS}, 2\beta_n)$.

To this step, it is obvious that $\chi_n, n = 1, 2, \ldots, N$ are *i.n.d.* Similarly, by employing *second order moment matching method*, $\chi = \sum_{n=1}^{N}\chi_n$ is approximated to be another *Gamma distribution* $\Gamma(k_\chi, \theta_\chi)$ with the same first and second order moments as:

$$k_\chi = \frac{N_{BS}(\sum_{n=1}^{N}\beta_n)^2}{\sum_{n=1}^{N}(\beta_n)^2} \quad and \quad \theta_\chi = \frac{2\sum_{n=1}^{N}(\beta_n)^2}{\sum_{n=1}^{N}\beta_n} \tag{7.19}$$

and the mean and variance are separately:

$$\mu_\chi = 2N_{BS}\sum_{n=1}^{N}\beta_n \quad and \quad \sigma_\chi^2 = 4N_{BS}\sum_{n=1}^{N}\beta_n^2 \tag{7.20}$$

where $\beta_n = e^{-\gamma d_n} d_n^{-\alpha}$.

At high SINR, the ergodic capacity is expressed as:

$$\begin{aligned}
C^d &= \mathbb{E}[\log(1+\frac{sinr_d}{N_{BS}}\cdot\sum_{n=1}^{N}(h_n^{ls})^2\|\underline{H}_n^{ss}\|^2)] \\
&= \mathbb{E}[\log(1+\frac{sinr_d}{N_{BS}}\cdot\chi)] \\
&\approx \mathbb{E}[\log(\frac{sinr_d}{N_{BS}}\cdot\chi)] \\
&\overset{(a)}{=} \log_2\frac{sinr_d}{N_{BS}}+\log_2 e\cdot\psi(k_\chi)+\log_2(\theta_\chi) \\
&\overset{(b)}{=} \log_2\frac{sinr_d}{N_{BS}}+\log_2 e[\ln k_\chi+\frac{1}{k_\chi}+O(\frac{1}{k_\chi^2})]+\log_2(\theta_\chi) \\
&\approx \log_2\frac{sinr_d}{N_{BS}}+\log_2 e\{\ln[\frac{N_{BS}(\sum_{n=1}^{N}\beta_n)^2}{\sum_{n=1}^{N}(\beta_n)^2}]+\frac{\sum_{n=1}^{N}(\beta_n)^2}{N_{BS}(\sum_{n=1}^{N}\beta_n)^2} \\
&+O(\frac{[\sum_{n=1}^{N}(\beta_n)^2]^2}{N_{BS}^2(\sum_{n=1}^{N}\beta_n)^4})\}+\log_2[\frac{2\sum_{n=1}^{N}(\beta_n)^2}{\sum_{n=1}^{N}\beta_n}]
\end{aligned} \tag{7.21}$$

With $I_d = \Theta((\frac{n}{b})^{(-\frac{\alpha}{2})})$, we can see that at high SINR the downlink ergodic capacity is upper bounded by $\Theta(log(\frac{Nn}{b}))$, namely, $C^d = O\big(\log(\frac{Nn}{b})\big)$.

We derive the ergodic capacity at low SINR as:

$$\begin{aligned}
C^d &= \mathbb{E}[\log(1+\frac{sinr_d}{N_{BS}}\cdot\sum_{n=1}^{N}(h_n^{ls})^2\|\underline{H}_n^{ss}\|^2)] \\
&= \mathbb{E}[\log(1+\frac{sinr_d}{N_{BS}}\cdot\chi)] \\
&\approx \mathbb{E}[\log_2 e\cdot\frac{sinr_d}{N_{BS}}\cdot\chi] \\
&\overset{(a)}{=} \log_2 e\cdot\frac{sinr_d}{N_{BS}}\mathbb{E}[\chi] \\
&= \log_2 e\cdot\frac{sinr_d}{N_{BS}}\cdot 2N_{BS}\sum_{n=1}^{N}\beta_n
\end{aligned} \tag{7.22}$$

It is clear that in the low SINR regime, the downlink ergodic capacity is upper bounded by $\Theta(\frac{Nn}{b})$, so that $C_{infra}^d = O\big(\frac{Nn}{b}\big)$.

Theorem 4: For a hybrid wireless network of n nodes and N distributed base stations over *Rayleigh* fading channels, if the total number of base stations $b = o(\frac{n}{\log n})$,

the *per-node downlink ergodic throughput capacity* under the *infrasctructure* transmission mode at high SINR is

$$T^d(n,b,N) = O\big(\frac{b}{Nn}\log(\frac{Nn}{b})W_d\big) \quad bit/s \tag{7.23}$$

And at low SINR:

$$T^d(n,b,N) = O\big(W_d\big) \quad bit/s \tag{7.24}$$

7.4 Conclusion

The above sections have illustrated the advantages of distributed base stations in hybrid wireless networks via information-theoretic arguments. With the introduction of distributed base stations, the hybrid wireless network can be interpreted as macroscopic multiple-antenna system. Cooperation among the base stations has been shown to be able to potentially increase the ergodic capacity of the network under the infrastructure mode, which is an indicator of spectrum efficiency, by an amount proportional to the the number of DBS with respect to the standard single-cell strategies in the hybrid wireless network. The uplink ergodic throughput capacity is $O\big(\log(\frac{NN_{BS}n}{b})W_u\big)$ at high SINR, and $O\big(\frac{NN_{BS}n}{b}W_u\big)$ at low SINR; while the downlink ergodic throughput capacity is $O\big(\frac{b}{Nn}\log(\frac{Nn}{b})W_d\big)$ at high SINR, and $O\big(W_d\big)$ at low SINR.

Chapter 8

Conclusion and Future Woks

This chapter concludes the whole dissertation. It begins with a summary of the dissertation results and contributions, follows with a discussion of future research directions in further investigation of HAN in Smart Grid communications.

8.1 Summary

This dissertation has focused on but not limited to Home Area Networks in Smart Grid Communications. The contributions of this dissertation are:

- *Capacity optimization and power allocation of IR-UWB user within the coexisting operating bandwidth with IEEE 802.11n user* (Chapter 2). Considering the operating frequencies of IEEE 802.11n, IEEE 802.11n system with either operating mode could be interference by UWB user, and the interference of IEEE 802.11n system to UWB user is also unavoidable. With the proposed power allocation scheme for IR-UWB user, the reliable communication is guaranteed for the coexisting IEEE 802.11n user, while IR-UWB achieves its maximized capacity.
- *Performance analysis of a dynamic HAN* (Chapter 3 and Chapter 4). Considering the power saving potential of the emerging WiFi Direct technique, we introduced WiFi Direct technique to HAN for Smart Grid communications. We evaluated the advantages of a dynamic HAN for Smart Grid with the emerging WiFi Direct technique from two perspectives: power saving and communication reliability of the dynamic HAN. Since the power consumption of the HAN is

directly related with the number as well as the working states of WiFi Direct devices, a Markov chain model is employed to represent a profile of the traffic intensity and the the number of WiFi Direct devices in active state. Furthermore, we investigated the downlink outage probability with multiple in-home users connected to the smart meter. Multiuser selection scheme is applied to the uplink of a dynamic HAN for Smart Grid communication scenario. To our best knowledge, this is the first study on performance analysis of multiuser selection scheme that is employed in dynamic HANs for Smart Grid communications.

- *Capacity Optimization in a Heterogeneous HAN* (Chapter 5). We modeled the communication scenario between the smart meter and in-home appliances as a heterogeneous multi-user network. The optimal power allocation algorithm was developed under the constraints that 1) each user should satisfy individual SINR requirement for successful heterogeneous communication; 2) the sum of transmit power allocated to each user is equal to the permissible total transmit power at the smart meter; 3) the allocated transmit power to each user is feasible. The optimization problem is mathematically shown to be convex and the optimal power allocation is thus derived. Furthermore, numerical results verify the capacity performance improvements of the proposed optimal power allocation scheme It is also shown that beamforming technique contributes to the optimal power allocation scheme.
- *hybrid Models of Power Line and Wireless Communications in HAN* (Chapter 6). To enhance HAN security for Smart Grid application, this dissertation incorporates the OFDM - based power line (PL) system into the HAN, and proposes two hybrid models of PL and wireless communications with transmit diversity and receive diversity, respectively. Simulation results validate the fea-

sibility of these new combinational solutions, and furthermore show that the hybrid models could tolerate jamming to the wireless system well.

- *Hybrid Wireless Networks with Distributed Base Stations* (Chapter 7). The ergodic throughput capacity, which is an indicator of spectrum efficiency, was investigated over the independent but not identically distributed composite fast fading channels. As opposed to the existing hybrid wireless networks in which the base station only serves individual cell area, the concept of distributed base stations (DBS) was introduced to achieve transmit/receive diversity. It is analytically shown that compared to the traditional hybrid wireless network, the ergodic throughput capacity of hybrid wireless networks with DBS scales with gain with $N \times N_{BS}$.

8.2 Future Directions

8.2.1 Improved Hybrid Models for HAN Security in Smart Grid

Wireless channel is mainly suffering from a thermal noise that is generally modeled as AWGN. But as to PL channel, not only the background noise, but also the impulsive noise exist in power lines, so that AWGN is not suitable to represent the PL noise any more. The noise existing in the power lines is classified into five types: colored background noise, narrowband noise, periodic impulsive noise asynchronous to the mains, periodic impulsive noise synchronous to the mains and asynchronous impulsive noise [91]. The PDF of impulsive noise can be expressed as a sum of Gaussian functions with different variances [82]. The Middleton's Class A model is employed in the previous work to characterize the PL noise, in which an important parameter called *Impulsive Index*, indicates the probability of pulses overlapping in time domain. In the previous work, simulation results revealed that BER performance of the hybrid

model varies with different values of *Impulsive Index*. In the future work, the effects of noise in PL channel will be theoretically analyzed from a perspective of information theory, especially Fano's Inequality[60].

In the previous work, Selection Combining (SC) scheme is employed at the receiver to recover the transmitted data. The received OFDM signal with the higher SNR is selected between the received signals propagated over the wireless channel and the PL channel, separately. This scheme is highly recommended for its easy implementation and good performance, especially when the transmitted information over the wireless channel is distorted by jamming. But using this combining scheme, it is not guaranteed that the output SNR is maximized. Based on this consideration, in the future work, we will explore other combining scheme for more reliable HAN communication.

8.2.2 Spectrum Efficiency of Wireless Hybrid Network with Correlated Distributed Base Stations

In this dissertation, the spectrum efficiency of wireless hybrid network with distributed base stations was investigated under the assumption that the distributed base stations are fully uncorrelated. We may turn to the topic of distributed source coding (DSC) in wireless hybrid network with correlated base stations. Especially in the downlink phase, it is likely that the distributed base stations transmit highly correlated data to a destination node. Thus DSC is performed at the distributed base stations. In this scenario, what we concern is the achievability of the rates for this hybrid wireless network. To address this problem, Slepian-Wolf theorem can be employed [60].

Appendix A

Computation of Uplink Outage Probability in the Absence of Interference

In this appendix, we compute the closed-form uplink outage probability in the absence of interference based on multiuser selection scheme.

$$\begin{aligned}
\mathbb{P}_{out}^{up} &= Pr[C(\eta_s) \leq R_{req}] \\
&= Pr[\log_2(1+\eta_s) \leq R_{req}] \\
&= Pr[1+\eta \leq 2^{R_{req}}] \\
&= Pr[\eta \leq 2^{R_{req}} - 1] \\
&= \int_0^{(2^{R_{req}}-1)} \overline{f}_{\eta_s}(\eta) d\eta
\end{aligned} \tag{A.1}$$

By taking (4.8) into (4.23),we can get:

$$\begin{aligned}
\mathbb{P}_{out} &= \int_0^{(2^{R_{req}}-1)} \{\sum_{K=0}^{M} \pi_K \frac{K}{\overline{\eta}} [1-\exp(-\frac{\eta}{\overline{\eta}})]^{(K-1)} \exp(-\frac{\eta}{\overline{\eta}})\} d\eta \\
&= \sum_{K=0}^{M} \pi_K F_{\eta_s}^K (2^{R_{req}} - 1) \\
&= \sum_{K=0}^{M} \pi_K [1-\exp(-\frac{2^{R_{req}}-1}{\overline{\eta}})]^K
\end{aligned} \tag{A.2}$$

Appendix B

Computation of Uplink Outage Probability in the Absence of Interference

In this appendix, we compute the closed-form uplink outage probability in the presence of MUI.

$$
\begin{aligned}
P_{iout}^{UP} &= Pr[\pi_K log_2(1+\gamma_K) \leq R_{req}] \\
&= \pi_K Pr[log_2(1+\gamma_K) \leq R_{req}] \\
&= \pi_K Pr[\gamma_K \leq 2^{R_{req}} - 1] \\
&= \pi_K Pr[\gamma_K(dB) \leq (2^{R_{req}} - 1)(dB)] \\
&= \pi_K Pr[\mathcal{P}_i^r(dB) - \mathcal{I}_K(dB) - \sigma^2(dB) \leq (2^{R_{req}} - 1)(dB)] \\
&= \pi_K Pr[\mathcal{P}_i^r(dB) - \mathcal{I}_K(dB) \leq (2^{R_{req}} - 1)(dB) - \sigma^2(dB)] \\
&= \pi_K Q(\frac{\mu_i - \mu_{I_K} - (2^{R_{req}} - 1)(dB) + \sigma^2(dB)}{\sqrt{\sigma_i^2 + \sigma_{I_K}^2}})
\end{aligned}
\tag{B.1}
$$

where μ_i can be easily obtained from (4.13) that:

$$
\mu_i = \mathcal{P}_i^t(dB) + G_t(dBi) + G_r(dBi) + 20\log(\frac{\lambda}{4\pi d_i}) \tag{B.2}
$$

Appendix C

Capacity Optimization in Heterogeneous HAN

Proof of $|\underline{H_k}^T \underline{V_j}|^2 = \lambda_j^2 \sum_{n=1}^{N} |\beta_{n,k}|^2$

In the notation of matrices, the matrix $\underline{V_j}^T \in \Re^{1\times N}$ has a singular value decomposition (SVD):

$$\underline{V_j}^T = \underline{U\Lambda V^*} \tag{C.1}$$

where $\underline{U} \in \Re^{1\times 1}$ and $\underline{V} \in \Re^{N\times N}$ are unitary matrices, and $\underline{UU^*} = \underline{U^*U} = \underline{VV^*} = \underline{V^*V} = \underline{I}$. $\underline{\Lambda} \in \Re^{1\times N}$ is the matrix with the first element as λ_j and all other elements as zero. λ_j^2 is the eigenvalue of the matrix $\underline{V_j}^T \underline{V_j}$ and also of $\underline{V_j V_j}^T$.

Thus, for real matrices $\underline{H_k}$ and $\underline{V_j}$, we can get :

$$\begin{aligned}
|\underline{H_k}^T \underline{V_j}|^2 &= |\underline{V_j H_k}^T|^2 \\
&= Tr[\underline{H_k V_j}^T \underline{V_j H_k}^T] \\
&= Tr[\underline{H_k U\Lambda V^* V\Lambda^* U}^T \underline{H_k}^T] \\
&= Tr[\underline{H_k U\Lambda\Lambda^* U}^T \underline{H_k}^T] \\
&= \lambda_j^2 Tr[\underline{H_k UU}^T \underline{H_k}^T] \\
&= \lambda_j^2 Tr[\underline{H_k H_k}^T]
\end{aligned} \tag{C.2}$$

We assume the channel gain from the n_{th} transmit antenna at the smart meter to the k_{th} user by $\beta_{n,k}$. Therefore,

$$\begin{aligned}
|\underline{H_k}^T \underline{V_j}|^2 &= \lambda_j^2 Tr[\underline{H_k H_k}^T] \\
&= \lambda_j^2 Tr[(\beta_{1,k} \quad \beta_{2,k} \ldots \beta_{N,k})(\beta_{1,k} \quad \beta_{2,k} \ldots \beta_{N,k})^T] \\
&= \lambda_j^2 \sum_{n=1}^{N} |\beta_{n,k}|^2
\end{aligned} \tag{C.3}$$

Similarly,

$$|\underline{H_k}^T \underline{V_k}|^2 = \lambda_k^2 \sum_{n=1}^{N} |\beta_{n,k}|^2 \tag{C.4}$$

Appendix D

Proof of Lemma 1

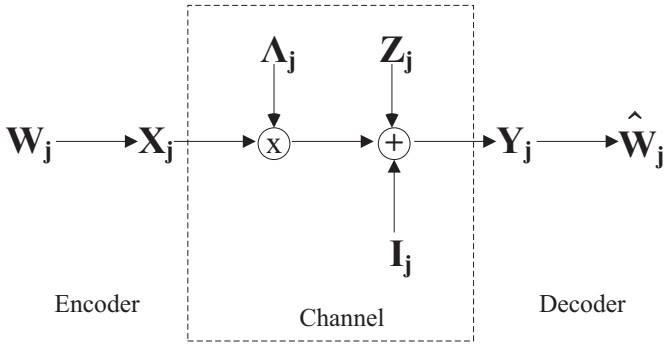

Figure D.1. The Sub-channel Converted from the MIMO channel via SVD.

Taking the uplink case of the source node ($k = 0$) for example, the capacity can be computed by decomposing the vector channel into a set of parallel scalar sub-channels. The vector $\underline{H}_0$ in (7.3) admits a singular value decomposition (SVD) with N singular values $\lambda_1, \lambda_2, \ldots, \lambda_N$ of the $\underline{H}_0$ [53].

From the perspective of information theory, we can rewrite the output for each sub-channel as [60]:

$$Y_j = \Lambda_j X_j + I_j + Z_j, \quad j = 1, 2, \ldots, N. \tag{D.1}$$

The equivalency is summarized in Figure D.1. We assume that for a certain time slot, all the messages W_j being sent out at rate R_j are independent and uniformly distributed over their respective ranges $\{1, 2, \ldots, 2^{R_j}\}$, corresponding to the codewords X_j, which is received by the receiver as a random sequence Y_j, including the effects of interference and noise in the link. And then the decoder maps the received signal to form an estimated message $\hat{W}_j$.

Define the probability of error,

$$P_e^j = Pr\{\hat{W}_j \neq W_j\} \tag{D.2}$$

associating with the independency of N sub-channels,

$$
\begin{aligned}
R &= H(W) \\
&= I(W;\hat{W}) + H(W|\hat{W}) \\
&\overset{(a)}{\leq} I(X;Y) + \epsilon \\
&= I(X_1, X_2, \ldots, X_N; Y_1, Y_2, \ldots, Y_N) + \epsilon \\
&= H(Y_1, Y_2, \ldots, Y_N) - H(Y_1, Y_2, \ldots, Y_N | X_1, X_2, \ldots, X_N) + \epsilon \\
&\overset{(b)}{=} H(Y_1, Y_2, \ldots, Y_N) \\
&\quad - H(I_1 + Z_1, I_2 + Z_2, \ldots, I_N + Z_N | X_1, X_2, \ldots, X_N) + \epsilon \\
&= H(Y_1, Y_2, \ldots, Y_N) - H(I_1 + Z_1, I_2 + Z_2, \ldots, I_N + Z_N) + \epsilon \\
&= H(Y_1, Y_2, \ldots, Y_N) - \sum_{j=1}^{N} H(I_j + Z_j) + \epsilon \\
&\leq \sum_{j=1}^{N} H(Y_j) - \sum_{j=1}^{N} H(I_j + Z_j) + \epsilon \\
&\leq \sum_{j=1}^{N} \big(H(Y_j) - H(I_j + Z_j) \big) + \epsilon \\
&\overset{(c)}{=} \sum_{j=1}^{N} \frac{1}{2} \log \big(1 + \frac{\mathcal{P}_u \lambda_j^2}{I_u + \sigma_n^2} \big) + \epsilon \\
&\overset{(d)}{\leq} \frac{1}{2} \log \big(1 + \frac{\sum_{j=1}^{N} \mathcal{P}_u \lambda_j^2}{I_u + \sigma_n^2} \big) + \epsilon
\end{aligned}
\tag{D.3}
$$

where (a) follows Fano's inequality and data processing inequality, where $\epsilon = \sum_{j=1}^{N}(1 + P_e^j R_j)$; (b) follows the that $H(Y|X) = H(X + I + Z|X) = H(I + Z|X)$; (c) is the definition of capacity; (d) follows Jensen's inequality.

References

[1] M. Sooriyabandara, and J. Ekanayake, "Smart Grid-Technologies for its realisation." *2010 IEEE International Conference on Sustainable Energy Technologies (ICSET)*, Dec. 2010, pp:1-4.

[2] A. Ghassemi, S. Bavarian, and L. Lampe, "Cognitive Radio for Smart Grid Communications." *2010 First IEEE International Conference on Smart Grid Communications*, 2010, pp:297-302.

[3] Y. Zhang, L. Wang, W. Sun, G. R. C., and A. M., "Distributed Intrusion Detection System in a Multi-Layer Network Architecture of Smart Grids." *IEEE Transanctions on Smart Grid*, Vol.2, Issue 4, 2011, pp:796-808.

[4] L. Yang, G. B. Giannakis, "Ultra-Wideband Communications: An Idea Whose Time Has Come. IEEE Signal Processing Magazine." Vol. 21, Issue 6:26-54, 2004.

[5] S. Wood and R. Aiello R, *Essentials of UWB*. 2008, Cambridge University Press. Cambridge, UK.

[6] J. Bellorado, S. S. Ghassemzadeh, and L. J. Greenstein, et.al., "Coexistence of Ultra-wideband systems with IEEE-802.11a Wireless LANs." GLEBECOM'03, 2013

[7] P. Yi, A. Iwayemi, and C. Zhou, "Developing ZigBee Deployment Guideline Under WiFi Interference for Smart Grid Applications." *IEEE Trans on Smart Grid*. Vol. 2, Issue 1, 2011, pp::110-120.

[8] F. Berens and P. Jung, "Wireless ultra-wide-band (UWB) communications: Technology, regulation, standardization, and application areas." 2010 IEEE ICUWB, Volume 1, pp:12-19.

[9] A. Huseyin, C. Zhining, and D. Benedetto, *Ultra Wideband Wireless Communication*. 2006, Wiley-Interscience, Hoboken, N.J., pp:10-11.

[10] Federal Communication Commission, Revision of part 15 of the commission's rules regarding ultra-wideband transmission systems, FIRST REPORT AND ORDER. ET Docket 98-153, FCC 02-48, February 14, 2002, pp:2-94.

[11] Z. Li, W. Zou, and B. Li, et.al., "Analysis on Coexistence of Ultra Wideband with OFDM-Based Communication Systems". *IEEE Transactions on Eletromagnetic Compatibility*. Vol.53, Issue 3, 2011, pp:823-830.

[12] M. Hamalainen, V. Hovinen, and R. Tesi, et.al., " On the UWB System Coexistence With GSM900, UMTS/WCDMA, and GPS." *IEEE Journal on Selected Areas in Communications*. Vol.2, No.9, Dec. 2002, pp:1712-1721.

[13] R. Giuliano and F. Mazzenga, "On the Coexistence of Power-Controlled Ultrawide-Band Systems With UMTS, GPS, DCS1800, and Fixed Wireless Systems." *IEEE Transactions on Vehicular Technology*. Vol.54, No.1, Jan. 2005, pp:62-80.

[14] A. Giorgetti, M. Chiani, and M. Z. Win, "The Effect of Narrowband Interference on Wideband Wireless Communication Systems." *IEEE Transactions on Communications*. Vol.53, No.12, Dec. 2005, pp:2139-2149.

[15] M. Chiani, and A. Giorgetti, "Coexistence Between UWB and Narrow-Band Wireless Communication Systems (Invited Paper)." *Proceedings of The IEEE*. Vol.97, No.2, Feb. 2009, pp:231-254.

[16] S. Kandeepan, G. Baldini, and R. Piesiewicz, "Preliminary experimental results on the spectrum sensing performances for UWB-Cognitive Radios for detecting." *IEEE 802.11n systems 6th International Symposium on Wireless Communication Systems (ISWCS)*, 2009, pp:111-115.

[17] R. Yang, K. S. Kwak, and Z. Zhou, "Distributed water-filling algorithm for direct-sequence ultra wideband cognitive radio network with limit on aggregate power emission." *IET Communications*, Volume 4, Issue 12, 2010, pp:1404-1414.

[18] G. Bansal, M. J. Hossain, and V. K. Bhargava, "Optimal and suboptimal power allocation schemes for OFDM-based cognitive radio systems." *IEEE Trans on Wireless Communications*, Vol. 7, NO. 11, Nov. 2008, pp:4710-4718.

[19] C W Tan, S Friedland, and S H Low, "Spectrum Management in multiuser cognitive wireless networks: Optimality and Algorithm." *IEEE Journal on Selected Areas in Communications*. Vol. 29, NO. 2, Feb. 2011, pp:421-430.

[20] J. Cai, K H Liu, X Shen, J W Mark, and T D Todd, "Power Allocation and Scheduling for Ultra-Wideband Wireless Networks." *IEEE Transactions on Vehicular Technology*. Vol.57, No.2, Mar. 2008, pp:1103-1112.

[21] H. Yoon, and J. Kim, "Collaborative Streaming-based Media Content Sharing in WiFi-enabled Home Networks." *IEEE Transactions on Consumer Electronics*, Volume 54, Issue 4, 2010, pp: 2193-2200.

[22] Wi-Fi Alliance, "Wi-Fi for the Smart Grid", $http : //www.wi - fi.org/knowledge_center_overview.php?docid = 4686$, Sep. 2010.

[23] Wi-Fi Alliance, "Wi-Fi CERTIFIED Wi-Fi Direct Frequently Asked Questions", $http : //www.wi - fi.org/files/20091019_Wi - Fi_Direct_FAQ.pdf$, 2011.

[24] Y. He, R. Yuan, X. Ma, and J. Li, "The IEEE 802.11 Power Saving Mechanism: An Experimental Study." *IEEE Wireless Communications and Networking Conference (WCNC), 2008*, pp: 1362-1367.

[25] C. H. Gan, and Y. B. Lin, "An Efficient Power Conservation Scheme for IEEE 802.11 Wireless Networks." *IEEE Transactions on Vehicular Technology*, Vol.58, No.4, May 2009, pp:1920-1929.

[26] I. Lee, J. Bo, E. Y. Choi, J. H. Lee, and S. K. Lee, "Analysis of Power Consumption and Efficient Power Saving Techniques for MIMO-OFDM-based Wiresless LAN receivers." *2011 Fourth International Conference on Sensor Technologies and Applications*, pp:597-601.

[27] M. Alizadeh, A. Scaglione, and R. J. Thomas, "From Packet to Power Switching: Digital Direct Load Scheduling." *IEEE Journal on Selected Areas in Communications*, Vol.30, No.6, Jul.2012, pp:1027-1036.

[28] T. T. Kim, and H. V. Poor, "Scheduling Power Consumption With Price Uncertainty." *IEEE Transanctions on Smart Grid*, Vol.2, No.3, Sep. 2011, pp:519-527.

[29] H. Li, L. Lai, and W. Zhang, "Communication Requirement for Reliable and Secure State Estimation and Control in Smart Grid." *IEEE Transanctions on Smart Grid*, Vol.2, No.3, Sep. 2011, pp:476-486.

[30] N. Yang, M. Elkashlan, and J. Yuan, "Outage Probability of Multisuer Relay Networks in Nakagami-m Fading Channels." *IEEE Transactions on Vehicular Technology*, Vol.59, No.5, May 2010, pp:2120-2132.

[31] O. Ali, C. Cardinal, and F. Gagnon, "Performance of Optimum Combining in a Poisson Field of Interferers and Rayleigh Fading Channels." *IEEE Transactions on Wireless Communications*, Vol.9, NO.8, Aug. 2010, pp: 2461-2467.

[32] Q. H. Spencer, C. B. Peel, A. L. Swindelhurst, and M. Haardt, "An Introduction to the Multi-User MIMO Dowlink." *IEEE Communication Magzine*, Oct.2004, pp:60-67.

[33] M. A. Azarm, R. Bari, and M. Yue, et.al, "Electrical Substation Reliability Evaluation with Emphasis on Evolving Interdependence on Communication Infrastructure." *In Proceedings of International Conference on Probabilistic Methods Applied to Power Systems*, Sep.2004, pp:487-491.

[34] A. Goldsmith, *Wireless Communications*, Cambridge University Press 2005, pp:390-392.

[35] M. Schubert, and H. Boche, "Solution of the Multiuser Downlink Beamforming Problem With Individual SINR Constraints." *IEEE Transactions on Vehicular Technology*, Vol.53, No.1, Jan.2004, pp:18-28.

[36] Z. Luo, and W. Yu, "An Introduction to Convex Optimization for Communications and Signal Processing," *IEEE Journal on Selected Areas in Communications*, Vol.24, No.8, Aug.2006, pp:1426-1438.

[37] E. Lee, M. Gerla, and S. Y. Oh, "Physical Layer Security in Wireless Smart Grid." *IEEE Communications Magazine*, Aug.2012, pp:46-52.

[38] S. Galli, A. Scaglione, and Z. Wang, "For the Grid and Through the Grid: The Role of Power Line Communications in the Smart Grid." *Invited paper, in Proceedings of the IEEE*, Vol.99, No.6, Jun.2011, pp:998-1027.

[39] HomePlug Powerline Alliance, Inc., HomePlug Green PHY^{TM}1.1 The Standard for In-Home Smart Grid powerline Communications: An application and technology overview. Oct.2012.

[40] M. Korki, N. Hosseinzadeh, and T. Moazzeni, "Performance Evaluation of a Narrowband Power Line Communications for Smart Grid with Noise Reduction Technique." *IEEE Transactions on Consumer Electronics*, Vol.57, No.4, Nov.2011, pp:1598-1606.

[41] M. Zimmermann, and K. Dosert, "A Multipath Model for the Powerline Channel." *IEEE Transactions on Communications*, Vol.50, No.4, Apr.2002, pp:553-559.

[42] S. Galli, "A Novel Approach to the Statistical Modeling of Wireline Channels." *IEEE Transactions on Communications*, Vol.59, No.5, May 2011, pp:1332-1345.

[43] S. W. Lai, and G. G. Messier,"The Wireless/Power-line Diversity Channel." *In Proceedings of 2010 IEEE International Conference on Communications (ICC)*, 2010, pp:1-5.

[44] M. A. Azarm, R. Bari, M. Yue, and Z. Musicki, "Electrical Substation Reliability Evaluation with Emphasis on Evolving Interdependence on Communication Infrastructure." in *Proceedings of International Conference on Probablistic Methods Applied to Power Systems*, Sep. 2004, pp:487-491.

[45] O. Dousse, P. Thiran, and M.Hasler, "Connectivity in ad-hoc and hybrid networks," *in the proceedings of 2002 INFOCOM*, vol. 2, pp. 1079-1088, 2002.

[46] D. Gesbert, S. Hanly, and H. Huang, et al., "Multi-Cell MIMO Cooperative Networks: A New Look at Interference," *Selected Areas in Communications, IEEE Journal on* , vol.28, no.9, pp.1380-1408, Dec. 2010.

[47] W. Choi and J. G. Andrews, "Downlink Performance and Capacity of Distributed Antenna Systems in a Multicell Environment," *IEEE Trans. Wireless Commun.*, vol. 6, no. 1, pp: 69-73, Jan. 2007.

[48] R. W. Heath, T. Wu, Y. H. Kwon, and A. C. K. Soong, "Multiuser MIMO in Distributed Antenna Systems With Out-of-Cell Interference," *IEEE Trans. Signal Process.*, vol. 59, No. 10, pp:4885-4899, Oct. 2011.

[49] M. Sawahashi, Y. Kishiyama, and A. Morimoto, et al., "Coordinated multipoint transmission/reception techniques for LTE-advanced [Coordinated and Distributed MIMO]," *Wireless Communications, IEEE* , vol.17, no.3, pp.26,34, June 2010.

[50] W. Feng, Y. Wang, and N. Ge, et al. "Virtual MIMO in Multi-Cell Distributed Antenna Systems: Coordinated Transmissions with Large-Scale CSIT," *IEEE J. Sel. Areas Commun.* Vol. 31, no. 10, pp: 2067-2081, Oct. 2013.

[51] P. Gupta and P. R. Kumar, "The Capacity of Wireless Networks," *IEEE Transactions on Information Theory*, vol.46, no.2, pp: 388-404, Mar. 2000.

[52] X. Wang and Q. Liang, "On the Throughput Capacity and Performance Analysis of Hybrid Wireless Networks over Fading Channels," *IEEE Trans. Wireless Commun.*, vol. 12, no. 6, pp: 2930-2940, Jun. 2013.

[53] D. Tse, P. Viswanath, *Fundamentals of Wireless Communication*, Cambridge University Press, Sep. 2004.

[54] M D Benedetto and G Giancola, *Understanding Ultra Wide Band Radio Fundamentals*. 2004, Prentice Hall

[55] A Roca, *Implementation of a WiMAX simulator in Simulink*. Diplomarbeit, Vienna, Feb. 2007.

[56] Z. Li, and Q. Liang, "Capacity Optimization of Ultra-wide Band System under the Coexistence with IEEE 802.11n." *11th International Symposium on Communications and Information Technologies (ISCIT)*, 2011, pp:553-557.

[57] IEEE 802.11n D.7.0. Part 11:Wireless LAN Medium Access Control (MAC) and Physical Layer (PHY) specifications, 2008, pp:245.

[58] C X Juan and Q Sheng, "Spectrum analysis of Ultra-wide band signal based on Gaussian pulse." Global Mobile Congress (GMC), 2010, pp:1-4.

[59] Electronic Communications Committee, ECC Report 64: the protection requirements of radio communications systems below 10.6GHz from generic UWB applications. Feb. 2005, pp:5-7, 24-27.

[60] T M Cover, J A Thomas, *Elements of Information Theory Second Edition*. 2006, John Wiley and Sons, Inc., Hoboken, New Jersey

[61] S Boyd and L Vandenberghe, *Convex Optimization*. 2004, Cambridge University Press

[62] A. Mitrofanova, "Lecture 3: Continuous times Markov chains. Possion Process. Birth and Death process." NYU, department of Computer Science, Dec.18, 2007.

[63] I. Humar, J. Zhang, Z. Wu, and L. Xiang, "Energy Saving Modeling and Performance Analysis in Multi-Power-State Base Station Systems", *2010 GreenCom and CPSCom*, 2010, pp:474-478.

[64] A. G. Hawkes, and A. M. Sykes, "Equilibrium Distributions of Finite-State Markov Processes." *IEEE Transactions on Reliability*, Volume 39, Issue 5, 1990, pp: 592-595.

[65] L. Kong, G. K. W. Wong, and D. H. K. Tsang, "Performance Study and System Optimization on Sleep Mode Operation in IEEE 802.16e." *IEEE Transactions on Wireless Communications*, VOL.8, NO.9, Sep. 2009, pp: 4518-4528.

[66] A. M. Saleh, and R. A. Valenzuela, "A Statistical Model for Indoor Multipath Propagation." *IEEE Jouranl on Selected Areas in Communications*, Vol.SAC-5, No.2, Feb. 1987, pp:128-137.

[67] M. K. Simon, and M. Alouini, *Digital Communication over Fading Channels 2nd Edition*, John Wiley Sons, Inc., Hoboken, New Jersey, Dec. 2004.

[68] W. Akkari, A. Belghith, and A. B. Mnaouer, "Enhancing power saving mechanisms for ad hoc networks using neighborhood information." *IEEE Wireless Communications and Mobile Computing Conference, 2008*, pp:794-800.

[69] A. A. M. Saleh, and R. A. Valenzuela, "A Statistical Model for Indoor Multipath Propagation." *IEEE Jouranl on Selected Areas in Communications*, Vol.SAC-5, No.2, Feb. 1987, pp:128-137.

[70] Q. Zou, A. Tarighat, and Ali. H. Sayed, "Performance Analysis of Multiband OFDM UWB Communications with Application to Range Improvement." *IEEE Transactions on Vehicular Technology*, Vol.56, No.6, Nov. 2007, pp: 3864-3878.

[71] X. Zhang, Z. Lv, W. Wang, "Performance Analysis of Multiuser Diversity in MiMO Systems with Antenna Selection." *IEEE Transactions on Wireless Communications*, Vol.7, No.1, Jan. 2008, pp: 15-21.

[72] S. S. Nam, H.-C. Yang, M.-S. Alouini, and D. I. Kim, "Impact of Interference on the Performance of Selection Based Parallel Multiuser Scheduling." *IEEE Transactions on Wireless Communications*, Vol.11, No.2, Feb. 2012, pp:531-536.

[73] N. Chang, R. Rashidzadeh, and M. Ahmadi, "Robust Indoor Positioning using Differential Wi-Fi Access Points." *IEEE Transactions on Consumer Electronics*, Vol.56, No.3, Aug. 2010, pp:1860-1867.

[74] A. Goldsmith, *Wireless Communications*. Cambridge University Press, 2005, pp: 172-180.

[75] G. L. Stuber, *Principles of Mobile Digital Communication 2nd Edition*, Kluwer Academic Publishers, 2002, pp:129-131.

[76] "IEEE 802.11n D.7.0. Part 11:Wireless LAN Medium Access Control (MAC) and Physical Layer (PHY) specifications." Sep. 2008, pp: 245.

[77] M. K. Simon and M.-S. Alouini, *Digital Communication over Fading Channels Second Edition*. John Wiley and Sons. Inc., Hoboken, New Jersey, 2005.

[78] H. Jafarkhani, *Space-Time Coding Theory and Practice*. Cambridge Universiry Press 2005, pp:48-49.

[79] A. Sheth, and R. Han, *An Implementation of Transmit Power Control in 802.11b Wireless Networks*, Technical Report CU-CS934-02, University of Colorado, 2002.

[80] Gunmmadi, R. H. Balakrishnan, and S. Seshan. "Metronome: Coordinating Spectrum Sharing in Heterogeneous Wireless Networks." *Communication Systems and Networks and Workshops*, 2009, pp:1-10.

[81] S. M. Alamouti, "A Simple Transmit Diversity Technique for Wireless Communications." *IEEE Journal on Select Areas in Communications*, Vol. 16, No. 8, Oct. 1998, pp:1451-1458.

[82] M. Katayama, T. Yamazato, and H. Okada, "A Mathematical Model of Noise in Narrowband Power Line Communication Systems." *IEEE Journal on Selected Areas in Communications*, Vol.24, No.7, Jul.2006, pp: 1267-1276.

[83] Y. Jiang, X. Hu, and X. Kai, et al., "Bayesian Estimation of Class A Noise Parameters with Hidden Channel States." 2007 International Symposium on Power Line Communications and Its Applications (ISPLC'07), pp:2-4.

[84] A. Mpitziopoulos, D. Gavalas, and C. Konstantopoulos, et.al, "A Survey on Jamming Attacks and Countermeasures in WSNs." *IEEE Communications Survey & Tutorials*, Vol.11, No.4, Sep.2009, pp:42-56.

[85] X. Zhu, P. Li,Y. Fang, and Y. Wang, "Throughput and Delay in Cooperative Wireless Networks With Partial Infrastructure." *IEEE Transactions on Vehicular Technology*, vol. 58, no. 8, pp. 4620-4626, Oct. 2009.

[86] W. Fu and D. Agrawal, "Capacity of Hybrid Wireless Mesh Networks with Random APs." *IEEE Transactions on Mobile Computing*, vol. 12, no. 1, pp: 136-150, Jan. 2013.

[87] T. S. Rappaport, *Wireless Communications: Principles and Practice, 2nd Edition*, Prentice Hall, 2002.

[88] D. Kirachaiwanich and Q. Liang, "Capacity of Wireless Hybrid Networks with Successive Interference Cancellation," in *Proc. 2010 IEEE Globecom*, pp. 1-5, Dec. 2010.

[89] B. Liu, P. Thiran and D. Towsley, "Capacity of Wireless Ad Hoc Network with with Infrastructure." *Proc. ACM MobiHoc*, Montreal, Canada, September 2007.

[90] J. G. Proaksi and M. Salehi, *Digital Communication*, 5th edition. McGraw-Hill, 2008.

[91] M. Gotz, M. Rapp, and K. Dostert, "Power Line Channel Charateristics and Their Effect on Communication System Design." *IEEE Communications Magazine*, Apr.2004, pp:78-86.

Biographical Statement

Zhuo Li received the Bachelor's degree in Network Engineering from the School of Communication and Information Engineering, University of Electronic and Scientific Technology of China, Chengdu, China, in 2004. She worked on the Master's degree in Circuits and Systems in the School of Information and Communication Engineering, Beijing University of Posts and Telecommunications, Beijing, China from 2008 to 2011. She is currently pursuing the Ph.D degree in Electrical Engineering at the University of Texas at Arlington, Texas, USA. Her research interests include ultra-wideband (UWB) communications, wireless communications in Smart Grid applications, and Home Area Network (HAN) security for Smart Grid.